Structure and Mechanism of RTEM-1 β-lactamase: The Role of Lysine 234

Thesis by

David M. Long

In Partial Fulfillment of the Requirements

for the Degree of

Doctor of Philosophy

California Institute of Technology

Pasadena, California

1991

(Submitted February 15, 1991)

To Mammy and Duke

Acknowledgments

I would like to thank my research advisor, Professor John H. Richards, for providing me with the opportunity to pursue "hair-brained schemes" in the laboratory and encouraging me to think and act independently. Jack's patience and unselfish attitude towards allowing his students to make lots of decisions and learn from their mistakes, as well as their successes, makes him a good advisor.

I wish to acknowledge the members of the Richards group for providing friendship, scientific and personal advice, and lots of loud conversation of a most unusual kind. I would like to thank Ilana Tamir and Scott Wolfe, who have both made substantial contributions to the work described in this thesis and who have been good friends. Special thanks go to Phoebe Ray for offering personal and professional advice, genuine friendship, and dates with her musician friends.

Thank you, Eric Ginsburg, Brad Jacobs, and Tom Povsic for granting me the opportunity to live with such refined "gents" as yourselves in the palace [hell hole] at 114 S. Meridith Ave.

Thank you, Eileen Ralicke for making my graduate life more interesting, for cheerfully engaging in life-threatening experiences with me, and for teaching me the value of a world where cows rule, herbal medicine is the only option, and there are no chemicals in the toothpaste or vegetables. You are a wonderful and talented person whom I admire and love very much.

I am most grateful and extend my deepest appreciation to my family for loving and supporting me in everything that I do which is

sensible. Thanks especially, Mom and Dad, for giving me encouragement, advice and opportunities that I will always value tremendously.

Abstract

Site-saturation mutagenesis has been used to substitute lysine 234 in RTEM-1 β–lactamase with 18 natural amino acids. Lysine 234 is conserved among the class A β–lactamases and has been implicated in x-ray diffraction and molecular modeling studies as a cationic residue that binds the C3 carboxylate common to most β–lactamase substrates (Hertzberg and Moult (1987) *Science*, **236**, 694.; Meows *et al.* (1990) *PROTEINS: Structure, Function, and Genetics*, **7**, 156.; Chapter 2 of this Thesis).

The 234 mutant proteins have significantly reduced activity towards hydrolysis of penicillin, ampicillin, and cephalosporin C and do not have observable phenotypic activity towards hydrolysis of cephalothin. With the exception of K234R, the phenotypic activities are essentially indistinguishable. The high phenotypic resistance of the K234R mutant shows that a positively charged guanidinium group can effectively substitute for the wild-type ammonium group of lysine 234. The uniformly reduced phenotypic activities of all other mutants indicate that the mutant amino acids do not interfere with or participate directly in the enzymatic reaction mechanism. Behavior of the mutants on anion exchange columns and analysis by circular dichroism spectroscopy show that the secondary and tertiary structures characteristic of the wild-type enzyme are not significantly disrupted by mutation.

Four mutants were purified to homogeneity and the steady-state kinetic parameters for hydrolysis of benzylpenicillin were measured

for each. The kinetics show that substituting lysine 234 with glutamate, glutamine, or valine causes a decrease in the apparent equilibrium-binding constant for benzylpenicillin of about three orders of magnitude. In contrast, the binding constant for the K234R mutant, which preserves the positive charge at position 234, is reduced by only one order of magnitude. These results indicate that lysine 234 is responsible for stabilizing the RTEM-1/benzylpenicillin complexes by approximately 4.5 kcal mol^{-1}, consistent with the formation of an intermolecular charged hydrogen bond.

The mutations have much less pronounced effects on the ability of the enzyme to catalyze the hydrolysis of benzylpenicillin under saturating substrate concentrations. K234R and K234E have the wild-type k_{cat}, while K234Q and K234V have k_{cat}s reduced by one and two orders of magnitude, respectively.

Analysis of the kinetic results shows that lysine 234 performs a uniform binding function in catalysis by RTEM-1 lactamase (Albery and Knowles (1976) *Biochemistry*, **15**, 5631). This contrasts with the differential binding role that has been determined for lysine 234 in catalysis by β–lactamase from *Bacillus licheniformis* (BL) (Ellerby *et al.* (1990), *Biochemistry*, **29**, 5797). The results indicate that RTEM-1 utilizes the binding capabilities of lysine 234 to increase the catalytic rate under low substrate concentrations, while BL utilizes it to increase the rate under conditions of high substrate concentration.

In Chapter 2, molecular modeling of the RTEM-1 β–lactamase active site is described. The models were based on the published

α–carbon trace of β–lactamase from *Staphylococcus aureus* PC1 (Hertzberg and Moult, *ibid.*) and were built in the absence of an experimentally determined high-resolution x-ray structure of a class A β–lactamase. The experiments were designed to yield structures useful for rationalizing the results of mutagenesis experiments and for formulating mechanistic ideas testable by experiment. The model structures are shown to compare favorably with the high-resolution structure of a class A β–lactamase published after the modeling was completed. Two working mechanisms for catalysis by RTEM-1 are proposed, based on the modeling, mutagenesis results, and on precedent.

Chapter four describes the development of methods for measuring enzymatic reaction rates with circular dichroism spectroscopy (CD). Application of the methods to two enzymes, β–lactamase and ribulose-1,5-bisphosphate carboxylase/oxygenase, is described. The general utility of the methods is addressed.

Table of Contents

List of Figures

CHAPTER 1

CHAPTER 2

CHAPTER 3

List of Tables

CHAPTER 1

CHAPTER 2

CHAPTER 3

CHAPTER 4

Abbreviations and Nomenclature

Mutants are designated by one-letter amino acid codes followed by the residue number and the replacement amino acid. For example, "K234R" designates lysine 234 replaced with arginine. "RTEM-1" refers to RTEM-1 β–lactamase encoded by plasmid pBR322, "PC1" refers to β–lactamase from *Staphylococcus aureus* PC1, and "BL" refers to β–lactamase from *Bacillus licheniformis* 749/C. "RuBP" is ribulose-1.5-bisphosphate. "CD" is circular dichroism spectroscopy. Black and white figures of protein structures are designed to be viewed with a pair of stereo glasses.

CHAPTER 1

Introduction: Some Interesting Aspects of Protein Chemistry and the Class A β-lactamases

Amino acids in folded proteins can have unusual chemical properties.

It is remarkable that the limited chemical diversity of the 20 natural amino acids is not more of a constraining factor when they combine to form the diverse group of over one million naturally occurring enzymes (1). The number of known chemical reactions that are catalyzed by enzymes is in the thousands, and many more exist that are still unknown or are only crudely characterized (2). One reason for the observed functional diversity in enzymes is that the chemical properties of amino acids in folded proteins are context dependent; their acidity, basicity, nucleophilicity, electrophilicity, and other chemical properties are greatly affected by the positions and identities of neighboring amino acids. The active sites of enzymes are curious places where acids and bases can have uncommon strengths, opposite charges can attract with abnormally high affinities, and nucleophiles and electrophiles can be transformed into particularly reactive species.

Acidic and basic amino acids in globular proteins can have ionization constants perturbed significantly from values measured in free solution (3). Notable examples of this effect include the active site lysine of acetoacetate decarboxylase (4). The ε-amino group of this lysine has a pKa of 5.9, over four pH units lower than the expected value of about 10. In papain, histidine 159 has a pKa of 3.4, a full 3 units below the value for imidizole in water (5), and in ribulose 1,5-bisphosphate carboxylase/oxygenase, the pKa of lysine 166 is two units below the expected value of 10 (6).

Significant perturbation of amino acid chemical properties in folded proteins is not limited to acid-base chemistry. The nucleophilicity of active-site serines of the serine proteases, β-lactamases, and some carboxypeptidases are increased considerably over normal values for these nucleophiles in free solution. In these cases the nucleophilic character is in some way enhanced by the position of the serine in the folded protein, although the precise reason for the increased reactivity is not fully understood. The serine nucleophiles of subtilisin, RTEM-1 β-lactamase, and the D-alanyl-D-alanine peptidase from *Streptomyces* R61 are positioned at the amino ends of α-helices, where higher nucleophilicities are thought to result from higher electrical potential at the positive (amino) end of the helix macrodipole (7,8).

The thermodynamics of protein folding and binding of small molecules by proteins are not thoroughly understood.

The physical forces that account for spontaneous folding of proteins are the same forces that stabilize enzyme-substrate complexes. Although the types of physical interactions--hydrogen bonds, salt bridges, hydrophobic interactions, and disulfide bonds--that have important thermodynamic consequences in protein folding and binding of small molecules have been identified and studied, the exact contributions that each makes to the overall energies of these processes are not well understood. It is not obvious why the thermodynamics of these changes need be so intractable, since the reason nature chose complex macromolecules where only a small

fraction of the structure participates directly in catalytic processes is not clear. The "spaghetti" that surrounds enzyme active sites is not just scaffolding that holds the reactive amino acids in place; it plays indirect but important catalytic roles that have not yet been fully characterized.

The free energies of enzyme/substrate binding and of protein folding are generally not large. Typical globular proteins are stable by only 5 to 15 kcals $mole^{-1}$, and many enzymes have substrate binding energies around 7 kcals $mole^{-1}$ (9). These relatively small energies derive from differences between large unfavorable and large favorable energy terms that are each made up of many contributing interactions. To predict the outcome of folding and binding events, energies of the individual interactions must be accurately determined, since small errors in these will result in gross errors in estimates of the free energy changes for overall processes. It is therefore essential to have a detailed understanding of individual interactions that influence the thermodynamics of protein folding and small molecule binding. Each species is, of course, fully hydrated, and this is an additional complicating factor in studies of protein folding and small molecule binding processes.

The functions of amino acids in proteins cannot be predicted from structural data alone.

The serine proteases were once thought to have active sites containing amino acids with binding functionality distinct and autonomous from catalytic functionality. Thus Aspartate 189 in trypsin, a serine protease with a negatively charged binding pocket

specific for arginyl or lysyl side chains, was thought to play the exclusive role of binding the cationic side chain of the amino acid residue at which cleavage takes place (10). Graf and co-workers tested this idea by mutating aspartate 189 to lysine in an attempt to create a protease with specificity for cleaving at aspartate and glutamate residues (11). Trypsin is a well-characterized enzyme, and the experiment was designed and performed with the benefit of both a high resolution x-ray structure and a wealth of biochemical information. In spite of this, it did not have the expected outcome. The D189K mutant trypsin had a severely reduced ability to cleave *any* peptide bonds, and similar to chymotrypsin, cleaved specifically at neutral amino acids. Since the mutant had significantly reduced activity and did not have the expected specificity, the previously held model of a binding pocket independent of an arrangement of catalytic residues is clearly an oversimplification. The results of this experiment demonstrate that the functional roles of amino acids in the active sites of enzymes can be interdependent and are not always the obvious or expected ones.

Matsumera *et al.* made mutations in T4 lysozyme that they predicted would increase the stability of the protein structure towards thermal and other denaturing influences (12). The mutations, carefully selected on the basis of high resolution x-ray structures and thorough computer analysis, were the introduction of cysteine residues designed to form intramolecular disulfide bridges. The researchers expected that each disulfide bond would contribute to the stability of the protein structure and increase resistance to denaturation; however, the experiment produced a quite remarkable

and somewhat unexpected result. Though some disulfide bonds had the predicted effect, others *decreased* the stability of T4 lysozyme. One would expect that introducing covalent cross links in the form of disulfide bonds would have the effect of increasing the structural stability of the protein. Apparently the energetic gain upon formation of some disulfide bonds did not exceed the energetic cost, yet the underlying reasons for this are not understood.

These examples of mutations with unexpected consequences have been used to illustrate that the folding and functional properties of proteins are not, currently at least, very well understood. Precisely how amino acid sequences dictate three-dimensional structures of proteins is a mystery. Furthermore, knowing the three-dimensional structure of an enzyme neither guarantees that the location of the active site can be determined, nor guarantees that the amino acid side chains that participate directly in catalysis can be identified.

Site-directed mutagenesis is a useful technique for studying the structures and functions of proteins.

It has been argued that protein mutagenesis experts do little more than increase the number of systems available to enzymologists for study, and that there are already too many proteins to investigate thoroughly, using our limited repertoire of techniques, most of which are complicated and difficult to apply. Of the estimated one million naturally occurring enzymes, only fifteen hundred are known and many fewer are structurally or functionally well characterized (1,2). To date there are over 550 structure files entered into the Brookhaven Protein Data Bank; however, in a substantial number of

cases several files have been entered that describe the structure of a single molecule (for example one that has been crystalized under different conditions) (13). Are the mutagenesis laboratories around the world simply increasing the already overwhelming number of enzymes, most of which have poorly understood structures and mechanisms? Or are they carefully selecting a few atoms out of thousands, or even tens of thousands, and gently replacing them in what amount to noninvasive procedures that create new molecules with properties leading to a deeper understanding of protein chemistry?

With the advent of recombinant DNA technology, it has become possible to design new polypeptide sequences and to produce them in quantities sufficient for detailed physical studies (14-16). Methods for making amino acid substitutions in proteins are numerous and can be conveniently divided into categories of oligonucleotide-directed and cassette mutagenesis. These mutagenic methods, when combined with the appropriate physical techniques for determining properties of protein variants, have led to otherwise inaccessible ideas about how enzymes function. Cassette methods are, in many cases, more flexible than oligonucleotide-directed, since they are well suited to experiments that entail simultaneous substitution of more than one amino acid at one or more positions in a protein. Site-saturation cassette mutagenesis (17,18), where all possible amino acid substitutions are made at one position, is a particularly useful technique for determining how single amino acids influence the catalytic and folding properties of enzymes. This mutagenic technique is somewhat less subjective than others that

involve choosing which amino acid(s) replace the original; it avoids drawing on preconceived notions about how the physical properties of amino acids dictate the functions they perform in folded proteins.

Using site-directed mutagenesis, subtle or extensive changes in the primary structures of proteins can be made with surgical precision, sometimes giving spectacular results in terms of furthering our understanding of enzyme mechanisms and the fundamental basis of catalysis itself (19-21). Virtually any protein-encoding DNA can be altered or constructed *de novo*, and as a result, genes coding for novel proteins are now commonplace. Single amino acids, or even entire folded domains, have been substituted in experiments designed to test hypotheses concerning catalysis by proteins (22,23), folding properties of proteins (24,25), evolutionary relationships between proteins (26,27), and the design of novel protein catalysts (28,29).

Many mutations in enzymes are silent or mildly deleterious. This is not unexpected, since most amino acid side chains do not participate directly in enzymatic reaction mechanisms, and primary sequence homologies of only 20-30% are enough to give similar tertiary folds in functionally related enzymes (30). On the other hand, mutations that have been confidently predicted to be innocuous have had catastrophic effects on the structural and/or functional integrity of enzymes. The reasons behind these results are often-times unclear. Many mutations that have been selected and designed to alter, in a specific fashion, the activity, specificity, or structure of an enzyme have not "worked" at all. These experiments have had, unfortunately for those attempting to understand enzyme

structures and mechanisms, completely unpredictable consequences. So there remains much to be learned about these interesting protein molecules.

RTEM-1 β-lactamase is an enzyme well suited for mechanistic and structural studies.

The experiments described in this thesis are all related to the enzyme RTEM-1 β-lactamase, which hydrolyzes the β-lactam of penicillin-type antibiotics rendering them ineffective as antibacterial agents (Figure 1). RTEM-1 β-lactamase is encoded by the ampicillin resistance gene (*Amp*^{r}) of the plasmid pBR322. Mature RTEM-1 has 263 amino acids (MW 28,500 Da) and is secreted into the periplasmic space of *E. coli* after a 23 amino acid leader sequence is cleaved from the amino terminus of the protein (31).

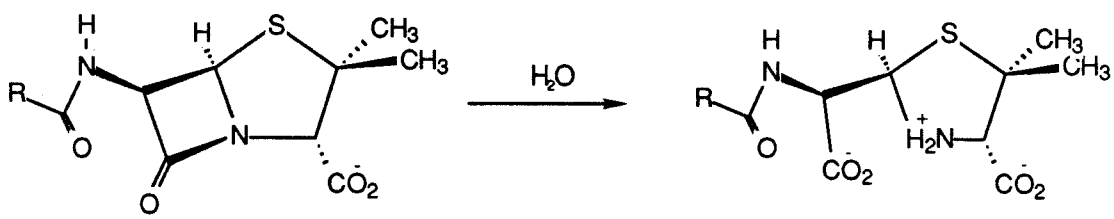

Figure 1. The hydrolysis reaction catalyzed by the β-lactamases. Hydrolysis of a penam antibiotic is shown; the R group is variable. The products of the reaction are ineffective as antibiotics.

RTEM-1 is a member of the class A β-lactamases, which have characteristic serine nucleophiles that participate directly in the β-lactam hydrolysis reaction. The class B β-lactamases are metalloenzymes that are mechanistically unrelated to the class A enzymes and are not discused in this thesis. The class C β-lactamases

are structurally and mechanistically similar to the class A enzymes, but in contrast to the class A enzymes, hydrolyze the cephem antibiotics more readily than the penam antibiotics. (32).

Some practical reasons make RTEM-1 an enzyme well suited to studies in protein processing, expression, folding, mutagenesis, and kinetics and mechanisms of enzymes. Colonies of *E. coli* that express the mature form of the enzyme in the periplasmic space are resistant to the deleterious effects of β-lactam antibiotics, and this provides a convenient method of screening for enzymatic activity based on phenotype. Expression of wild-type and sequence variants of the enzyme at levels acceptable for most studies is generally not a problem, and can be accomplished using the natural RTEM-1 promoter or synthetic promoters such as *tac* (17). Following extrusion from the periplasmic space with hypoosmotic solutions, the enzyme can be purified to homogeneity in relatively high yield, using ion-exchange chromatography (see Chapter 3 for details).

The class A β-lactamases have similar tertiary structures.

The sequence alignment of four well-studied class A β-lactamases is shown in Figure 2 (33). Although the structural information contained in such sequence alignments is limited, in conjunction with results from mutagenesis and biochemical experiments, these comparisons can be used to identify amino acids that might play important structural or functional roles in enzymes.

The tertiary structures of three class A β-lactamases have been reported to moderate or high resolution. In 1987 the structure of β-lactamase from *Staphylococcus aureus* PC1 was reported to 2.5Å

resolution (34), and more recently the structures of β-lactamase from *Bacillus licheniformis* 749/C and from *Streptomyces albus* have been solved to 2.0Å and 3.0Å resolution, respectively (35,36). The tertiary folds of the three enzymes are similar with a root-mean-square difference in α-carbon coordinates of about 1.3 Å (Figure 4). The common motif is a unique α+β structure that has 11 α-helices and 5 strands of antiparallel β-pleated sheet. The tertiary structure of these enzymes has few similarities to the functionally related serine proteases.

The relatively high primary-structure homologies (Figures 2 and 3) among the four β-lactamases are evidence that their three-dimensional structures are similar. Sequence homologies of 20-30% are generally thought to be a sufficient condition to assume similar tertiary structures, as exemplified by the serine proteases, which have homologies on this level and nearly identical tertiary structures (30). The homology between RTEM-1 and the enzymes from *Staphylococcus aureus* PC1 or *Bacillus licheniformis* 749/C is 30% and 33%, respectively.

The class A β-lactamases bind β-lactam antibiotics in a cleft of the globular protein structure.

The location of the active site in the three-dimensional structure of the class A β-lactamases is revealed by the conserved serine residue at position 70. This amino acid is modified in active-site labeling experiments and is known to be a nucleophile which, during the β-lactam hydrolysis reaction, attacks the β-lactam carbonyl carbon of the substrate (37-41). The hydroxyl group of serine 70

lies in an exposed position on the floor of a cleft in the protein structure; the cleft has dimensions appropriate to accommodate binding of molecules the size of β–lactam antibiotics (Figure 5). The fused ring structure of the β–lactam antibiotics gives these compounds a rigid yet bent conformation that is complementary to the shape of the active-site cleft. The cleft is lined with numerous conserved residues, some of which participate directly in the hydrolysis reaction and have putative catalytic roles discussed in Chapter 2.

Since during the β–lactam hydrolysis reaction, the hydroxyl group of serine 70 is covalently modified by the carbonyl carbon of the β–lactam bond, these two groups must be placed in close proximity in models of the Michaelis complex. A second point of contact is suggested by model building (Chapter 2) and mutagenesis experiments (Chapter 3) that support an electrostatic interaction between the carboxylate of the antibiotic and the ammonium group of lysine 234. Accordingly, the serine 70/carbonyl carbon and lysine 234/carboxylate contacts have been invoked as key features in models of the Michaelis complex and covalent intermediates along the reaction pathway (Chapter 2). A model of the Michaelis complex, the construction and details of which are discused in Chapter 2, is depicted in Figure 6.

The mechanism of β–lactam hydrolysis by the class A β–lactamases has been only partially characterized.

The task of determining the detailed mechanism of the class A β–lactamases has not been accomplished. However, mutagenic,

genetic, kinetic, and biochemical experiments have identified some of the amino acids that participate in catalysis and the reactions that constitute some of the steps in the mechanism. Detailed mechanistic interpretation of experimental results has been facilitated by knowing the tertiary structure of the class A β–lactamases.

The accepted model kinetic scheme for the class A β–lactamases is shown in Figure 7 (37-40). Subsequent to initial binding of the substrate, this model consists of two steps: acylation of the enzyme at the conserved serine 70, and deacylation of the serine 70 residue. The products of the deacylation step are written as the free species since product dissociation is not rate-limiting for the class A β–lactamases (40).

In multiple turnover experiments, the steady-state rate constants for hydrolysis of β–lactam antibiotics have been measured directly by two spectroscopic methods. The original method, reported by Waley (41), is based on absorbance decreases at around 230 nm upon hydrolysis of the β–lactam chromophore. A new method, developed in the Richards laboratory and described in Chapter 4, relies on changes in the chiroptical properties of the antibiotic fused ring system upon hydrolysis of the β–lactam. While neither method is appropriate for all rate measurements, combined use of the two allows measurements for almost all mutant RTEM-1 β–lactamases under most reaction conditions. The steady-state rate constants determined by these methods, which have been reported in the literature or measured by members of the Richards group (but are unpublished), are collected in Table 1.

Transient-state kinetic experiments designed to measure the elemental rate constants of the β–lactamase reaction have provided useful mechanistic information. Anderson and co-workers have developed a stopped-flow method based on hydrolysis of a fluorogenic substrate (37,38), and Waley's group have developed a versatile chemical quenched-flow method that can be used to measure hydrolysis rates of a variety of antibiotic substrates (39,40). The published kinetic data measured by the latter method are collected in Table 2.

An important aspect of β–lactamase kinetics is that for a given class A enzyme (data for which are entered into Table 1), the first-order rate constants k_{-1}, k_2, and k_3 are approximately equal, although deacylation (k_3) in each case is partially rate-limiting. Christensen *et al.* have pointed out that this condition is an indication that the class A β–lactamases have evolved to achieve optimal catalytic efficiency (40). The data in Table 2 also show that K_S, the equilibrium-dissociation constants for enzyme and substrate, are *not equal to* the K_M values but are about twice as large. The expression for K_M (Figure 7) reduces to K_S under two conditions: if $k_2 \ll k_{-1}$ and $k_2 \ll k_3$, or if $k_3 \sim k_{-1}$.

Mutagenesis studies have revealed some details of the class A β–lactamase mechanism.

One of the earliest β–lactamase mutagenesis studies was designed to verify the role of the conserved serine 70 as a nucleophile that was known to be covalently modified during the hydrolysis of labelled substrates (42,43). Fisher and co-workers had shown that

after quenching the hydrolysis of ^{14}C-cefoxitin by denaturation, gel filtration analysis indicated that during the reaction the enzyme was esterified, probably at the serine 70 hydroxyl group (44). Mutagenic studies revealed that substitution of serine 70 with amino acids other than cysteine results in complete inactivation of the enzyme (45). The absolute requirement for a nucleophile at position 70 is consistent with the now well-established role of serine 70 as an attacking nucleophile that has reactivity analogous to that observed for the active-site serine in the serine proteases (46). Combined with results from the aforementioned labeling experiments, the mutagenic studies have not only unequivocally identified serine 70 as the active-site nucleophile, but have also revealed that the nucleophile must be a primary one (the threonine mutant is not active), and that a sulfur nucleophile is surprisingly effective at this position (the S70C mutant has a turnover number about 2% of that of the wild-type enzyme (45)).

A particularly interesting site-saturation experiment revealed that the conserved threonine 71 in RTEM-1 does not participate directly in the reaction mechanism; however, it is responsible for stabilizing the folded structure of the active protein. Schultz and Richards substituted threonine 71 with all possible amino acids, and found that fourteen of the nineteen mutants have appreciable activity towards hydrolysis of ampicillin; however, all nineteen mutants have destabilized structures as judged by Western blot analyses (17). The location of the threonine 71 side chain as seen in the common three-dimensional fold of the class A β-lactamases explains only some of these results. In the folded protein, threonine

71 occupies a position near the amino end of an α-helix, with the side chain directed away from the floor of the active-site cleft projecting into the interior of the protein, where it makes intimate contact with other buried residues and stabilizes the folded structure. The surprising result is that proline at position 71 has a relatively smaller destabilizing effect, as does histidine at position 71. It is not obvious why at position 71 these residues disrupt the structure to a lesser extent than do other amino acids.

In addition to the mutagenesis experiments performed at serine 70 and threonine 71, one other mutagenesis experiment has clearly identified a specific function for an amino acid in the active site of RTEM-1 β–lactamase. Chapter 3 describes a site-saturation experiment performed on lysine 234 of RTEM-1 β–lactamase and kinetic characterization of selected mutants. In conjunction with the computer modeling studies presented in Chapter 2, these experiments have established the role of lysine 234 as a cationic anchor that interacts with the anionic carboxylate, which is a conserved feature of all good β–lactamase substrates. Removing the ammonium group at position 234 by substituting lysine 234 with neutral or negatively charged amino acids severely compromises the enzyme's ability to bind substrate; however, the substitutions do not, at least in some cases, significantly change the pseudo-first-order rate at which the enzyme catalyzes β–lactam hydrolysis.

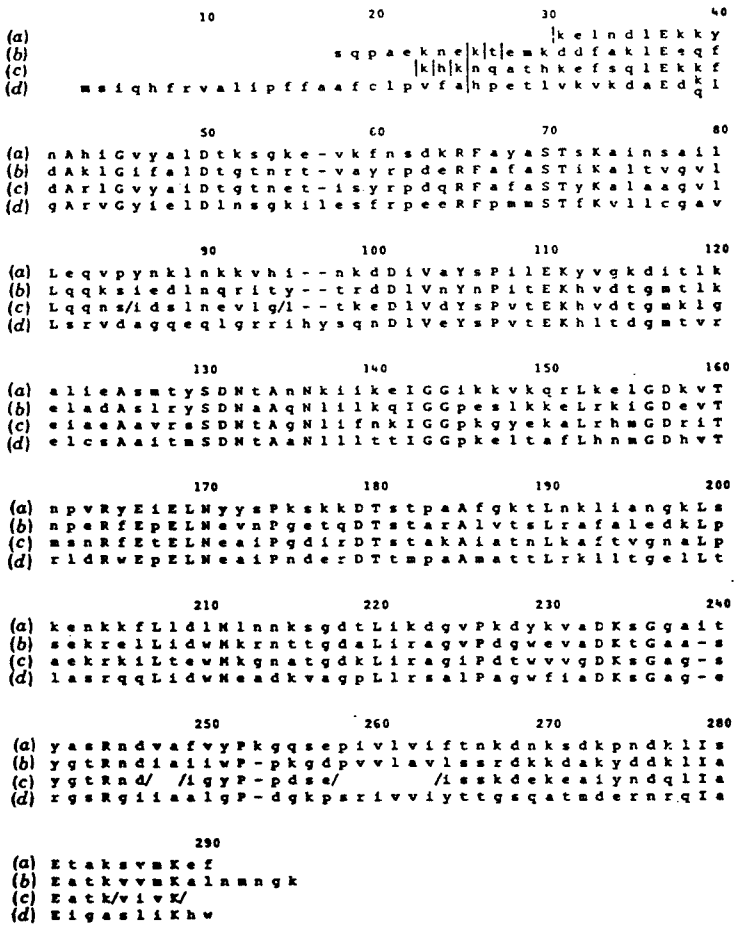

Figure 2. Amino acid sequence alignment of four class A β–lactamases. The sequences are: (*a*) *Staphylococcus aureus* PC1; (*b*) *Bacillus licheniformis* 749/C; (*c*) *Bacillus cereus* 569/H lactamase 1; (*d*) *Escherichia coli* pBR322 RTEM-1. Numbering starts from the N-terminus of the longest form of the *B. licheniformis* enzyme that has been isolated, and takes account of the gaps postulated in the currently known sequences to obtain optimal matching. The vertical bars show the N-termini of naturally released enzymatically active molecules. Residues that are identical in all four molecules are shown in capitals, other residues in lower case letters. The one-letter codes are used for amino acids. The figure was taken from Ambler,R. P. (1980)*Phil. Trans. R. Soc. Lond.* B, **289**, 321-331.

	a)	b)	c)	d)
a) *Staphylococcus aureus* PC1	100	41	38	30
b) *Bacillus licheniformis* 749/C		100	56	33
c) *Bacillis cereus* 569/HI			100	34
d) *Escherichia coli* RTEM-1				100

Figure 3. Homology matrix for four class A β–lactamases. The numbers are percentages of conserved residues.

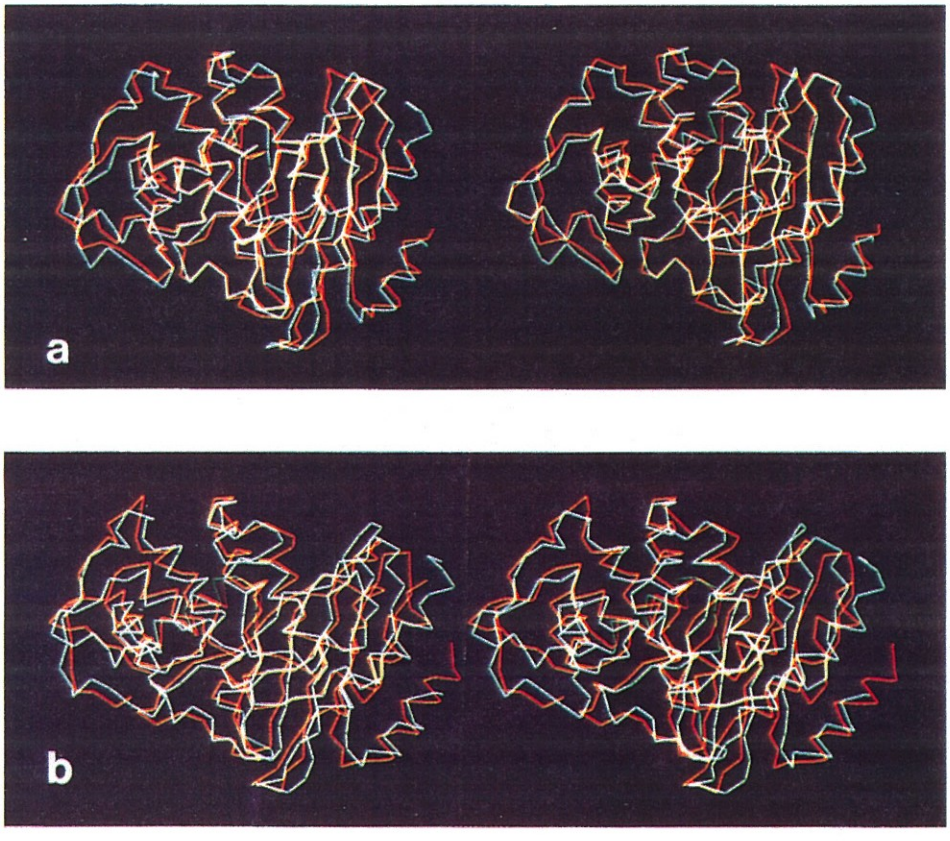

Figure 4. α−carbon backbone comparison of three class A β−lactamases. a) *B. licheniformis* and *S. aureus*, and b) *B. licheniformis* and *S. albus* G enzyme (36).

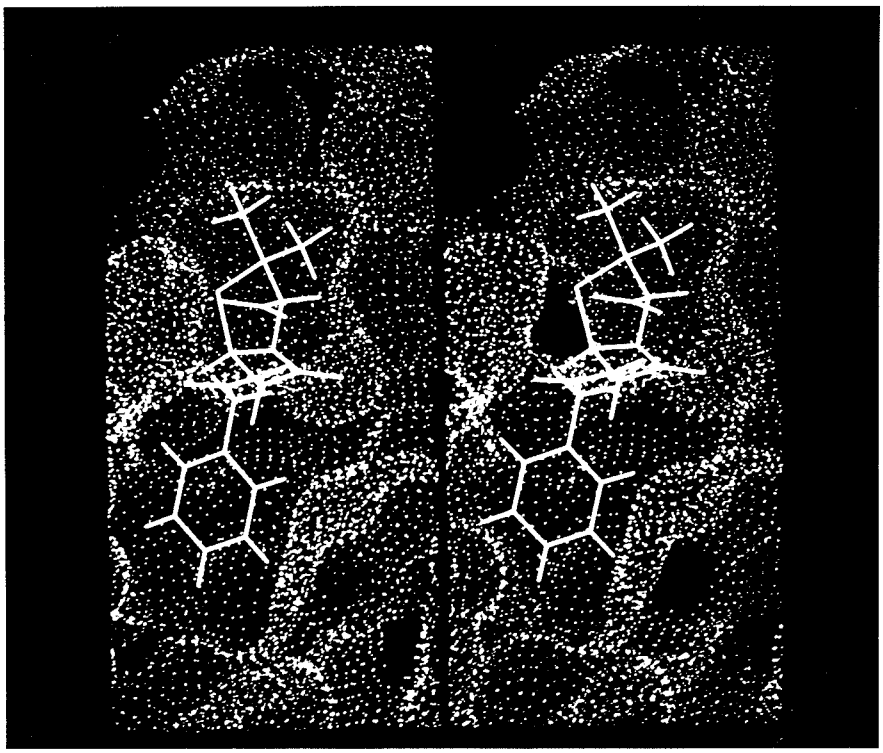

Figure 5. The Class A β–lactamase active site. The position of the bound substrate was determined by computer modeling.

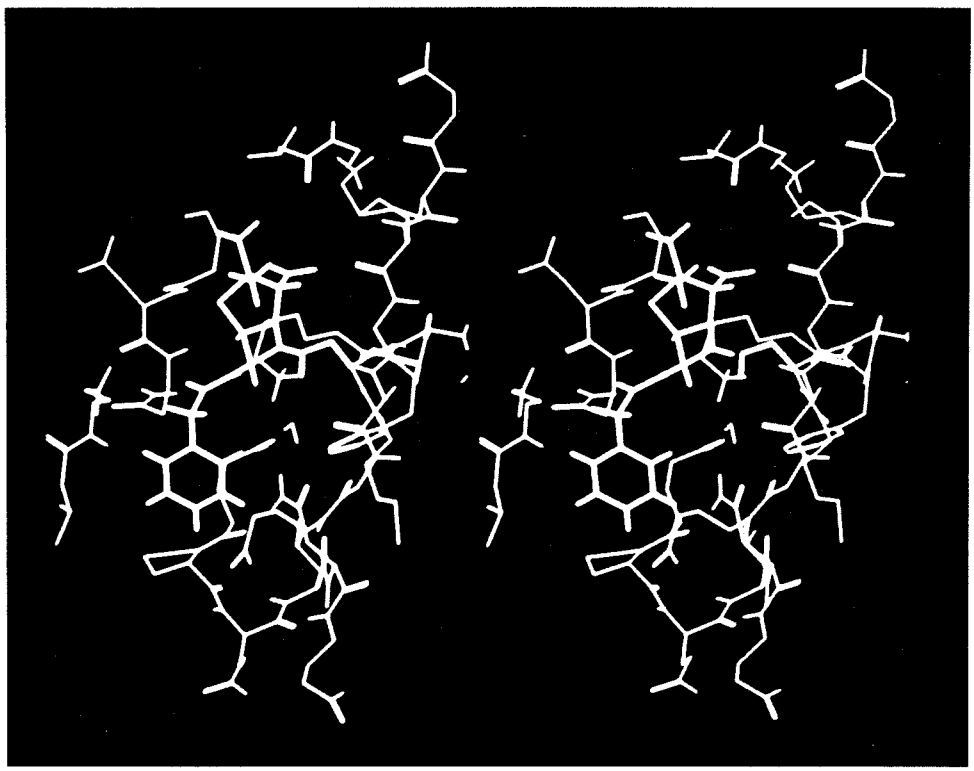

Figure 6. A model of the RTEM-1 β−lactamase Michaelis complex with benzylpenicillin. The fused ring system of the bound antibiotic is visible in the foreground.

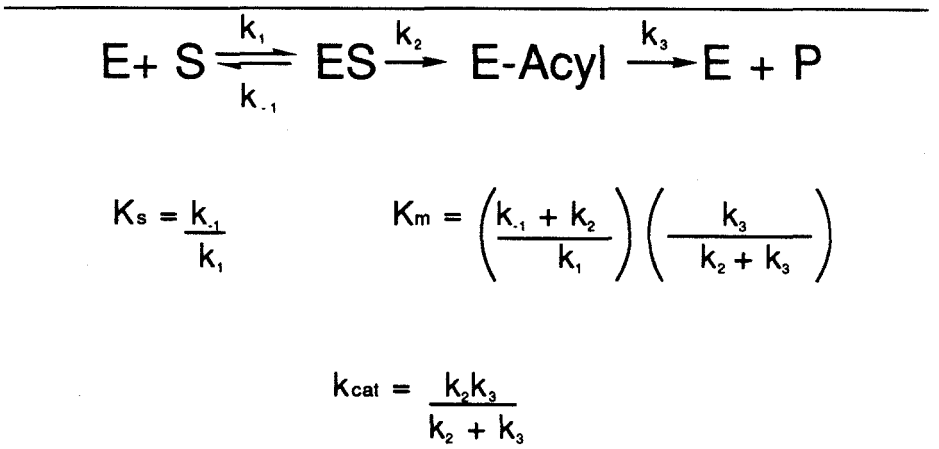

Figure 7. The acyl-enzyme mechanism for the class A β–lactamases. E is the enzyme, S is the substrate, ES is the Michaelis complex, E-Acyl is the acyl-enzyme, and P is the product. The steady-state rate constants are shown in terms of the elemental rate constants. Ks is the equilibrium dissociation constant for E and S, KM is the Michaelis constant and kcat is the pseudo-first-order rate constant (turnover number).

Table 1. Steady-state kinetic parameters for wild-type and mutant RTEM-1 β–lactamases. The units of kcat, KM, and kcat/KM are s^{-1}, μM, and $M^{-1}s^{-1}$, respectively. Substrate abbreviations are BP, benzylpenicillin; CO, cephalothin; AMP, ampicillin; CC, cephalosporin C. The structures of these compounds are shown in Figure 7. The enzyme AEC is the K73C mutant derivatized with ethylene imine as in Reference 1. The asterisk (*) indicates that these parameters were estimated from progress curve fitting that gives rough estimates only (see Chapter 4 for discussion). References: 1, Carroll, S., Long, D., and Richards, J., *Biochemistry*, submitted; 2, Healey, W., Labgold, M., and Richards, J., (1989) *Proteins: Structure, Function and Genetics*, **6**,275.; 3, Schultz, S. and Richards, J.(1986) *Proc. Natl. Acad. Sci. USA*, **83**, 1588.; 4, Richmond, T., unpublished results; 5, Emerling, M. Ph. D. Thesis, 1991, Calif. Inst. Tech.; 6, Chapter 3 of this thesis; 7, Christensen, H., Martin, M., and Waley, S.(1990) *Biochem. J.*, **266**, 853.; 8, Sigal, I., DeGrado, W., Thomas, B., and Petteway, S. (1984) *J. Biol. Chem.*, **259**, 5327.; 9, Schultz, S., Dalbadie-McFarland, G., Neitzel, J., and Richards, J. (1987) *Proteins: Structure, Function and Genetics*, **2**,290.

Enzyme	Substrate	kcat	KM	kcat/KM	ref.
WT*	CO	120	190	$6X10^{5}$	1
WT	BP	980	42	$2.36X10^{7}$	7
WT	AMP	1482	10.5	$1.42X10^{8}$	6
WT*	CC	687	57	$8.2X10^{4}$	2
K73R	BP	0.3	43	$6.9X10^{3}$	1
K73C	BP	0.25	21	$1.2X10^{4}$	1
K73R	CO	$7X10^{-3}$	136	51	1
AEC	CO	38	660	$5X10^{4}$	1
A237N*	BP	840	144	$5.8X10^{6}$	2
A237T*	BP	315	54	$5.8X10^{6}$	2
A237N*	AMP	2670	633	$4.3X10^{6}$	2
A237T*	AMP	225	45	$5.1X10^{6}$	2
A237N*	CO	230	101	$2.3X10^{6}$	2
A237T*	CO	50	66	$7.5X10^{5}$	2
A237N*	CC	299	956	$3.1X10^{5}$	2
A237T*	CC	29	199	$1.5X10^{5}$	2
T71S	BP	300	21	$1.6X10^{7}$	3
T71I	BP	1530	350	$4.4X10^{7}$	3
E166D*	BP	25	22	$1.1X10^{6}$	4
E166H*	BP	13	22	$5.9X10^{5}$	4
S130T	BP	2.4	22	$1.12X10^{5}$	5
S130G	BP	247	96	$2.6X10^{6}$	5
S130N	BP	7.9	143	$5.52X10^{4}$	5
S130Q	BP	0.06	47	$1.33X10^{3}$	5
K234E	AMP	1553	14000	$1.11X10^{5}$	6
K234V	AMP	62	17600	$3.49X10^{3}$	6
K234R	AMP	951	133	$7.12X10^{6}$	6
K234Q	AMP	138	22000	$6.29X10^{3}$	6
S70C	AMP	50	120	$4.17X10^{5}$	8
S70C	BP	20	60	$3.33X10^{5}$	8
C77S	BP	1950	24	$8.12X10^{7}$	9

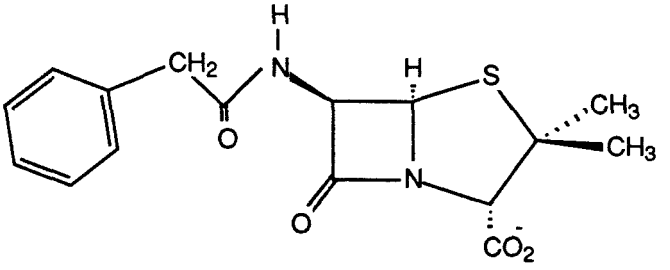

Benzylpenicillin (BP)

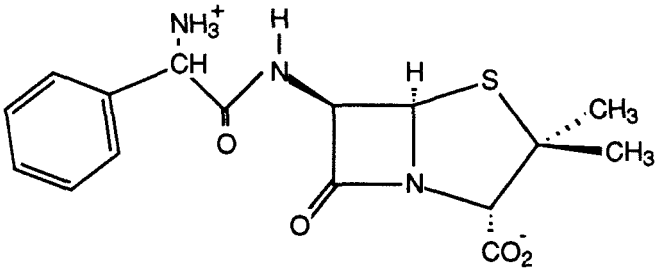

Ampicillin (AMP)

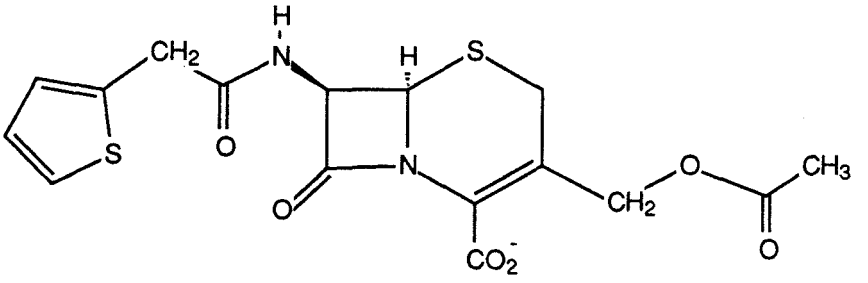

Cephalothin (CO)

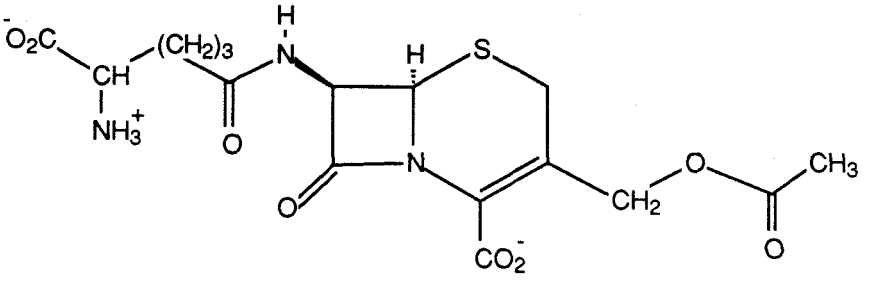

Cephalosporin C (CC)

Figure 8. Structures of some common β-lactam antibiotics (kinetic data are contained in Tables 1 and 2).

Table 2. Rate constants for the hydrolysis of benzylpenicillin measured by Christensen *et al.* (40). The steady-state parameters kcat and KM were measured from progress curves at pH 7.0 and 20°C. k_2 and k_3 were measured with the acid quenched-flow method, and k_1 and k_{-1} were measured in the presence of sucrose or glycerol. The β–lactamase from *B. cereus* is shown as β–lactamase 1, the enzyme from *S. aureus* is shown as PC1, and enzyme from *E. coli* is shown as RTEM-1.

Rate Constant	Units	β–lactamase 1	PC1	RTEM-1
k_1	$\mu M^{-1}s^{-1}$	41(3)	22(2)	123(10)
k_{-1}	s^{-1}	2320(700)	196(30)	11800(1500)
k_2	s^{-1}	4090(210)	173(10)	2800(300)
k_3	s^{-1}	3610(200)	96(10)	1500(200)
kcat	s^{-1}	1920(60)	62(3)	980(100)
kcat/KM	$\mu M^{-1}s^{-1}$	26.2(4)	10.3(1)	23.6(5)
KM	μM	73(5)	6.0(1)	42(5)
Ks	μM	57(14)	8.9(2)	96(9)

References

1. Knowles, J. (1987) *Science*, **236**, 1252.
2. Fersht, A. (1985) *Enzyme Structure and Mechanism, second Ed.*,W. H Freeman and Co., New York, 17.
3. *Ibid*, 174.
4. Schmidt, D. E., Jr. and Westheimer, F. H. (1971) *Biochemistry*, **10**, 1249.
5. Johnson, F., Lewis, S., and Shafer, J. (1981) *Biochemistry*, **20**, 44.
6. Hartman, F., Stringer, C., Milanez, S., and Lee, E. (1986) *Phil. Trans. R. Soc. Lond. B*, **313**, 379.
7. Hol, W. (1985) in *Prog. Biophys. Mol. Biol.*, **45**, 149.
8. Shoemaker, K., Kim, P., York, E., Stewart, J., and Baldwin, R. (1987) *Nature (London)*, **326**, 563.
9. Pace, N. (1975) *CRC Crit. Rev. of Biochem.*, **1**, 1.
10. Rhulmann, A., Kukla, D., Schwager, P., Bartels, K., and Huber, R. (1973) *J. Mol. Biol.*, **77**, 417.
11. Graf, L., Craik, C., Patthy, A., Roczniak, S., Fletterick, R., and Rutter, W. (1987) *Biochemistry*, **26**, 2616.
12. Matsumura, M., Becktel, W., Levitt, M., and Matthews, B. (1989) *Proc. Natl. Acad. Sci. U.S.A.*, **86**, 6562.
13. Bernstein, F. (1977) *J. Mol. Biol.*, **112**, 535.
14. Shortle, D. and Botstein, D. (1985) *Science*, **229**, 1193.
15. Richards, J. (1986) *Nature (London)*, **323**, 11.
16. Zoller, J. and Smith, M. (1983) *Meth. Enzymol.*, **100**, 468.

17. Schultz, S. C. and Richards, J. H. (1986) *Proc. Natl. Acad. Sci. U.S.A.*, **83**, 1588.

18. Lim, W. and Sauer, R. (1989) *Nature (London)*, **339**, 31.

19. Dalbadie-McFarland, G., Cohen, L., Riggs, A., Moln, C., Itakura, K., and Richards, J. (1982) *Proc. Natl. Acad. Sci. U.S.A.*, **79**, 6409.

20. Benkovic, S., Fierke, C., and Naylor, A. (1988) *Science*, **239**, 1105.

21. Fersht, A., Shi, J.-P., Knill-Jones, J., Lowe, D., Wilkinson, A., Blow, D., Brick, P., Carter, P., Waye, M., and Winter, G. (1985) *Nature (London)*, **314**, 235.

22. Gutteridge, S., Sigal, I., Thomas, B., Arentzen, R., Cordova, A., and Lorimer, G. (1984) *The EMBO J.*, **3**, 2737.

23. Malcom, B., Rosenberg, S., Corey, M., Allen, J., Baetselier, A., and Kirsch, J. (1989) *Proc. Natl. Acad. Sci. U.S.A.*, **86**, 133.

24. Shortle, D. and Lin, D. (1985) *Genetics*, **110**, 559.

25. Wells, J. and Powers, D. (1986) *J. Biol. Chem.*, **261**, 6564.

26. Chang, Y.-H., Labgold, M., and Richards, J. (1990) *Proc. Natl. Acad. Sci. U.S.A.*, **87**, 2823.

27. Mas, M., Chen, C., Hitzman, R., and Riggs, A. (1986) *Science*, **233**, 788.

28. Regan, L. and DeGrado, W. (1988) *Science*, **241**, 976.

29. Hecht, M., Richardson, J., Richardson, D., and Ogden, R. (1990) *Science*, **249**, 884.

30. Hartly, B. S. (1974) *Symp. Soc. Gen. Microbiol.*, **24**, 152.

31. Sutcliffe, J. (1978) *Proc. Natl. Acad. Sci. U.S.A.*, **75**, 3737.

32. Sykes, R. (1982) *J. Infect. Dis.*, **145**, 762.

33. Ambler, R. (1980) *Phil. Trans. R. Soc. Lond. B*, **289**, 321.

34. Hertzberg, O. and Moult, J.(1987) *Science*, **236**, 694.

35. Dideberg, O, Charlier, P., Wery, J.-P., Dehottay, P., Dursart, J., Erpicum, T., and Ghuysen, J.-M. (1987) *Biochem. J.*, **245**, 911.

36. Meows, P. C., Knox, J. R., Dideberg, O., Charlier, P., and Frere, J.-M. (1990) *Proteins: Structure, Function, and Genetics*, **7**, 156.

37. Anderson, E. G. and Pratt, R. F. (1981) *J. Biol. Chem.*, **256**, 11401.

38. Anderson, E. G. and Pratt, R. F. (1983) *J. Biol. Chem.*, **258**, 13120.

39. Martin, M. T. and Waley, S. (1988) *Biochem. J.*, **254**, 923.

40. Christensen, H., Martin, M., and Waley, S. (1990) *Biochem. J.*, **266**, 853.

41. Waley, S. (1974) *Biochem J.*, **139**, 789.

42. Pratt, R. and Loosemore, M. (1978) *Proc. Natl. Acad. Sci. U.S.A.*, **75**, 4154.

43. Knott-Hunziker, V., Waley, S., Orlek, B., and Sammes, P. (1979) *FEBS Letts.*, **99**, 59.

44. Fisher, J., Belasco, J., Khosla, S., and Knowles, J. (1980) *Biochemistry*, **19**, 2895.

45. Sigal, I., Harwood, B., and Arentzen, R. (1982) *Proc. Natl. Acad. Sci. U.S.A.*, **79**, 7157.

46. Kraut, J. (1977) *Annu. Rev. Biochem.*, **46**, 331.

CHAPTER 2

Structural and Mechanistic Ideas from Molecular Modeling of the RTEM-1 β–lactamase Active Site

Introduction

Understanding enzymatic reaction mechanisms relies heavily on knowing the three-dimensional structures of enzymes. Mechanistic studies often make significant progress when tertiary structures are solved using crystallography or multidimensional NMR, the two techniques currently available for determining protein structures. These methods are indispensable tools to the enzymologist, but require expertise that is often found only in laboratories that specialize in structure determination.

The results of site-directed mutagenesis experiments are particularly difficult to interpret without knowing the three-dimensional structure of the protein. Choosing the amino acids which, if mutated, would provide clues to the enzyme's mechanism is a more rational venture when a high-resolution structure is available. The folding and catalytic properties of mutant enzymes are sometimes radically different from those of wild-type enzymes, and the precise reason for the observed effects depends on the position of the mutated side chain in the folded enzyme and on the question of whether it participates directly in the reaction mechanism or not. The predicament caused by a lack of a tertiary structural information would be less severe if all amino acids conserved within each class of enzymes were direct participants in reaction mechanisms. This, however, is virtually never true.

Even without knowing the tertiary structure, significant progress can be made towards understanding the mechanism of an enzyme. It is worthwhile to carry out mutagenesis and kinetic experiments, assuming that when a structure does become available, more

detailed interpretation of results will become possible. In these situations crystallographic or NMR data, even if limited, can be combined with computer-assisted molecular modeling methods to construct working three-dimensional models. While being used to develop or test hypotheses that would otherwise go unformulated, models can be modified as experimental data, describing structures and mechanisms in increasing detail, become available.

This chapter describes molecular modeling experiments that were conducted in the absence of an experimentally determined high-resolution structure of the class A β–lactamases. The modeling studies were carried out for two primary reasons. First, no alternative approach to understanding the structures was available, since results from laboratories specializing in structure determination of the class A β–lactamases were not forthcoming, and second, modeling provided the opportunity to assess the utility of some general and easily executable methods for introducing detail into low- or moderate-resolution protein structures.

The structure solved by Hertzberg and Moult of the class A β–lactamase from *Staphylococcus aureus* PC1 ("PC1") to 2.5 Å resolution is the only experimental data that was used to construct the model of the RTEM-1 β–lactamase ("RTEM-1") active-site described (1). The crystallographers entered the α–carbon coordinates of PC1 into the Brookhaven Protein Data Bank (2); however, they omitted the coordinates of the side-chain atoms. In principle the 2.5 Å x-ray structure defines atomic coordinates with an uncertainty of about 0.4 Å (3).

In the modeling studies described here, the α–carbon coordinates of PC1 were used as a framework upon which the side chains of RTEM-1, for which no high-resolution structure is available, were "hung." The 30% primary structure homology between the two enzymes provides a sound basis for assuming that the α–carbon coordinates of RTEM-1 are similar to those determined experimentally for PC1. Considering dynamic properties of the proteins in solution, the two enzymes' active sites probably have few differences that would be easily distinguishable even by high-resolution crystallography.

We have used simple computer-assisted molecular modeling methods as a complement to experimental approaches in efforts to understand the structure and mechanism of the class A β–lactamases. In addition to allowing formulation of mechanistic ideas, computer modeling has been used to explain the results of mutagenesis experiments.

Molecular modeling of the RTEM-1 β–lactamase active site

The position and general shape of the active site in the class A β–lactamases was revealed in the structure of PC1 by the location of the conserved serine 70, which is in an exposed position on the floor of a cleft lined with conserved residues (1). The cleft is fully defined by six fragments of the class A β–lactamase fold that range in length from two to seven amino acids and that come together in three-dimensional space to form a depression in the surface of the protein shown in Figure 1. The six sequences that make up the active site are shown in Figure 2 and are referred to as the

"active-site peptides," and are distinguished from one another by designating their residue numbers according to the Ambler system (4). For example, active-site peptide 233-239 is the β-sheet sequence that makes up the right-hand border of the cleft as shown in Figure 3. The relative positions of the active-site peptides in the folded structure are evident in Figure 3.

The level of structural refinement depicted in Figure 3 is a common situation in protein structural studies as indicated by the number of low- and moderate-resolution x-ray structures that have been entered into the Brookhaven Protein Data bank (2). Cases for which only the structure of a single member of a class of phylogenetically related proteins is known are common, and hence it is of general interest to know if simple computer modeling techniques can be used to add or substitute amino acid side chains onto experimentally determined α-carbon frameworks.

The α-carbon and β-atom positions are fully defined by the ϕ and φ angles that describe an α-carbon peptide trace. This becomes obvious by viewing a diagram of planar peptide bonds (Figure 4) and recognizing that the ϕ and φ angles, which describe the trace of the peptide chain, constrain the positions of all four ligands at the tetrahedral α-carbon and so, in addition to those of the α-carbons, define the positions of β-hydrogens and β-side-chain atoms.

The problem of determining the coordinates of side-chain atoms for a protein fold described by a set of ϕ and φ angles thus reduces to determining the state of freely rotating angles that describe the conformation of each side chain. Each side chain has a specific number of rotational degrees of freedom that are presumably

constrained in the nondenatured protein structure. The number of rotational degrees of freedom characteristic of each amino acid side chain are collected in Table 1. Most side chains have two degrees of rotational freedom, and although glycine, alanine, and proline each have none--the conformations of these amino acids are fully defined by ϕ and φ angles--lysine and arginine each have the relatively large number of four.

To construct a model of the RTEM-1 active site from the α–carbon trace of PC1, six peptides were built with the RTEM-1 active-site peptide sequences, and while allowing the ϕ and φ angles to vary, the α-carbons of these were superimposed on the experimentally determined α-carbons of the PC1 structure. The operation amounted to free translation of the RTEM-1 active-site peptides and free rotation about ϕ and φ angles, and yielded a structure with the RTEM-1 active-site sequence and α–carbon coordinates and β–atom coordinates identical to those determined experimentally for the PC1 enzyme (Figure 5).

Up to this point the modeling operations did not involve energy calculations and were simply the addition of the RTEM-1 side chains onto the the PC1 α–carbon frame work in operations that defined the positions of the α and β atoms and the active-site peptide, main chain atoms. Nine of the twenty-five amino acids that are constituents of the active-site peptides are different in RTEM-1 and PC1 (Figure 6), which is a homology of 64%.

Construction of the RTEM-1 model was completed by performing molecular mechanics calculations in which the minimum energy conformations of the active-site amino acid side chains were

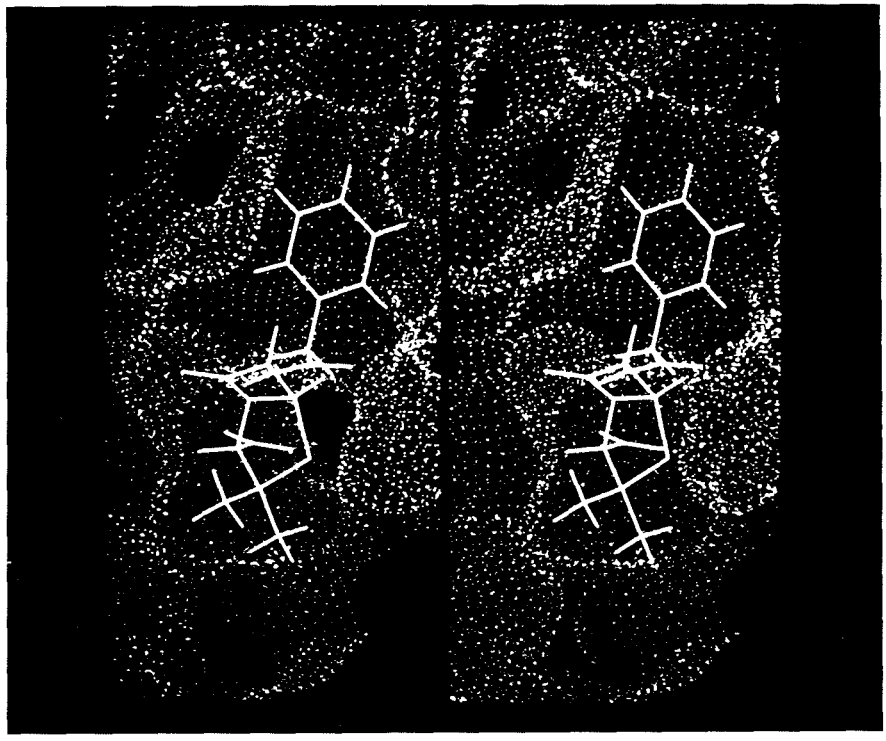

Figure 1. Surface representation of the RTEM-1 model active-site cleft. A model of benzylpenicillin is bound in the cleft.

69-73	Met-Ser-Thr-Phe-Lys
103-104	Val-Glu
130-132	Ser-Asp-Asn
166-171	Glu-Pro-Glu-Leu-Asn-Glu
216-217	Val-Ala
233-238	Asp-Lys-Ser-Gly-Ala-Gly

Figure 2. Primary sequences of the RTEM-1 active-site peptides. Numbering is according to Ambler (4).

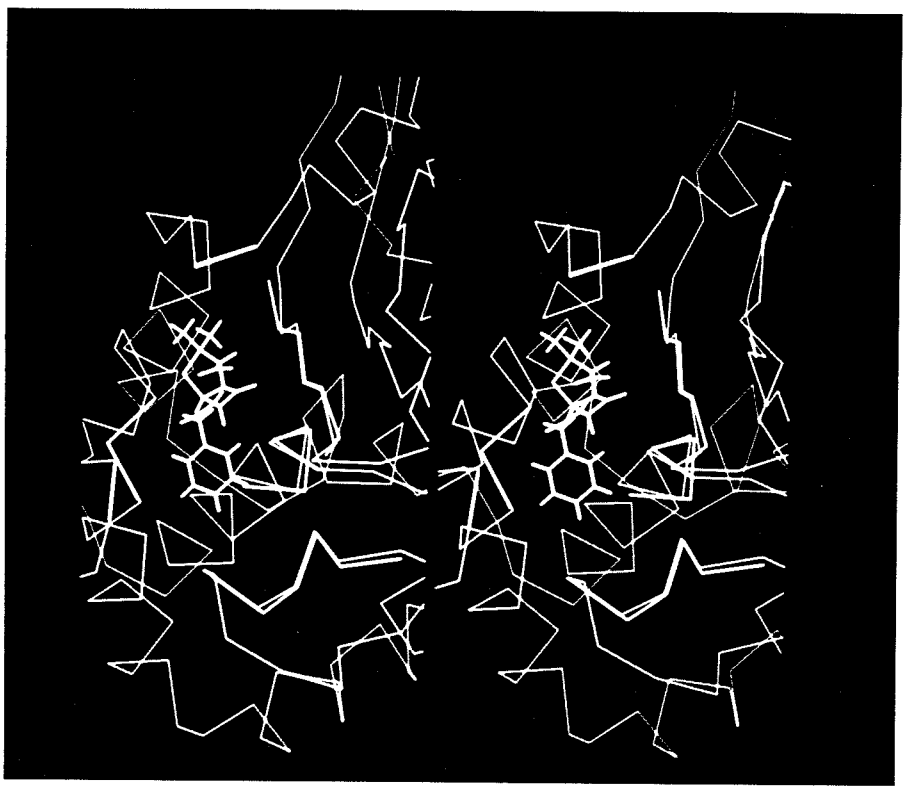

Figure 3. The RTEM-1 active-site peptides overlaid on the α-carbon trace of PC1. The active-site peptides are represented as α-carbon traces and are in boldface. Benzylpenicillin bound in the cleft is visible in the foreground.

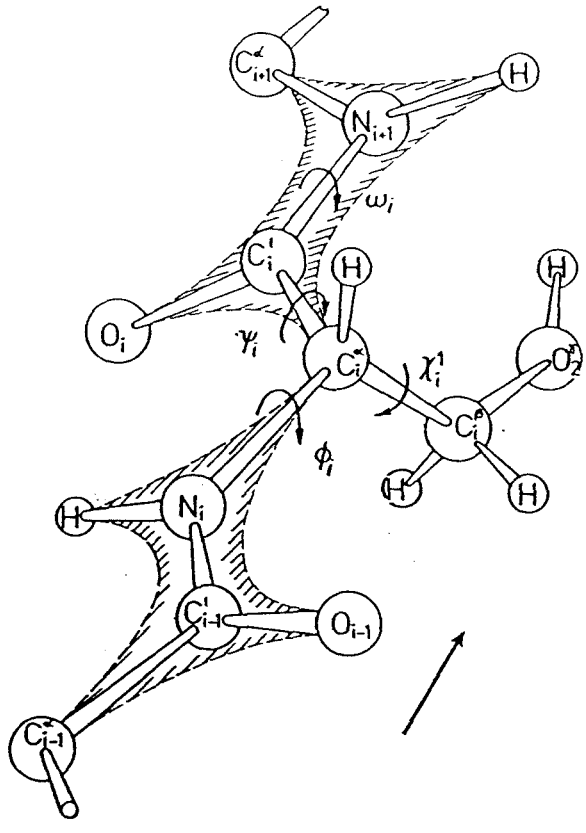

Figure 4. Schematic diagram showing the definition of ϕ and φ angles that define the fold of a peptide chain. Fixing ϕ and φ constrains the positions of β atoms as well as all main chain atoms. The direction of the peptide chain is indicated. A serine residue is inserted to illustrate the side chain rotational angles (χ) which were estimated in molecular modeling experiments From Schulz, G. E. and Schirmer, R. H. (1979) *Principles of Protein Structure*, Springer-Verlag, New York, p. 19.

Table 1. Rotational degrees of freedom for the natural amino acid side chains.

Amino Acid	Number of Rotational Degrees of Freedom
Alanine	0
Cysteine	1
Leucine	2
Methionine	3
Glutamate	3
Glutamine	3
Histidine	2
Lysine	4
Valine	1
Isoleucine	2
Phenylalanine	2
Tyrosine	2
Tryptophan	2
Threonine	1
Glysine	0
Serine	1
Aspartate	2
Asparagine	2
Proline	0
Arginine	4

Figure 5. Schematic diagram of the molecular modeling procedures used to create a model of the RTEM-1 active site. In step (A) amino acids are assembled into the RTEM-1 active-site peptides; in step (B) the α–carbons of the RTEM-1 active-site peptides are superimposed on the experimentally determined α–carbon coordinates of PC1 β–lactamase; in step (C) the minimum energy conformations of the PC1αC/RTEM-1 side chains are estimated using molecular mechanics calculations.

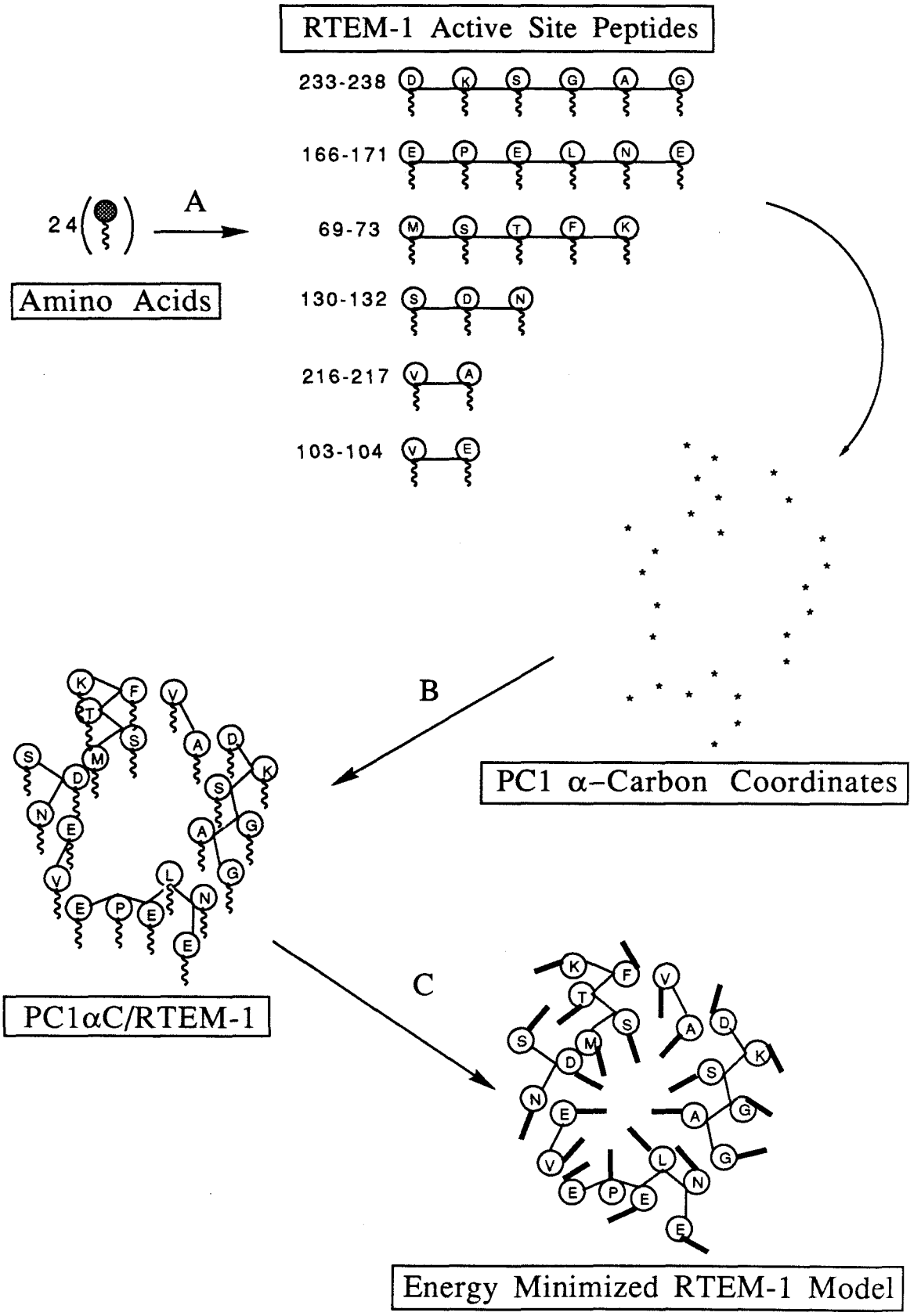
RTEM-1 Active Site Peptides
233-238
166-171
69-73
130-132
216-217
103-104
24
A
Amino Acids
B
PC1 α–Carbon Coordinates
PC1αC/RTEM-1
C
Energy Minimized RTEM-1 Model

RTEM-1	69-73	Met-Ser-Thr-Phe-Lys
PC1	69-73	Ala----------Ser-----
RTEM-1	103-104	Val-Glu
PC1	103-104	-----Ala
RTEM-1	130-132	Ser-Asp-Asn
	130-132	----------
RTEM-1	166-171	Glu-Pro-Glu-Leu-Asn-Glu
PC1	166-171	-----Ile----------Tyr
RTEM-1	216-217	Val-Ala
	216-217	Ser-Gly
RTEM-1	233-238	Asp-Lys-Ser-Gly-Ala-Gly
PC1	233-238	----------Gly-Ala

Figure 6. Sequences of the RTEM-1 and PC1 β-lactamase active-site peptides. Numbering is according to Ambler (4). Homologous residues are shown in the PC1 sequence as dashed lines (----). The peptides are 60% homologous.

determined (Figure 5). The active-site amino acids of RTEM-1 have a total of 40 rotational degrees of freedom, and so these operations required that in principle a 40-dimensional space be searched for the optimum combination of side-chain conformations. This was accomplished in several ways, sometimes allowing all 40 degrees of freedom in the model to vary and in other experiments allowing only a subset of the rotational angles to vary in any given energy calculation.

For the energy calculations the Dreiding force field (5) was intentionally selected over those that are considered to be more sophisticated, such as AMBER (6) or CHARMM (7). In these molecular modeling applications, the degree of sophistication of the force field is not considered important for two principal reasons. First, the detailed energetics of interacting amino acids in proteins are difficult systems to model, because using any of the currently available methods, even single hydrophobic interactions, charge/charge interactions, or hydrogen bonds (all modeled in the absence of solvent), are difficult to analyze. And second, almost at the outset, it was clear that the primary determinant of side chain conformations is simple volume exclusion that results in the most sterically favorable packing arrangement. All of the force fields estimate the steric size and shape of the amino acids relatively well.

In addition to models of the active site, models of Michaelis complexes were built that incorporate the x-ray structure of benzylpenicillin that was retrieved from the Cambridge Crystallographic Data Bank with the assistance of Danilo Casimiro. Reaction intermediates such as acyl-enzymes and tetrahedral

intermediates were constructed using the methods described here and were compared to the x-ray structure of the closely related D-alanyl-D-alanine carboxypeptidase from *Streptomyces* R61 complexed with its inhibitor benzylpenicillin. In the Discussion Section, the active-site model is compared to an x-ray structure of a class A β–lactamase that was published after the molecular modeling was completed.

Materials and Methods

Computer Hardware

All molecular modeling was performed on a Digital Equipment VAXstation 3500 with an Evans and Sutherland model ES390 graphics terminal.

Computer Software

The Biograf molecular modeling program version 2.1 from BioDesign Inc. (Pasadena, CA.) was used to display molecular representations and to perform molecular mechanics calculations.

Construction of the Active-Site Peptides

The RTEM-1 active-site peptides were constructed in the PEPTIDE option of the BUILD operations using Biograf's standard amino acid fragment library. The peptides were stored as separate Biograf files in extended conformation (ϕ and φ angles 180°) after the carboxyl and amino termini atoms (CO_2^- and NH_4^+) of each were deleted in the EDIT option in the BUILD operations.

Superimposing the RTEM-1 active-site peptides on the α–carbon coordinates of PC1

For each of the six RTEM-1 active-site peptides, the α–carbon of the N-terminal amino acid was superimposed on the corresponding α–carbon atom in the PC1 x-ray structure by using the DOCK option in the Biograf ROTATE operations. In separate manipulations performed in the MODELING options using the ROT BOND operation, the ϕ and φ angles of the active-site peptides were adjusted sequentially so as to allow the RTEM-1 α–carbon positions to overlap with those of the PC1 structure. These operations were performed with the peptides displayed as α–carbon traces but by updating files containing the complete coordinates of each active-site peptide. Refinement of the RTEM-1 peptide conformations resulted in no more than 0.2Å difference in α–carbon positions between the model and the x-ray structure. The structure generated by these operations is hereafter referred to as PC1αC/RTEM-1.

Modeling side chain conformations using molecular mechanics calculations

To avoid overloading Biograf prior to implementing molecular mechanics calculations, the conformational angles of side chains in PC1αC/RTEM-1 were manually adjusted in the MODEL operations using the ROT BOND option so that minimal overlap occurred. Minimum energy conformations of side chains were modeled by several molecular mechanics methods, all of which employed the Dreiding force field and the conjugate gradient method of energy minimization. Energy minimizations were performed in the ENERGY operations using the MECHANICS option and the default potential parameters of Biograf. Typically less than 1000 cycles of

minimization were required to attain conditions of convergence as defined by Biograf. The energy calculation setup procedures required designating atoms as fixed or moveable according to the following Biograf definitions: Moveable--those that contribute to the energy expression and can move during the calculations in response to the forces acting on them, and Fixed--those that contribute to the energy expression but cannot move during the calculations. The main chain atoms and β atoms of PC1αC/RTEM-1 were assigned fixed positions, and in separate experiments either all or only a subset of the side chain atoms were designated as moveable. The reliability of the minimization procedures was judged by comparing side chain conformations of structures that were minimized starting from different initial side chain conformations. Similarly, from the minimized PC1αC/RTEM-1 structures, subsets of moveable atoms were chosen in minimization experiments designed to assess reproducibility of the methods. For example, in separate experiments the side chains of each active-site peptide in the minimized PC1αC/RTEM-1 structure were designated as moveable while all others were designated as fixed in minimizations starting from different initial side-chain conformations.

Construction of Michaelis complex models

The x-ray structure of benzylpenicillin was retrieved from the Cambridge Crystallographic Data Bank and used in the construction of models of Michaelis complexes. Using the DOCK option of the Biograf MODEL operations, the antibiotic structure was docked onto the energy-minimized PC1αC/RTEM-1 structure so that the antibiotic carboxylate and the ammonium group of lysine 234 were in close

proximity, as were the hydroxyl group of serine 70 and the carbonyl carbon of the β–lactam (these interactions have been verified empirically; see Chapters 1 and 3). After designating the main chain atoms of the PC1αC/RTEM-1 structure as fixed and the atoms of the antibiotic and side chains as moveable, the complex was energy-minimized using the previously described methods.

Construction of reaction intermediates

Covalent bonds in models of reaction intermediates were formed and broken either by direct editing of Biograf files (making the appropriate changes in connectivities, atom types, and charges), or by making changes in the EDIT option of the FAST BLD operations of Biograf. Molecular mechanics simulations to determine minimum energy structures were executed as described previously. All side-chain atoms and all atoms that derive from the antibiotic structure were designated as moveable and the main chain atoms as fixed in these operations.

Quantitative comparison of the Bacillus licheniformis β–lactamase structure and the computer-generated model of RTEM-1

Within the the active-site peptides, RTEM-1 and β–lactamase from *B. licheniformis* (BL) have 16 conserved amino acids. The root-mean-square difference (RMS) between the positions of the nonhydrogen atoms of the side chains and α–carbons of the conserved residues were computed from the model and the 2 Å resolution x-ray structure of the BL published after the modeling was complete (9). The analysis involved a total of 77 atoms from each structure.

Results

By employing a computer modeling approach, we have constructed a working model of the RTEM-1 active site using as a basis set the α−carbon coordinates determined by x-ray crystallography for the closely related β−lactamase from *Staphylococcus aureus* PC1. The methods provide the opportunity to construct models in the absence of high-resolution structures, and are of general interest because they allow incorporation of structural detail that is sometimes not reported with moderate resolution x-ray data. The techniques are useful both in terms of exploiting to the fullest extent the inherent information contained in α−carbon traces and in constructing models of proteins for which only the structures of phylogenetically related ones have been solved. We should point out that in no case will our methods yield structures with resolution better than that of the x-ray data from which they were derived.

The energy minimization operations used to determine low-energy side-chain conformations for the RTEM-1 model yielded several minimized structures; however, none had atomic coordinates that differed significantly more than the approximate 0.4 Å expected from the limiting resolution of the PC1 x-ray structure upon which the models were based (1,3). One explanation for this is that the active-site side chains of the RTEM-1 model fit together in a manner similar to the pieces of a jigsaw puzzle and so have minimum energy conformations governed mainly by steric factors that are relatively easy to model.

Details of the model RTEM-1 active-site structure are shown in Figures 7 through 17. Notable features include the exposed position of the hydroxyl group of serine 70 on the floor of the active-site cleft (Figure 7), the close proximity of the charged lysine 73 and glutamate 166 (Figure 8), the exposed ammonium group of lysine 234 that is the only charged residue for which no counter ion exists (in the form of an oppositely charged residue, Figure 9), and the relatively open end of the substrate binding cleft which accommodates the variable side group of the antibiotics (Figure 10). Figure 11 shows how in the model structure the amino acid side chains fit together tightly in the floor of the active-site, giving it a well-defined shape These same general features of the RTEM-1 model were indicated as important features of the PC1 β–lactamase structure that was solved by Hertzberg and Moult and the structure of the related D-alanyl-D-alanine carboxypeptidase from *Streptomyces* R61 that was solved by Kelly and co-workers (1,8).

After molecular modeling of the RTEM-1 active site was complete, a high-resolution structure of the class A β–lactamase from *Bacillus licheniformis* (BL) was published (9). This provided the opportunity to estimate the accuracy of the RTEM-1 model and to assess the reliability of the modeling methods. A quantitative comparison between the RTEM-1 model and the high-resolution BL structure revealed that the RMS difference in the positions of the conserved atoms, a total of 77 from 16 different side chains, is 1.6 Å. The side chains of serine 130, glutamate 171, and valine 103 are on the periphery of the RTEM-1 model and as such are either solvent-accessible or else interact with side chains of the protein

which were absent in the modeling. If these are disregarded in the analysis, the RMS difference in side chain coordinates is reduced to 1.3 Å. If the RMS difference is calculated for the six residues that are on the floor of the active-site cleft--serine 70, threonine 71, lysine 73, glutamate 166, asparigine 170, and lysine 234--the RMS difference is 0.9 Å. All of these residues except threonine 71 are believed to be directly involved in the catalytic mechanism

How accurately the model reflects the actual structure of RTEM-1 depends on differences between the PC1 and RTEM-1 structures, uncertainty in the PC1 structure, and additional uncertainty introduced by limitations inherent in the modeling procedures. If the molecular modeling is maximally effective, then the uncertainty in the model coordinates will be no more than the uncertainty in the PC1 x-ray structure from which it was derived. If it is assumed that the actual positions of the conserved atoms of PC1, BL, and RTEM-1 are identical, then by comparing the RTEM-1 model with the independently determined BL structure, the minimum achievable difference in atomic coordinates should be the sum of the uncertainties in the α-carbons of the PC1 structure and the BL structure, which is about $\pm$ 0.7 Å (the uncertainty in the BL coordinates is estimated to be about $\pm$ 0.3 Å from the RMS difference of two independent molecules in the asymmetric unit of one crystallographic unit cell (9), and the uncertainty in the PC1 structure estimated from the 2.5 Å resolution x-ray data is about $\pm$ 0.4 Å (3)).

For six important catalytic residues, the 0.9 Å RMS difference between the model's atomic positions and BL's is only 0.2 Å greater

than the estimated minimum achievable value of 0.7 Å. This small difference is a reflection of the similarities of the PC1 and BL structures and is an indication that the atomic coordinates of the model and the actual RTEM-1 structure are defined with an uncertainty of not less than ± 0.6 Å (i.e., the sum of the uncertainty in the PC1 structure, ± 0.4 Å, and the additional uncertainty introduced by the modeling procedures, ± 0.2 Å).

One important assumption was made in the previous argument that will not hold in all cases: The positions of the conserved atoms in the active sites of the three β–lactamase structures were assumed to be identical. The high level of primary-structure homology between the three enzymes argues that the structural differences between RTEM-1 and PC1 are no more extensive than the limited differences that have been observed between BL and PC1.

The RTEM-1 model was combined with the x-ray structure of benzylpenicillin in a model of the noncovalent Michaelis complex. Using the docking capabilities of the Biograf program prior to energy minimization, the antibiotic was positioned so that serine 70 was close to the carbonyl carbon of the β–lactam, and the ammonium group of lysine 234 was close to the exocyclic carboxylate of the antibiotic. (As indicated previously, these interactions had been established empirically- see Chapter 3 and (10).) Energy minimization of the antibiotic/enzyme complex resulted in the identification of intermolecular hydrogen bonds that have been suggested by Hertzberg and Moult and Kelly *et al.* (1,8). The lengths and angles of some intermolecular hydrogen bonds of the Michaelis model are compared in Table 2 to those modeled or determined

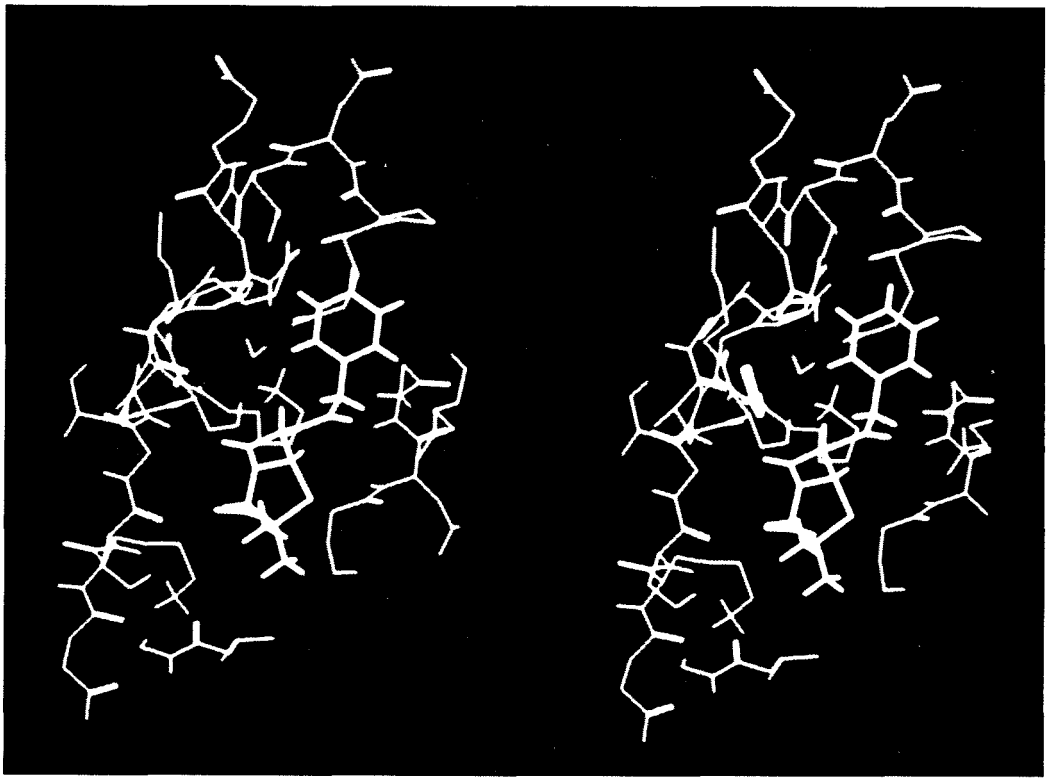

Figure 7. The hydroxyl group of serine 70 on the floor of the RTEM-1 active-site cleft. The side chain of serine 70 (arrow) is near the carbonyl carbon of the bound antibiotic.

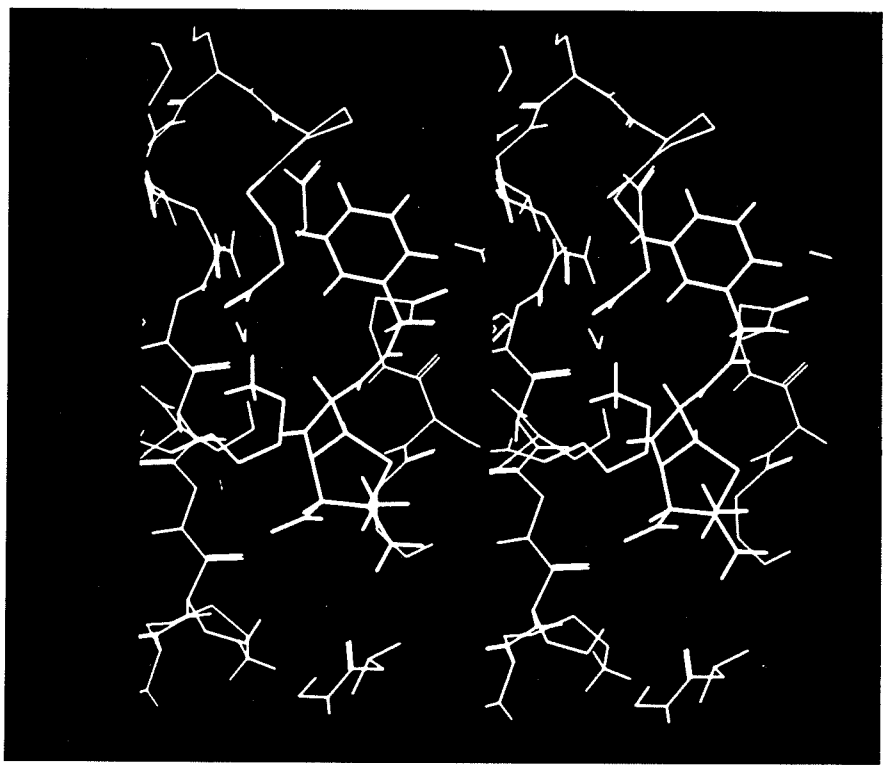

Figure 8. The side chains of glutamate 166 and lysine 73 (bold, background to left of antibiotic) in the RTEM-1 active-site cleft.

(a)

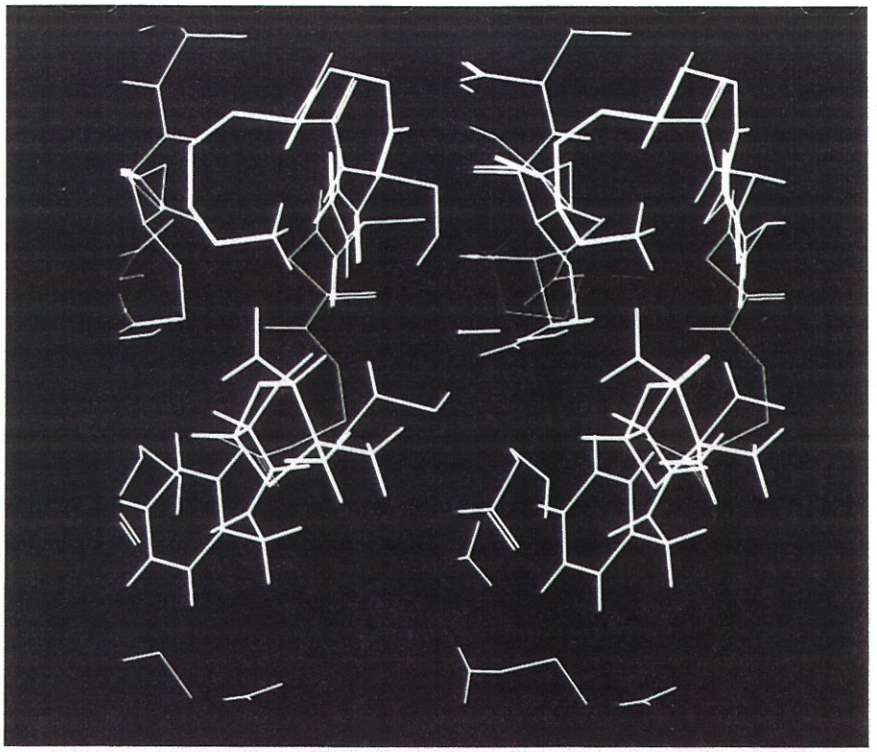

(b)

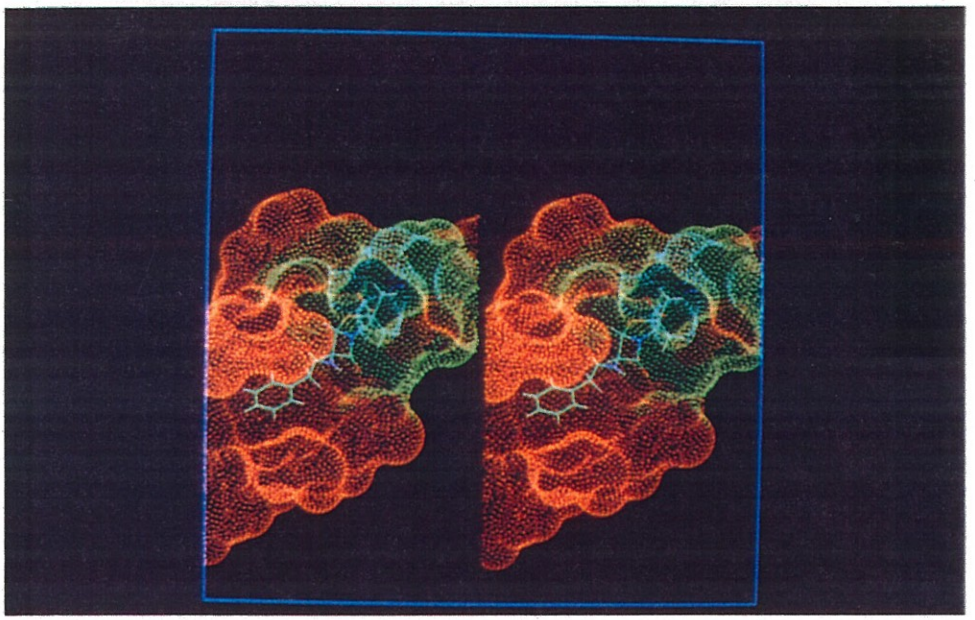

Figure 9. (a) The ammonium group of lysine 234 in the RTEM-1 active-site cleft. (b) Surface representation colored according to relative electrostatic potential. Orange designates positive potential and blue designates neutral potential (calculations considered only the enzyme and not the bound substrate as shown).

(a)

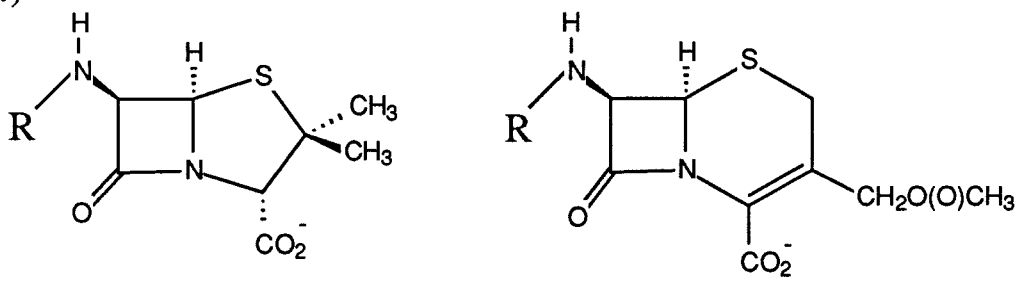

(I) (II)

(b)

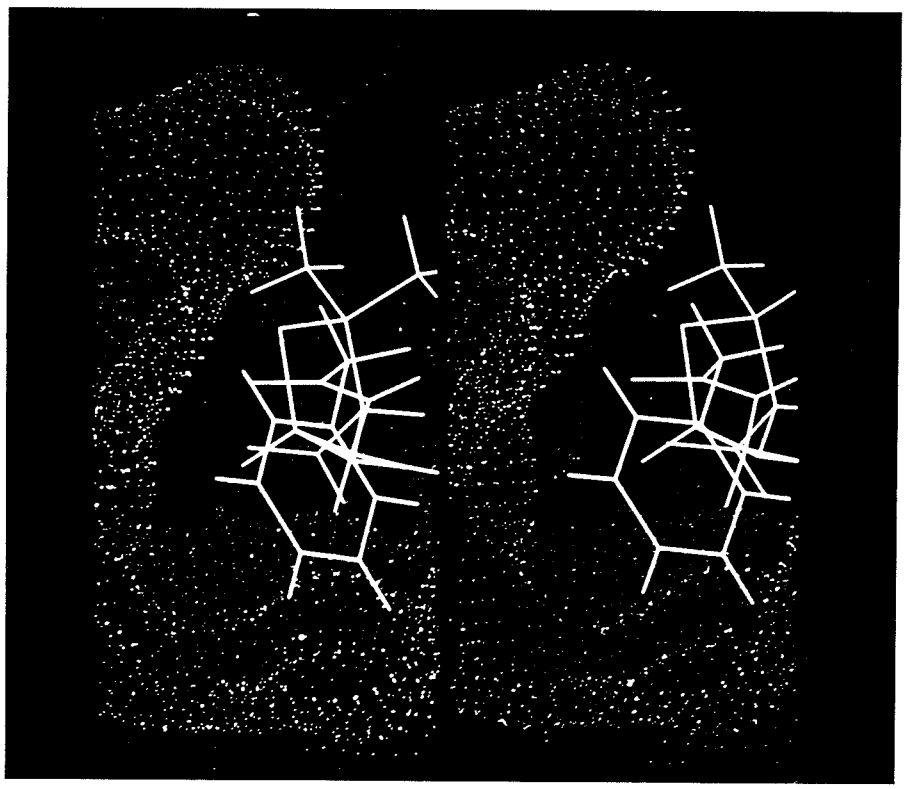

Figure 10. (a) The side group (R) of the penam (I) and the cepheme (II) antibiotics. (b) The open "end" of the RTEM-1 active-site cleft which accounts for the allowable variability in the substrate side group structure.

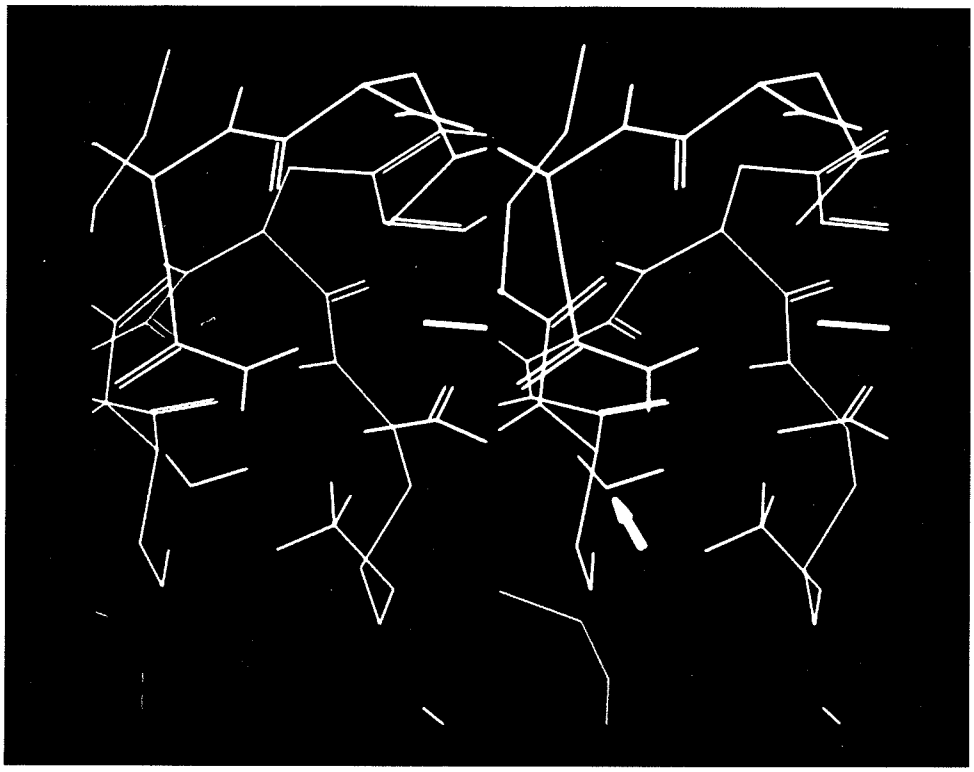

Figure 11. The RTEM-1 active-site showing the steric complementarity between the active site side chains. The arrow points to the bound water molecule discused in the text. Serine 70 is below the water, lysine 73 to the lower right, asperigine 170 above, and the carboxylate of glutamate 166 to the upper right.

Table 2. Intermolecular hydrogen bond distances in the RTEM-1/benzylpenicillin model Michaelis complex. "RTEM-1 Model" are values from this work, "*B. licheniformis* Model" are values from a model of *B. licheniformis* β–lactamase complexed with benzylpenicillin (Meows, P., Knox, J., Dideberg, O., Charlier, P., and Frere, J.-M. (1990) *PROTEINS: Structure, Function, and Genetics*, 7, 156.), "R61/Cephalosporin C" are values taken from the x-ray structure of D-alanyl-D-alanine carboxypeptidase from *Streptomyces* R61 complexed with cephalosporin C (Kelly, J., Knox. J., Zhao, H., Frere, J.-M., and Ghuysen, J.-M. (1989) *J. Mol. Biol.*, **209**, 281.), and "Trypsin/BPTI" are values taken directly from the x-ray structure of trypsin complexed with bovine pancreatic trypsin inhibitor (Brookhaven Protein Data Bank structure file "2PTC" (Huber, R., Eisenhofer, D.)). Parenthetical values are modeled and all others are empirically determined. Distances are in angstroms. The schematic figure shows the hydrogen bonds listed in the table. For Trypsin/BPTI distances (a) and (b) describe this systems oxyanion hole, and distance (c) describes the BPTI/aspartate 189 electrostatic interaction.

	Hydrogen bond length (Å)				
	a	b	c	d	e
RTEM-1					
Model	3.2	5.1	3.1	5.0	3.6
B. licheniformis					
Model	2.8	2.8	3.2	2.9	3.5
R61/Cephalosporin C	-	(2.1)	(3.4)	(3.5)	-
Complex	-	-	4	3	-
Trypsin/BPTI	3.1	2.8	3.7	-	-

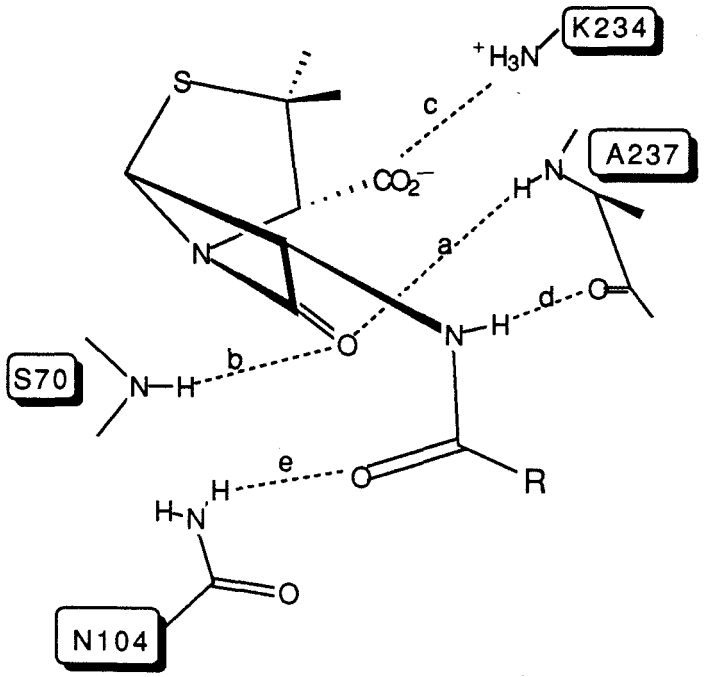

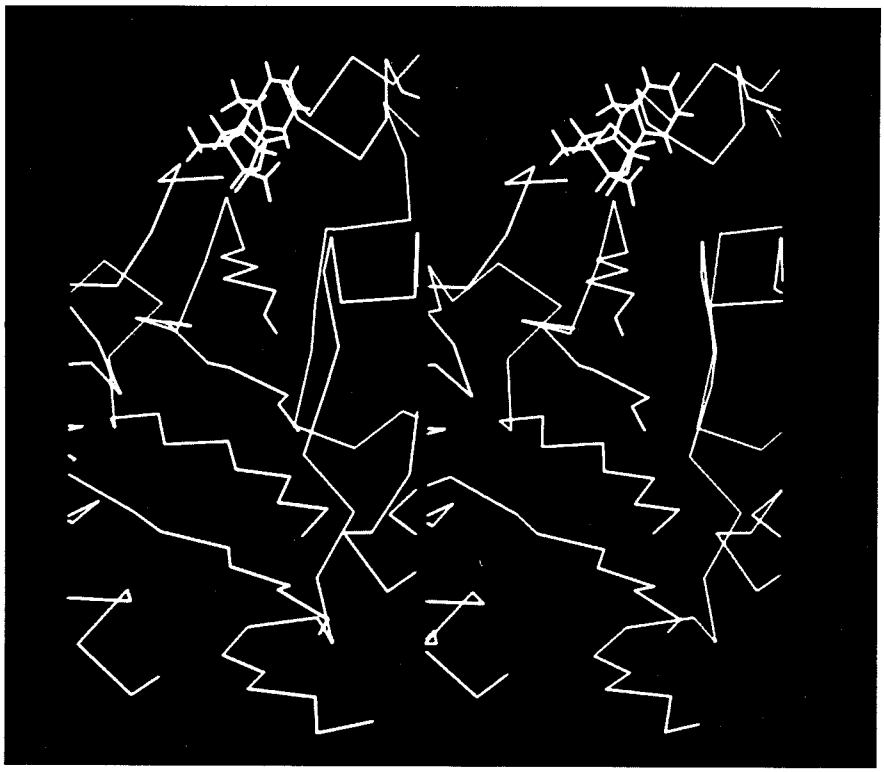

Figure 12. The "sixth strand β-sheet" binding mode of benzylpenicillin. The five-stranded antiparallel β-pleated sheet of the PC1 α-carbon trace is evident "below" the bound benzylpenicillin structure (bold).

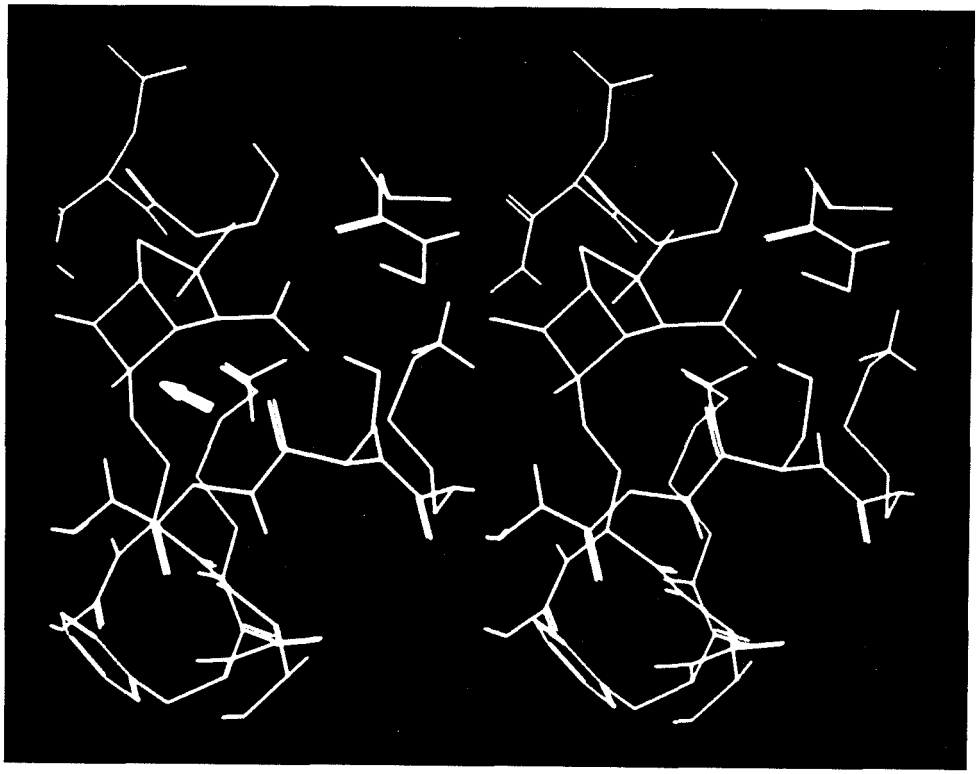

Figure 13. The tetrahedral intermediate formed during acylation of serine 70. The arrow points to the tetrahedral carbon.

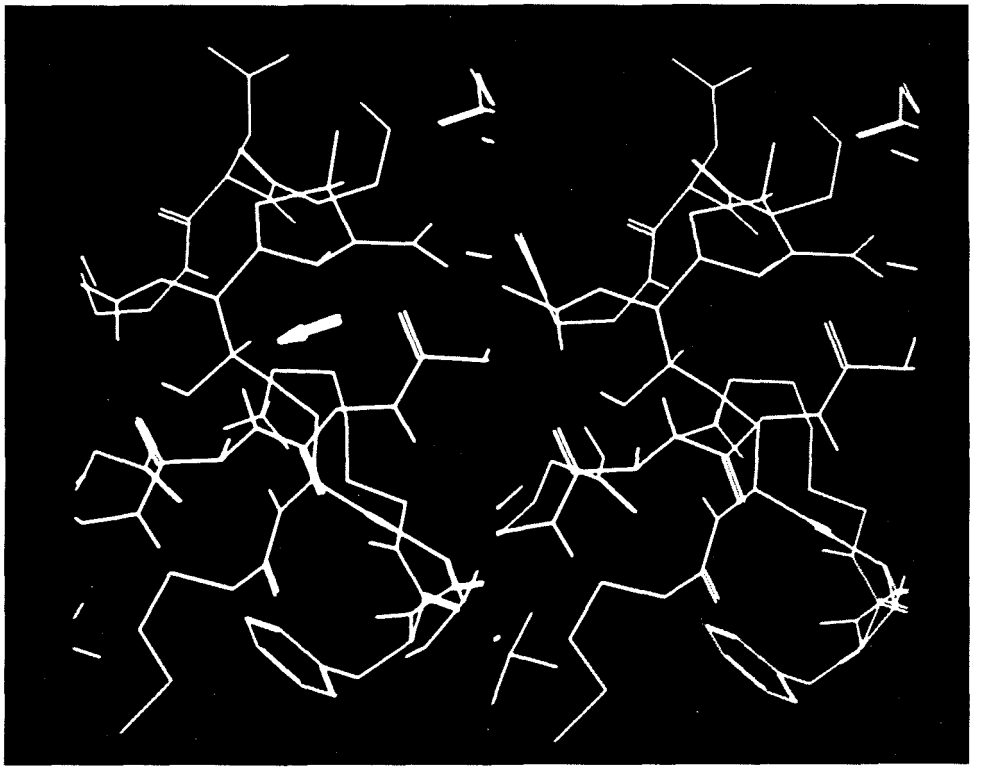

Figure 14. The tetrahedral intermediate formed during deacylation of serine 70. The arrow points to the tetrahedral carbon..

experimentally by other researchers. A striking feature of the modeled enzyme/substrate complex is that the shape of the rigid antibiotic, which contains two amide bonds, mimics a peptide in the extended conformation, and in the complex the antibiotic binds essentially as the sixth strand of an otherwise five-stranded antiparallel β–pleated sheet that is an integral part of the tertiary structure of the protein (Figure 12). This binding mode was also pointed out as a key feature of the covalent complexes between β–lactam antibiotics and the D-alanyl-D-alanine carboxypeptidase from *Streptomyces* R61 (8).

Significant features of the model complex are the hydrogen bonds between the carbonyl oxygen of the β–lactam and the main chain amide hydrogens of serine 70 and alanine 237. Together these bonds could constitute an oxyanion hole that stabilizes tetrahedral intermediates along the reaction pathway of β–lactam hydrolysis in a manner similar to the oxyanion hole that is an important factor in catalysis by the serine proteases (11). Although the geometries of the hydrogen bonds that make up the putative oxyanion hole are not optimum in the ground-state model for the Michaelis complex, models of tetrahedral intermediates along the reaction pathway (Figures 13 and 14) indicate that transformation of the β–lactam carbonyl carbon to a tetrahedral center does not preclude these putative hydrogen bonds as judged by angular and distance geometries (Table 3). Crystallographic studies have shown that the oxyanion hole is an authentic feature of the D-alanyl-D-alanine carboxypeptidase from *Streptomyces* R61 complexed with β–lactam antibiotics (28).

Discussion

The molecular modeling techniques we describe are applicable to any protein for which an α–carbon trace is known and are based on exploiting the inherent information in ϕ and φ angle values. The primary utilities of the methods are the ability to add detail into moderate-resolution protein structures determined by x-ray crystallography or two-dimensional NMR and to construct working models of proteins for which only structures of phylogenetically related ones have been determined.

Application of computer-assisted molecular modeling to the RTEM-1 β–lactamase active site has helped formulate rational ideas about the effects of active-site mutations and the mechanism of the class A β–lactamases. Molecular modeling supports and illustrates the experimentally determined roles that serine 70, lysine 234, and threonine 71 play in the RTEM-1 mechanism and suggests how lysine 73 and glutamate 166 might participate in the acylation and deacylation steps of the catalytic mechanism. The following discussion of the mechanistic chemistry of the class A β–lactamases is based on experimental evidence and molecular modeling results.

Model structures of enzyme/substrate complexes indicate that the side chain of the bound substrate projects along the axes of the active-site cleft and to a significant degree is sterically unhindered and remains solvated even while the antibiotic is bound. Thus the models explain why the class A β–lactamases readily hydrolyze substrates with a variety of side chain structures, but are considerably less promiscuous toward hydrolysis of most other variations in the β–lactam antibiotic structure.

Molecular modeling shows that the side chain of threonine 71, even though in close proximity to those with important catalytic roles, projects away from the accessible portion of the active site and into the interior of the protein where it makes contacts with other side chains (Figure 15). This is consistent with mutagenesis results that have established the role of threonine 71 in the mechanism of RTEM-1 as catalytically unimportant but vital for stabilization of the folded protein structure (12).

The enzyme/substrate complexes, whether they be ground-state or higher-energy, are stabilized to a significant extent by electrostatic association of an ammonium group (enzyme-derived, lysine 234) and a carboxylate group (substrate-derived). This is supported by these molecular modeling studies, the mutagenesis experiments presented in Chapter 3, and published x-ray diffraction studies (1,8). Mutations at lysine 234 in RTEM-1 have dramatic effects on the ability of the enzyme to bind substrate but do not effect the ability of the enzyme to catalyze the hydrolysis reaction under pseudo-first-order conditions. Replacing lysine 234 with glutamine, for example, has no observable affect on k_{cat} but increases K_M by three orders of magnitude, indicating that this residue plays primarily a binding role that is consistent with the model structures in which the aforementioned charged groups interact over a distance of 3.0Å (Figure 16).

Although the mechanism of the class A β–lactamases is not known, it is now well established that serine 70 is acylated by the β–lactam during the hydrolysis reaction (Figure 17) (13,14). The incipient acyl-enzyme intermediate is hydrolyzed by an unknown mechanism

to yield the free enzyme that is available for subsequent rounds of catalysis. The mechanistic roles of serine 70, lysine 234, and threonine 71 described in the preceding paragraphs have been firmly established by experimental methods, but there remain a number of unanswered questions about the mechanism of acylation and deacylation of serine 70. In the acylation step neither the residue responsible for deprotonation of serine 70, if one exists, nor the origin of the proton that is donated to the β-lactam nitrogen during or before the ring opening step of the mechanism is known. The deacylation step of the mechanism is no better characterized. Hydrolysis of the acyl-enzyme might be general base-catalyzed by a side chain in the active site or could occur by another mechanism. Both transient-state (15,16) and steady-state (17) kinetic experiments performed on mutant enzymes will provide useful information for defining the sequence of chemical transformations that are the catalytic mechanism of the class A β-lactamases.

We propose two working catalytic mechanisms--the charge relay (CR) and the bound water (BW) mechanisms--both of which we favor on the basis of geometric features of models and x-ray structures and on the basis of enzymological precedent. The two mechanisms have common features, including the mode of substrate binding, which is driven by salt-bridge formation and is effectively the extension of an antiparallel β-pleated sheet that is a part of the enzymes' secondary structure (Figure 12). In the proposed mechanisms the substrate binds so that the variable side chain is relatively exposed to solvent, the hydroxyl group of serine 70 is the attacking nucleophile, and tetrahedral intermediates are stabilized

by an oxyanion hole--the main chain amide N-H bonds of serine 70 and alanine 237--which is directly analogous to the one active in the serine proteases (Figures 13 and 14).

Central to the task of determining the mechanism of the class A β-lactamases is answering the question of how the serine 70 hydroxyl group is deprotonated when this residue nucleophilically attacks the carbonyl carbon of the β-lactam ring to form the acyl-enzyme. In the charge-relay (CR) mechanism (Figure 18), lysine 73 acts as a general base to remove the serine proton in a manner directly analogous to the function of histidine 57 in the serine proteases (11). In both the RTEM-1 model and published x-ray structures of BL and the D-alanyl-D-alanine carboxypeptidase from *Streptomyces* R61 (8,9), the ε-nitrogen of lysine 73 is near enough to the serine hydroxyl group to hydrogen bond to and is the only amino acid that is close enough to act directly on the serine as a general base.

The CR mechanism is essentially the familiar serine protease mechanism with the catalytic triad in the former case being made up of serine 70, lysine 73, and glutamate 166, and the catalytic triad in the latter case being serine 195, histidine 57, and aspartate 102. As judged by modeling and x-ray studies, the positions of the three residues in the class A β-lactamase active site are appropriate for a charge-relay system. The ε-nitrogen of lysine 73 is positioned near the amid nitrogen of the β-lactam to which it donates the serine proton in the deacylation step of the mechanism, and glutamate 166 is located close enough to interact with lysine 73, which would

presumably stabilize the charged form of the latter side chain (Figure 18).

Site-directed mutagenesis at lysine 73 has implicated an important catalytic role for this active-site amino acid. Mutations at lysine 73 have little effect on the ability of RTEM-1 to bind antibiotic substrates but have a dramatic effect on the catalytic properties of the enzyme (18). For example, the K73R and the K73C mutants both have k_{cat}s reduced by about four orders of magnitude but have K_Ms virtually the same as that of the wild-type enzyme. These results indicate that the primary function of this residue is to stabilize non-ground-state species or to participate directly in the catalytic mechanism, possibly as a general acid or a general base, depending on the whether the side chain is protonated or deprotonated at the pertinent stage in the reaction. Lysine 73 does not play a direct role in substrate binding, and replacing it with others does not significantly disrupt the apparent abilities of the binding residues to perform their functions. Western blot analysis of the lysine 73 mutants shows that replacing the wild-type residue with others has a relatively small effect on the structural stability of the protein. These mutagenesis results are consistent with a general base role for lysine 73 as is invoked in the CR mechanism.

A pitfall of the CR mechanism is that to invoke a general base function for lysine 73 requires that the ammonium group of this residue is in fact not an ammonium group at all, but is, at least in the ground-state enzyme/substrate complex, an amino group (deprotonated) that has a pKa somehow reduced below the expected value of 10. However, there is ample precedent for unusual

ionization constants for amino acid side chains in folded proteins. Examples of lysine residues with depressed pKas include the active-site lysine in acetoacetate decarboxylase (pK=5.9, over four units lower than expected) (19) and lysine 166 in ribulose 1,5-bisphosphate carboxylase/oxygenase (pK=8, two units lower than expected) (20). Lysine 73 is positioned near the amino terminus of an 11 residue α–helix. The work of Hol and co-workers has shown that the macrodipole of this helix is expected to reduce the pKa of a lysine positioned near the amino terminus (21).

The full details of the proposed CR mechanism are illustrated in Figure 18. The direct analogy between the well-known serine protease mechanism and the CR mechanism makes it an attractive target for experimental verification (22). The extensive body of information that has been gathered on the serine proteases will undoubtedly be valuable in efforts to verify the authenticity of this proposed class A β–lactamase mechanism.

Since other than lysine 73 there is no amino acid side chain near enough the serine hydroxyl group to act as a general base in the established acylation step of the mechanism, as part of these molecular modeling studies we have considered the possibility that glutamate 166 might act as a general base and deprotonate the hydroxyl group of serine 70 via a water molecule bound by hydrogen bonds in the active site of the enzyme. On the basis of this, the bound water (BW) mechanism, which is supported by ample precedent in protein chemistry, is being proposed (Figure 19). The BW mechanism solves the serine deprotonation problem by invoking a proton-relay step that occurs between glutamate 166 and serine 70

via a water molecule that is strongly hydrogen bonded to both of these residues (Figure 21). Although several possible active-site water binding sites were considered in the modeling studies, only one mode satisfied a set of criteria that were considered required of any water that performs a proton-relay function and that is the source of hydroxide responsible for hydrolysis of the acyl-enzyme intermediate. The criteria were:

1. The binding site must be the appropriate size and shape to accommodate a water molecule.
2. Binding water must not preclude binding of substrate; that is, bound water must not interfere sterically or in any other way with formation of enzyme/substrate complexes.
3. The water must be bound by at least one hydrogen bond acceptor that has the ability to act as a general base, and it must be bound by the hydrogen bond donating hydroxyl group of serine 70.
4. The bound water must be positioned so that hydroxide generated by general base catalysis can participate in hydrolysis of the acyl-enzyme intermediate.

Calculating the solvent-accessible surface of the active-site cleft shows a depression that is the appropriate size to accommodate a water molecule between serine 70 and glutamate 166. The hydrophilic walls of the depression are formed by two hydrogen bond acceptors, the side chains of asparagine 170 and glutamate 166, and one hydrogen bond donor, the hydroxyl group of serine 70, making a total of three intermolecular hydrogen bonds that could anchor a water molecule at this site. A model of the water/enzyme

complex shows that the geometry and volume of the water-binding site is close to optimal as judged by distances and angles of putative hydrogen bonds (Figure 21). According to models of the tertiary substrate/water/enzyme complex, water bound in this position does not interfere with substrate binding.

A site-saturation mutagenesis experiment performed at glutamate 166, one of the putative water-binding residues, revealed that this residue plays an important catalytic role but does not participate directly in substrate binding. The K_Ms measured for mutants at this position are, within experimental error, the same as the wild-type value; however, in all cases the k_{cat}s for the mutants are reduced by at least two orders of magnitude (23). The mutations have a less pronounced effect on the catalytic properties of the enzyme as compared to mutations at lysine 73; however, they do show that the primary function of glutamate 166 is catalytic in nature. Although mutagenesis experiments indicate that lysine 73 and glutamate 166 are catalytically important, they have not allowed unequivocal assignment of specific roles to these amino acids.

One has only to consider high-resolution x-ray structures of proteins to be convinced that "bound water" is a useful term that describes solvent in and around the folded structures of proteins. Evidence supporting the BW mechanism comes from enzymological precedent for proton-relay mechanisms that involve water and other "multidentate" hydrogen bonding species. In dihydrofolate reductase, a proton transfer takes place via a water bound by aspartate 27, tryptophan 21 and dihydrofolate, and in horse liver alcohol dehydrogenase, a proton is transferred from a water-free

pocket to bulk solvent via a network of hydrogen bonds which involves serine 48, histidine 51, and the bridging 2'-hydroxyl group of the coenzyme ribose ring (24,25).

In models of the RTEM-1/benzylpenicillin acyl-enzyme intermediate, the water molecule is bound by the carboxylate of glutamate 166 at an angle of 102° 3.3Å from the acyl carbonyl carbon (Figure 21). The theoretical work of Houk's group has predicted that the optimum angle for nucleophilic attack on a carbonyl group is about 105°, depending on the specific reaction (26,27). Deprotonation of the bound water by glutamate 166, followed by nucleophilic attack by hydroxide on the acylated hydroxyl group of serine 70 are, therefore, reasonable events to propose as the deacylation steps of the mechanism.

The mechanisms and structures of a class A β–lactamase and the D-alanyl-D-alanine carboxypeptidase from *Streptomyces* R61 ("R61") have similarities as well as differences that are potentially useful in mechanistic studies of the class A β–lactamases and that have relevance to the CR and BW mechanisms which we have proposed. R61 is the well-characterized penicillin-recognizing enzyme that is a target of β–lactam antibiotics, which through formation of stable acyl-enzymes ($t_{1/2}$ for hydrolysis on the order of hours), inhibit this enzyme's essential cell wall cross linking activity. The pertinent question to be answered is, what structural features of R61 make it deacylate so much more slowly than β–lactamase deacylates? A comparison of the x-ray structures of the two proteins has revealed that in three-dimensional space β–lactamase has glutamate 166 and R61 has phenylalanine 164 (28). The nonconservative replacement

of a hydrophilic residue for a hydrophobic one could account, at least partially, for the observed differences between the two enzymes' activities. The proposed BW mechanism can be considered inconsistent with this "mutation" that is a characteristic difference between the two β–lactam-recognizing enzymes. One who subscribes to the BW mechanism would expect that replacing glutamate 166 (a general base that acts through a bound water molecule) with a hydrophobic residue might severely slow the rate of acylation, as well as the rate of deacylation of the active-site serine. However, R61 is known to undergo acylation at a rapid rate, and so the BW mechanism, as depicted in Figure 20, seems to be inconsistent with this observation.

The observed differences between the activities of RTEM-1 and R61 and the results of mutagenesis experiments performed on the serine protease trypsin are consistent with the CR mechanism we have proposed (Figure 18). If the catalytic triad of β–lactamase is serine 70/lysine 73/glutamate 166 as is proposed in the CR mechanism, then the effects of mutations at aspartate 102 in trypsin, or at glutamate 166 in β–lactamase, might be expected to mimic the observed activity difference between R61 and β–lactamase, since like the mutant enzymes, these two enzymes have catalytic triads that differ only in the "third" position (R61 has Ser65/Lys62/Phe164 while β–lactamase has Ser70/Lys73/Glu166). Replacing glutamate 166 in RTEM-1 β–lactamase with histidine or aspartate causes a two order-of-magnitude reduction in k_{cat} but has no observable effect on K_M (23). Similarly, when aspartate 102 in trypsin is replaced by asparagine, k_{cat} drops by four orders of magnitude but K_M is

unaffected (29). Preliminary results indicate that β–lactamase mutants at position 166 do not deacylate as efficiently as the wild-type enzyme (30). Although the results have to be confirmed before deemed conclusive, they indicate that these mutants could have properties in common with R61.

In addition to the previously mentioned amino acids, mutagenesis studies indicate that serine 130 might have a direct role in the reactions catalyzed by RTEM-1 β–lactamase (31). Replacing this side chain with other residues causes k_{cat} decreases of as much as four orders of magnitude, but only minor changes in K_M values. In three-dimensional space, serine 130 corresponds to tyrosine 150 in the structurally and evolutionarily related class C β–lactamase from *Citrobacter freundii* (32). Oefner *et al.* have invoked a general base role of deprotonation of the active-site serine for the anionic form of the tyrosine in β–lactamase from *Citrobacter freundii* (32); however, an analogous role for the serine residue at this position in RTEM-1 is unlikely, considering the high pKa of primary alcohols (typically 16) and realizing that there is no enzymological precedent for participation of a serine anion in general base catalysis. Consistent with the mutagenic and crystallographic results is a role for serine 130 as a water-binding side chain that is required in the deacylation steps of the catalytic mechanism. The serine 130 water-binding role is consistent with the CR mechanism we have proposed, since this mechanism requires that a water is bound appropriately for deprotonation by lysine 73 followed by nucleophilic attack by hydroxide on the acyl-enzyme. These experimental results are inconsistent with the BW mechanism, since in this scheme all

catalytically important residues, including those that bind water, are accounted for and do not involve serine 130.

Distinguishing between the mechanisms we have proposed, or others that might be authentic, cannot be accomplished through modeling or other theoretical approaches, but is a task amenable to experimental methods such as mutagenesis, x-ray crystallography, and transient-state kinetic methods.

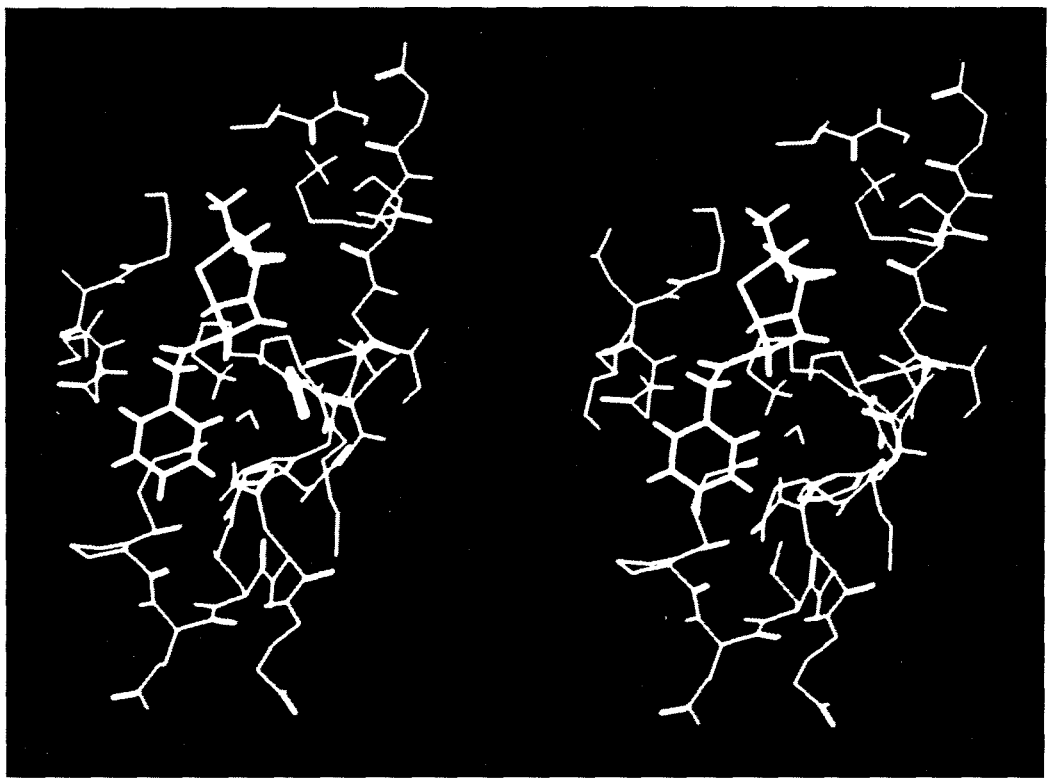

Figure 15. The side chain of threonine 71 (far right, serine 70 shown with arrow) shown projecting away from the bound substrate and into the interior of the class A β-lactamase folded protein.

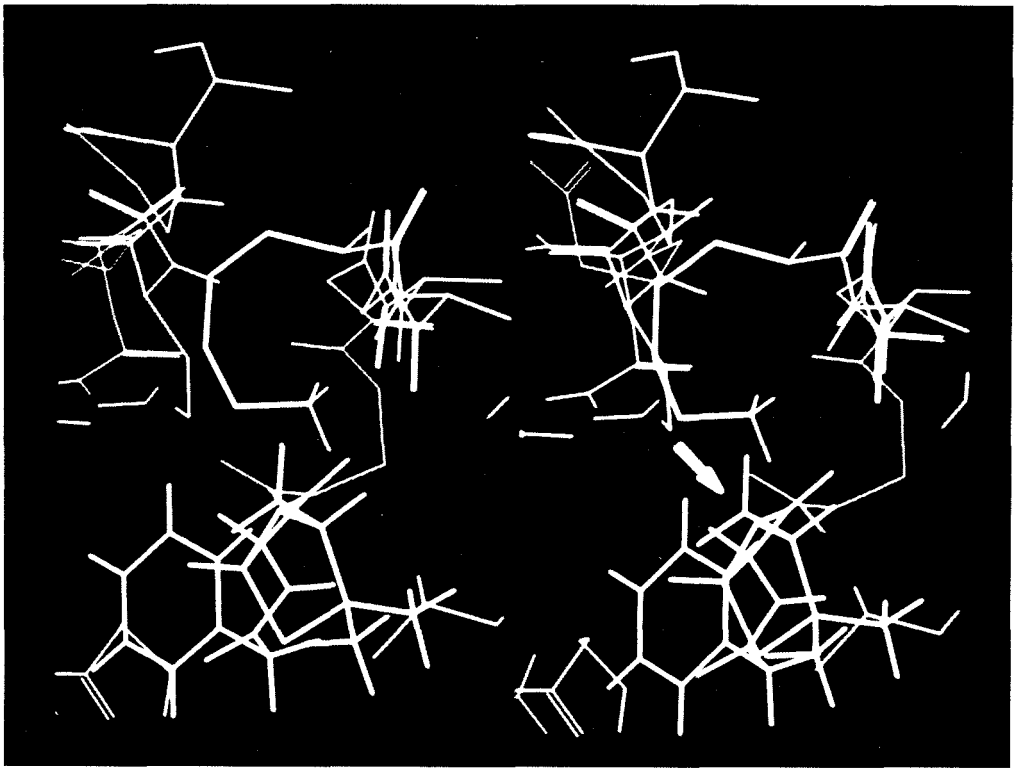

Figure 16. The carboxylate of benzylpenicillin and the ammonium group of lysine 234 in the RTEM-1/benzylpenicillin complex. The arrow points to the carboxylate.

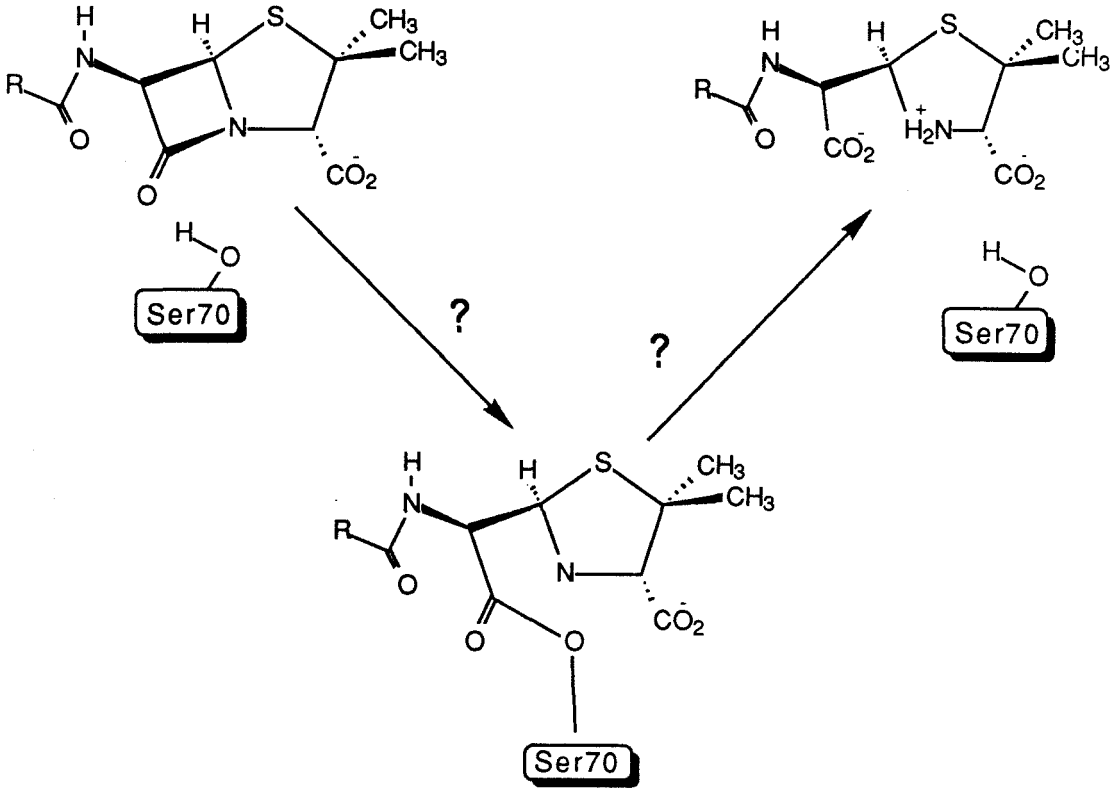

Figure 17. The general acyl-enzyme mechanism of the class A β–lactamases.

Figure 18. The proposed charge relay (CR) mechanism of the class A β–lactamases. (i) is the Michaelis complex, (ii) is the tetrahedral intermediate formed in the acylation step, (iii) is the acyl-enzyme, (iv) is the tertrahedral intermediate formed in the deacylation step.

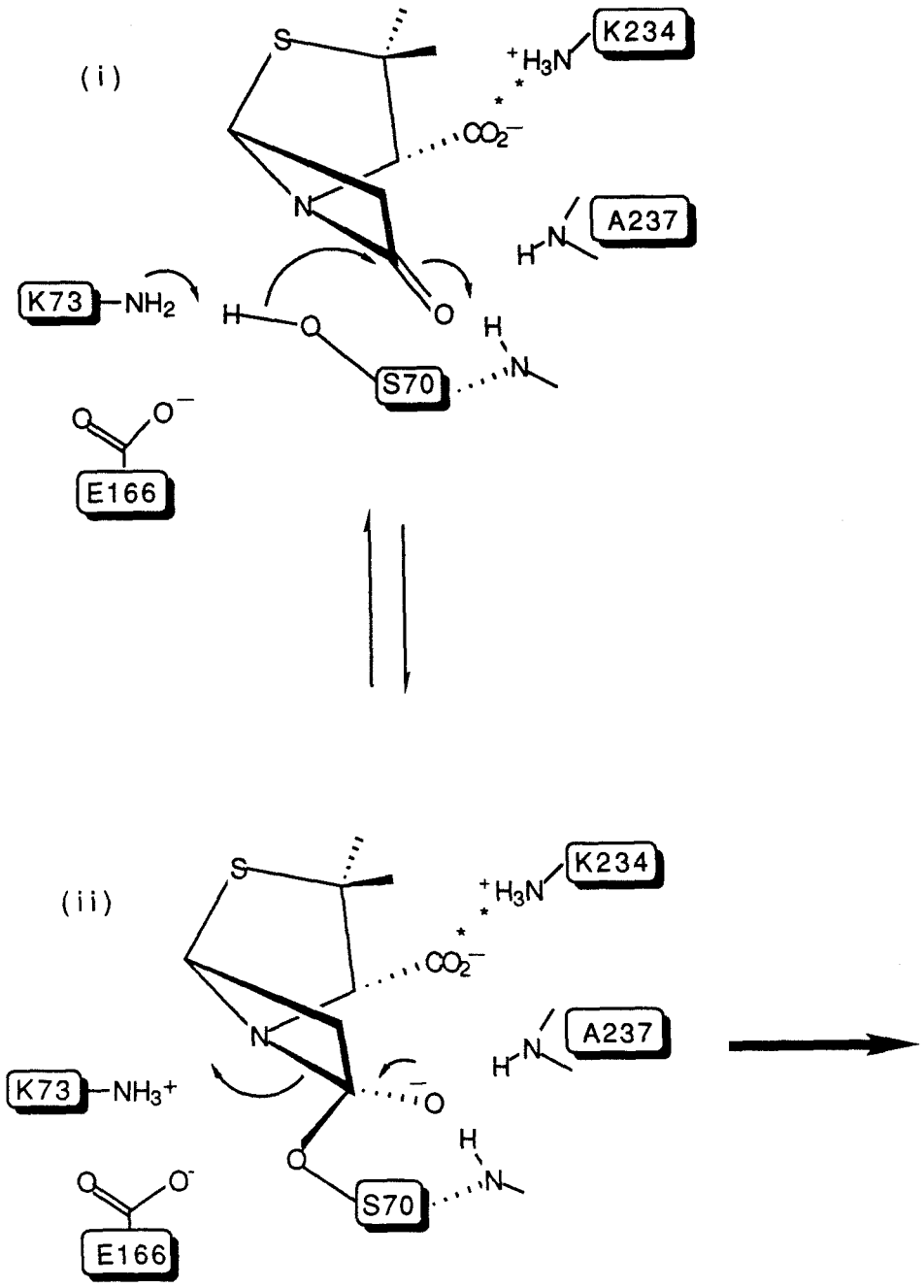
(i)
K234
A237
K73
S70
E166
(ii)
K234
A237
K73
S70
E166

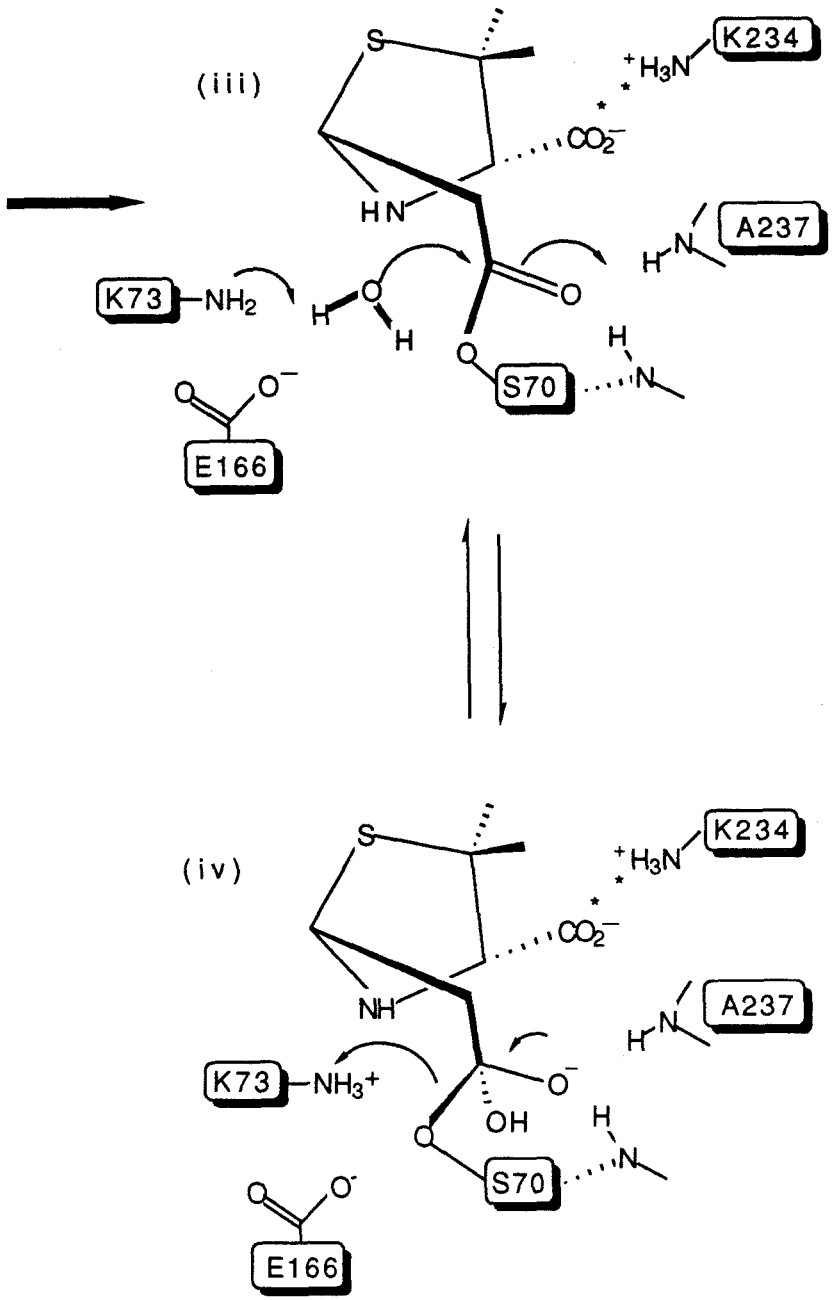
(iii)
S
K234
$^{+}H_3N$
CO_2^-
HN
A237
H
N
K73
NH_2
H
O
H
O
H
N
S70
O
O^-
E166
(iv)
S
K234
$^{+}H_3N$
CO_2^-
NH
A237
H
N
K73
NH_3^+
O^-
OH
H
N
S70
O
O^-
E166

Figure 19. The proposed bound water (BW) mechanism for the class A β–lactamases. (i) is the Michaelis complex, (ii) is the tetrahedral intermediate formed in the acylation step, (iii) is the acyl-enzyme after a proton migration from E166 to K73 (not shown), and (iv) is the tetrahedral intermediate formed in the deacylation step. Dashed lines (---) indicate hydrogen bonds.

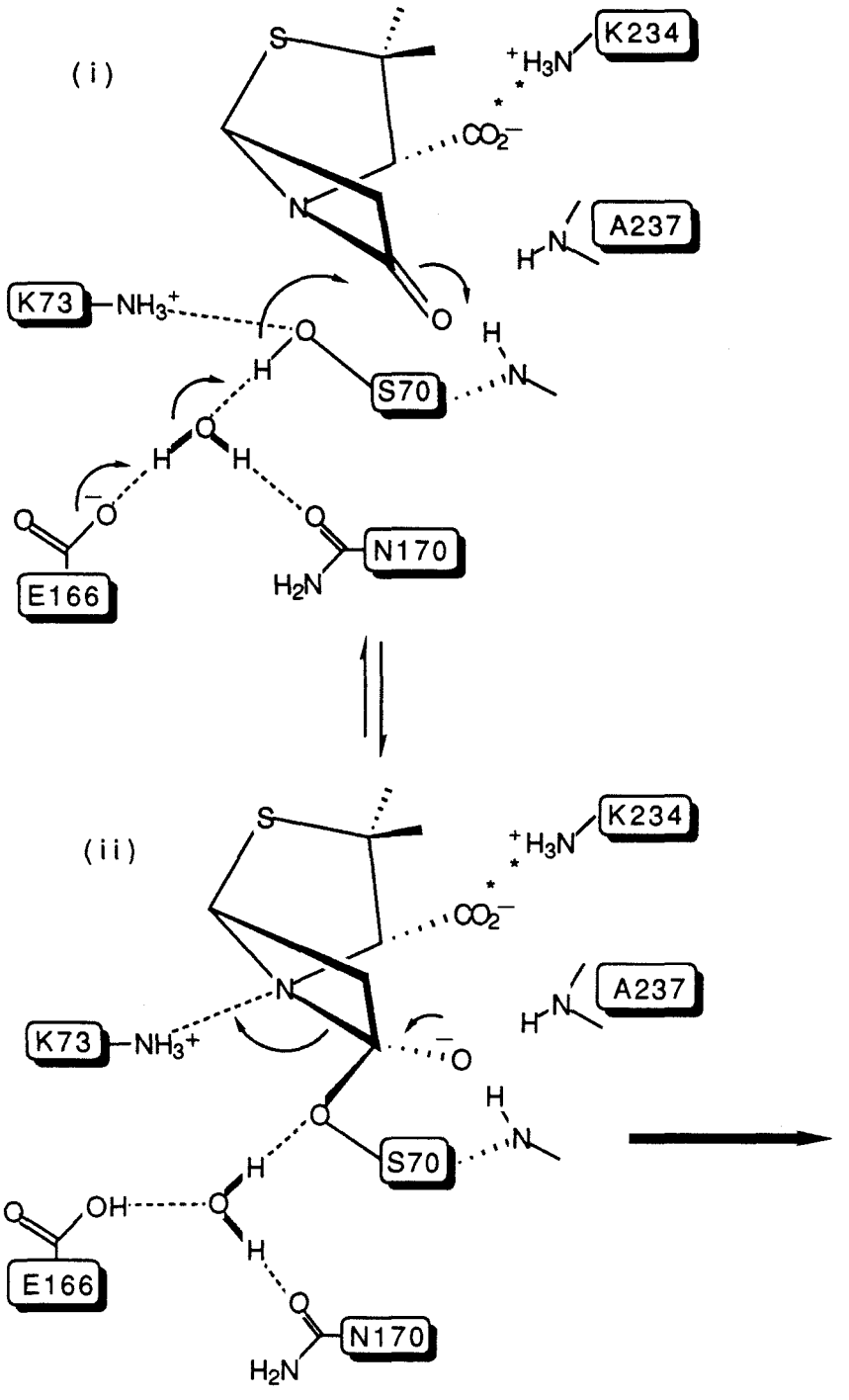
(i)
K234
A237
K73
S70
N170
E166
(ii)
K234
A237
K73
S70
N170
E166

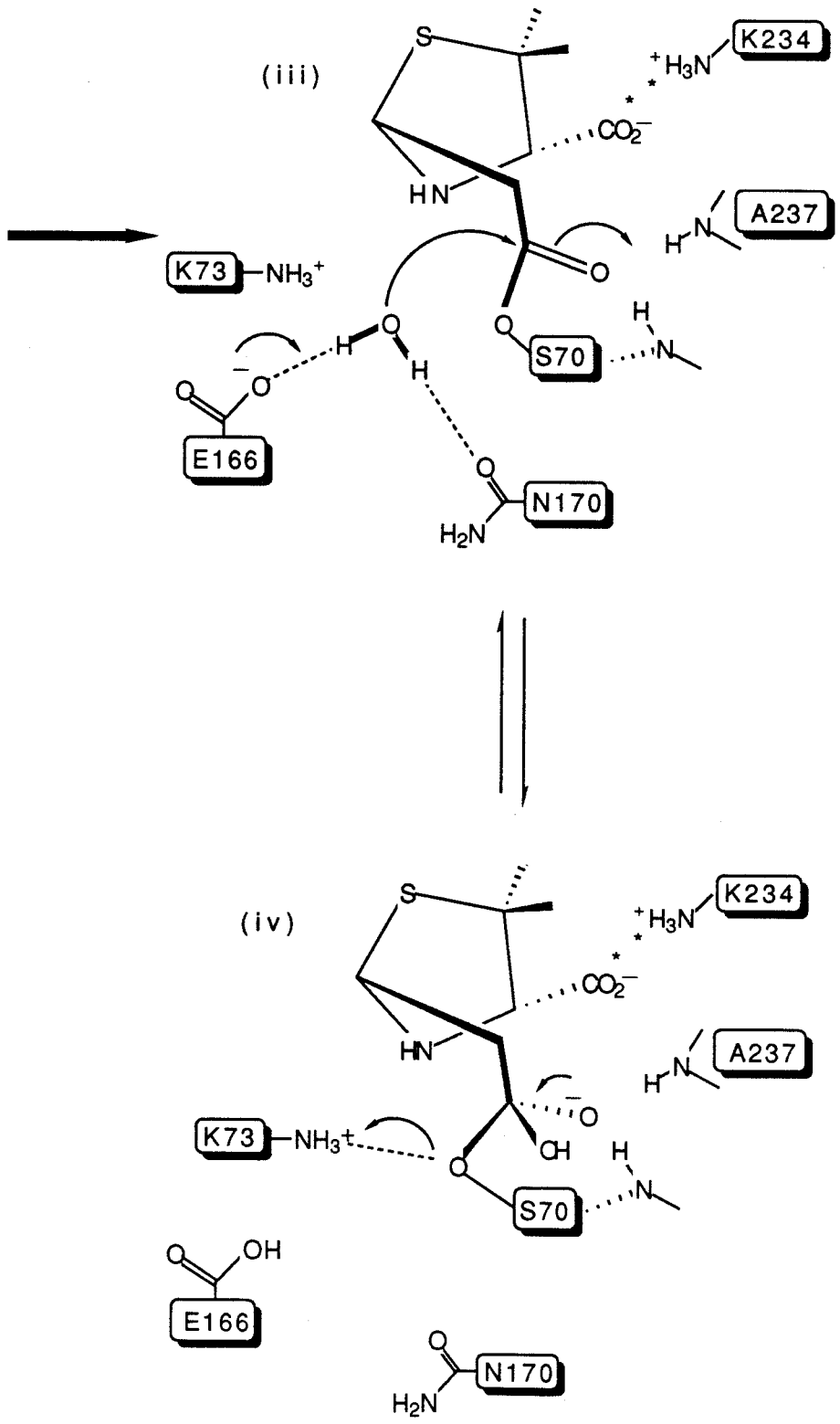
(iii)
K234
A237
K73
S70
E166
N170
(iv)
K234
A237
K73
S70
E166
N170

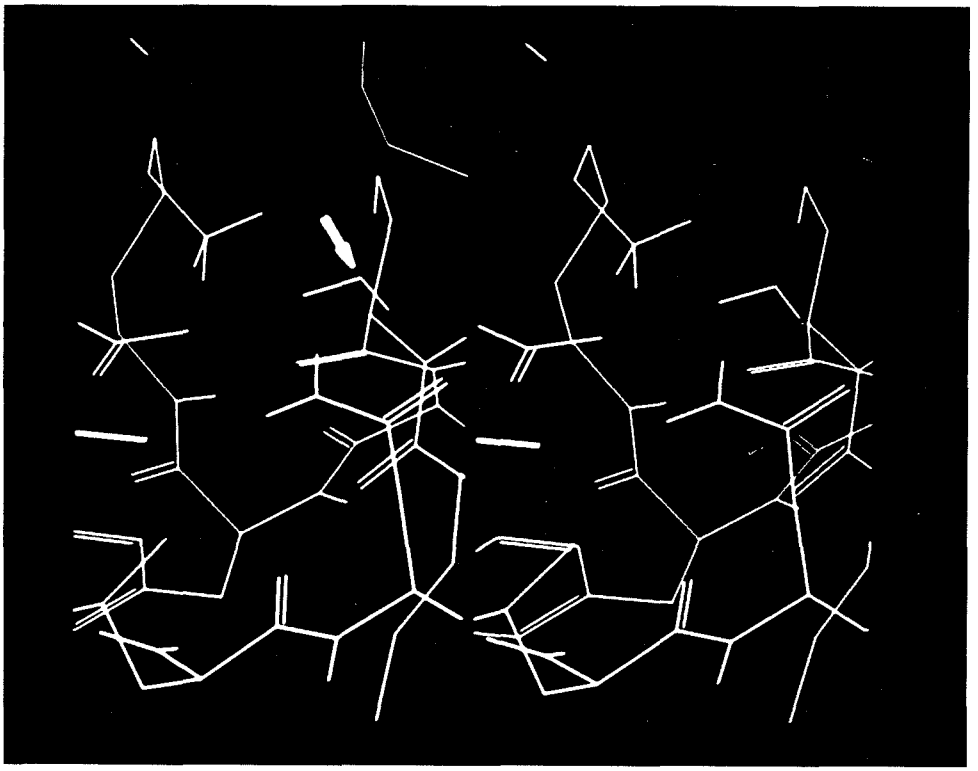

Figure 20. The water molecule (arrow) bound by serine 70 (upper right), glutamate 166 (carboxylate to left), and asparagine 170 (middle right) that is invoked in the BW mechanism.

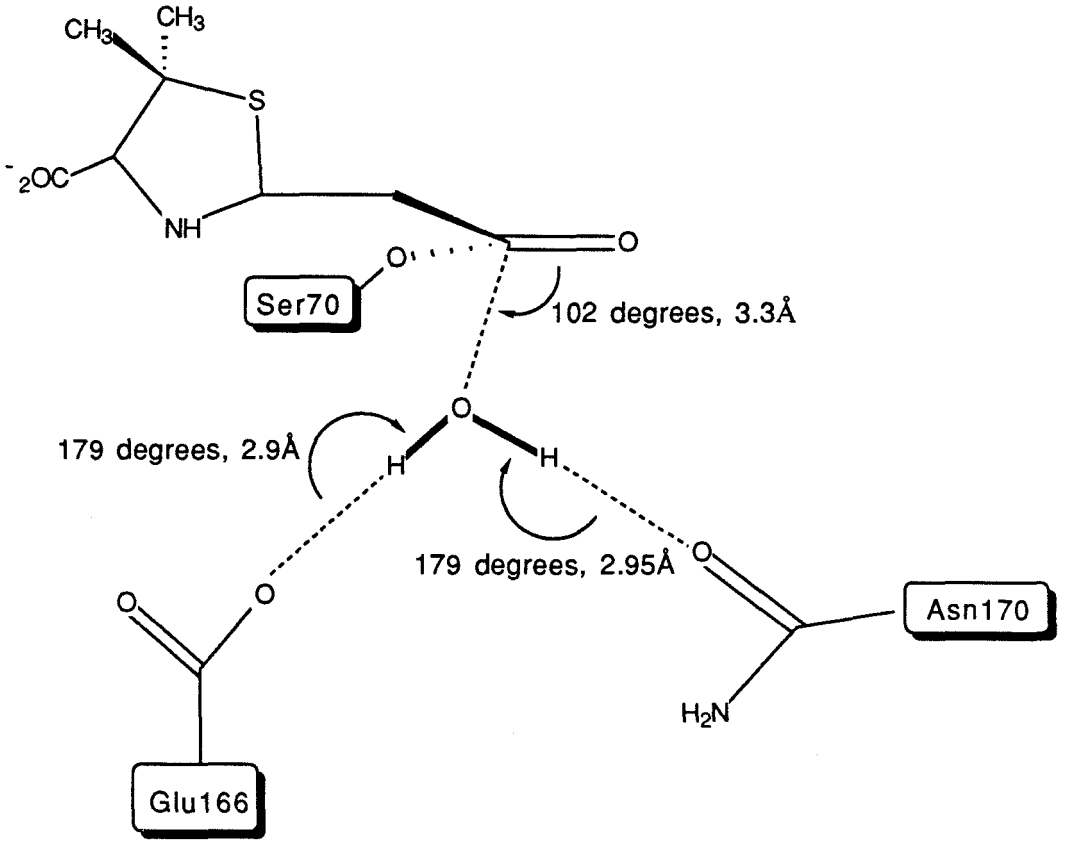

Figure 21. Schematic diagram showing the spatial relationship between the bound water and the acyl-enzyme carbonyl group.

Table 3. Geometric features of the oxyanion holes in the Michaelis complex (MM; Figure 12), the tetrahedral intermediate formed in the acylation step (TI1; Figure 13), and the tetrahedral intermediate formed in the deacylation step (TI2; Figure 14) of the modeled mechanisms. Values are distances in angstroms followed by angles in degrees.

	Bond to A237 amid H	Bond to S70 amid H
MM	3.2,155	5.1,144
TI1	3.8,127	4.1,125
TI2	4.1,128	4.2,121

References

1. Hertzberg, O. and Moult, J.(1987) *Science*, **236**, 694.
2. Bernstein, F. (1977) *J. Mol. Biol.*, **112**, 535.
3. Fersht, A. (1985) *Enzyme Structure and Mechanism, second Ed.*,W. H Freeman and Co., New York, p.6.
4. Ambler, R. (1980) *Phil. Trans. R. Soc. Lond. B*, **289**, 321.
5 Mayo, S., Olafson, B., and Goddard, W. (1990) *J. Phys. Chem.*, **94**, 8897.
6. Weiner, S., and Kollman, P. (1984) *J. Amer. Chem. Soc.*, **106**, 765.
7. Brooks, B., and Bruccoleri, R. (1983) *J. Comp. Chem.*, **4**, 187.
8. Kelly, J., Knox. J., Zhao, H., Frere, J.-M., and Ghuysen, J.-M. (1989) *J. Mol. Biol.*, **209**, 281.
9. Meows, P. C., Knox, J. R., Dideberg, O., Charlier, P., and Frere, J.-M. (1990) *Proteins: Structure, Function, and Genetics*, **7**, 156.
10. Fisher, J., Belasco, J., Khosla, S., and Knowles, J. (1980) *Biochemistry*, **19**, 2895.
11. Kraut, J. (1977) *Annu. Rev. Biochem.*, **46**, 331.
12. Schultz, S. C. and Richards, J. H. (1986) *Proc. Natl. Acad. Sci. U.S.A.*, **83**, 1588.
13. Pratt, R. and Loosemore, M. (1978) *Proc. Natl. Acad. Sci. U.S.A.*, **75**, 4154.
14. Knott-Hunziker, V., Waley, S., Orlek, B., and Sammes, P. (1979) *FEBS Letts.*, **99**, 59.
15. Martin, M. T. and Waley, S. G. (1988) *Biochem. J.*, **254**, 923.
16. Christensen, H., Martin, M., and Waley, S. (1990) *Biochem. J.*, **266**, 853.

17. Waley, S. G. (1974) *Biochem J.*, **139**, 789.

18. Carroll. S., Long, D. and Richards, J., *Biochemistry*, in press.

19. Schmidt, D. E., Jr. and Westheimer, F. H. (1971) *Biochemistry*, **10**, 1249.

20. Hartman, F., Stringer, C., Milanez, S., and Lee, E. (1986) *Phil. Trans. R. Soc. Lond. B*, **313**, 379.

21. Hol, W. (1985) in *Prog. Biophys. Mol. Biol.*, **45**, 149.

22. Blow, D. (1976) *Acc. Chem. Res.*, **9**, 145.

23. Todd Richmond, unpublished results.

24. Filman, D. J., Bolin, J. T., Mathews, D. A., and Kraut, J. (1982) *J. Biol. Chem.*, **257**, 13663.

25. Andersson, P., Kvassman, J., Linstrom, A., Olden, B., and Pattersson, G. (1981) *Eur. J. Biochem.*, **113**, 425.

26. Li, Y., Paddon-Row, M., and Houk, K. (1988) *J. Amer. Chem. Soc.*, **110**, 3684.

27. Yun-Dong, W. and Houk, K. (1987) *J. Amer. Chem. Soc.*, **109**, 908.

28. Knox, J. R., and Kelly, J. A. (1989) in *Chemical and Biochemical Problems in Molecular Recognition*, Stanley Roberts ed., Royal Society of Chemistry.

29. Craik, C., Roczniak, S., Largman, C., and Rutter, W. (1987) *Science*, **237**, 909.

30. Diane Hollenbaugh, unpublished results.

31. Michael Emerling, unpublished results.

32. Oefner, C., D'Arcy, A., Daly, J. J., Gubernator, K., Charnas, R. L., Heinze, I., Hubschwerlen, C., and Winkler, F. K. (1990) *Nature (London)*, **343**, 284.

CHAPTER 3

The Role of Lysine 234 in RTEM-1 β–lactamase Studied by Site-Saturation Mutagenesis

Introduction

Electrostatic interactions between charged amino acids, cofactors, and small molecules are important determinants of enzyme folding, allosteric, and catalytic properties. Intramolecular salt bridges in folded proteins have been widely observed (1-3), and the free energies of substrate binding by many enzymes, including phosphofructokinase (4), tyrosyl-tRNA synthetase (5), aspartate aminotransferase (6), and trypsin (7), have important electrostatic contributions. Electrostatic catalysis, where polar transition states are stabilized by charged groups in proteins, is an important determinant of enzymatic activity in lysozyme and the serine proteases as well as in other systems (8,9).

The energies of charge-charge interactions in proteins are difficult to predict or measure, mainly because they depend so strongly on the anomalous dielectric properties of the protein media through which they take place (Equation 1) (10).

$$E = \frac{332}{\varepsilon} \cdot \frac{q_1 q_2}{r_{12}}$$

Equation 1. Coulomb's law. The potential energy E (kcal mol^{-1}) of two point charges q_1 and q_2 (electron charges) separated by a distance r (angstroms). ε is the effective dielectric constant.

The dielectric constant of a material, for example, one that is positioned between two plates of a capacitor, is a macroscopic property that is not very useful for describing interactions on the molecular level. The effective dielectric constant arises from the polarizability of the medium that separates interacting charges *as*

well as the medium that is near but not necessarily between interacting charges (11). The heterogeneity and asymmetry characteristic of folded proteins results in highly variable and difficult-to-predict dielectric constants within the interiors and near the surfaces of protein molecules, and consequently the contributions that electrostatics make to the stabilization of ground-state and highe-energy intermediates in enzymatic catalysis are not what would be expected from models that assume a uniform dielectric constant in the active sites of enzymes (12,13).

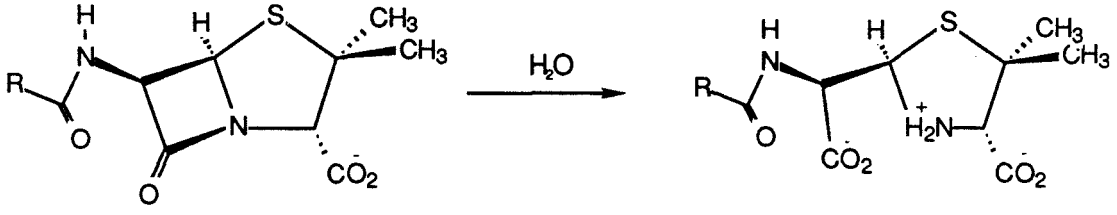

Figure 1. The hydrolysis reaction catalyzed by the β–lactamases. Hydrolysis of a penam antibiotic is shown; the R group is variable. The products of the reaction are ineffective as antibiotics.

We report here a mutagenesis study of the electrostatic role of lysine 234 in binding and catalysis by RTEM-1 β–lactamase (RTEM-1). RTEM-1 binds and hydrolyzes the β–lactam of penicillin-type antibiotics in reactions that convert these normally potent antibacterial agents into innocuous products (Figure 1). In studies of synthetic antibiotics, comparisons with a related carboxypeptidase system, x-ray diffraction studies, and molecular modeling studies, the carboxylate at C3, which is required for efficient hydrolysis by RTEM-1, has been implicated as an electrostatic anchor that interacts with the positively charged

ammonium group of lysine 234 in the class A β–lactamase active site (Figure 2) (14-16).

Class A β–lactamases such as RTEM-1 destroy β–lactam antibiotics that otherwise form covalent complexes with the DD-peptidases, inhibiting the essential cell wall cross-linking activity of these enzymes that are required for cell viability (17,18). Comparisons of the primary and higher-order structures of the class A β–lactamases with the DD-peptidases have led to the identification of a positively charged amino acid that is conserved among members of these evolutionarily related classes of enzymes (Figures 3, 4, and 5) (19,20). The positive residue--lysine 234 in the β–lactamases and histidine 298 in the DD-peptidases--is located in the enzymes' active site, and unlike all other charged residues in the two active sites, appears to have no counterion (a negatively charged amino acid) near enough to interact electrostatically (Figure 6). These unique features of the lysine 234/histidine 298 residue implies that it could participate in intermolecular charge-charge interactions and that its function could be to interact electrostatically with the carboxylate common to all substrates of the β–lactamases and the DD-peptidases.

Evidence supporting an electrostatic role for the antibiotic C3 carboxylate comes from comparing the structures of the β–lactamase and DD-peptidase substrates (Figure 7), and from the observation that β–lactam antibiotics that lack the C3 carboxylate are generally both poor β–lactamase substrates *and* poor DD-peptidase substrates that have low antibacterial activity (21,22).

In the crystal structure of the D-alanyl-D-alanine carboxypeptidase from *Streptomyces* R61 (DD-peptidase R61)

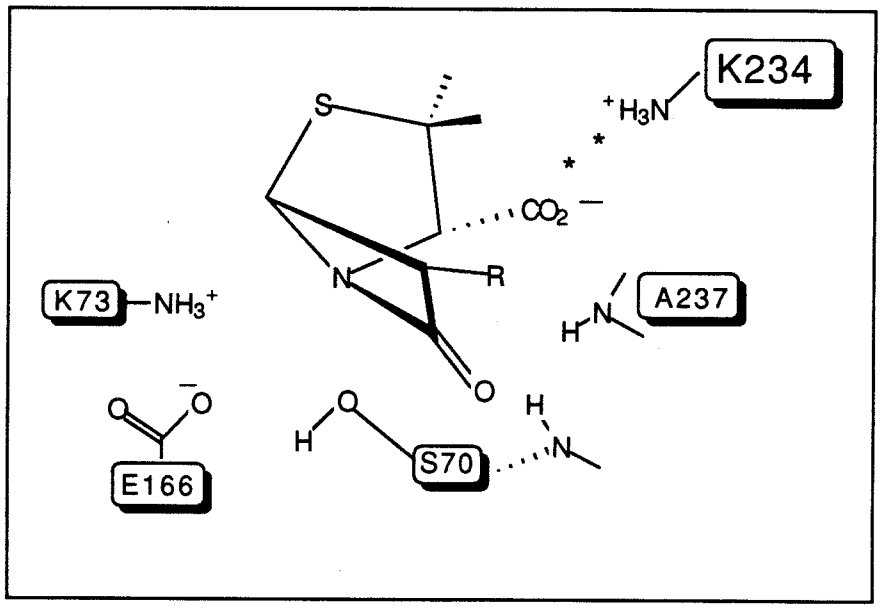

Figure 2. Schematic diagram showing the RTEM-1 active-site amino acids and the putative Lysine 234/C3 carboxylate salt bridge.

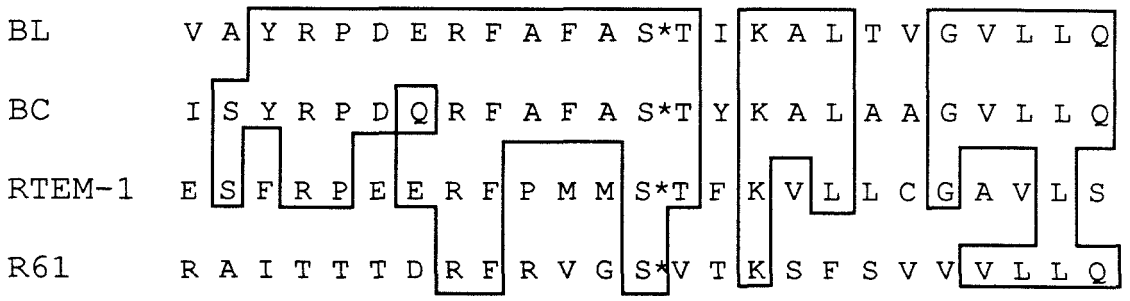

Figure 3. Primary sequence comparison of the class A β–lactamases and the DD-peptidases. The active-site serine is indicated as S*. BL, BC, and RTEM-1 are β–lactamases from *B. licheniformis*, *B. cereus*, and *E. coli*, respectively. R61 is the DD-peptidase from *Streptomyces* R61. Boxed residues are conserved.

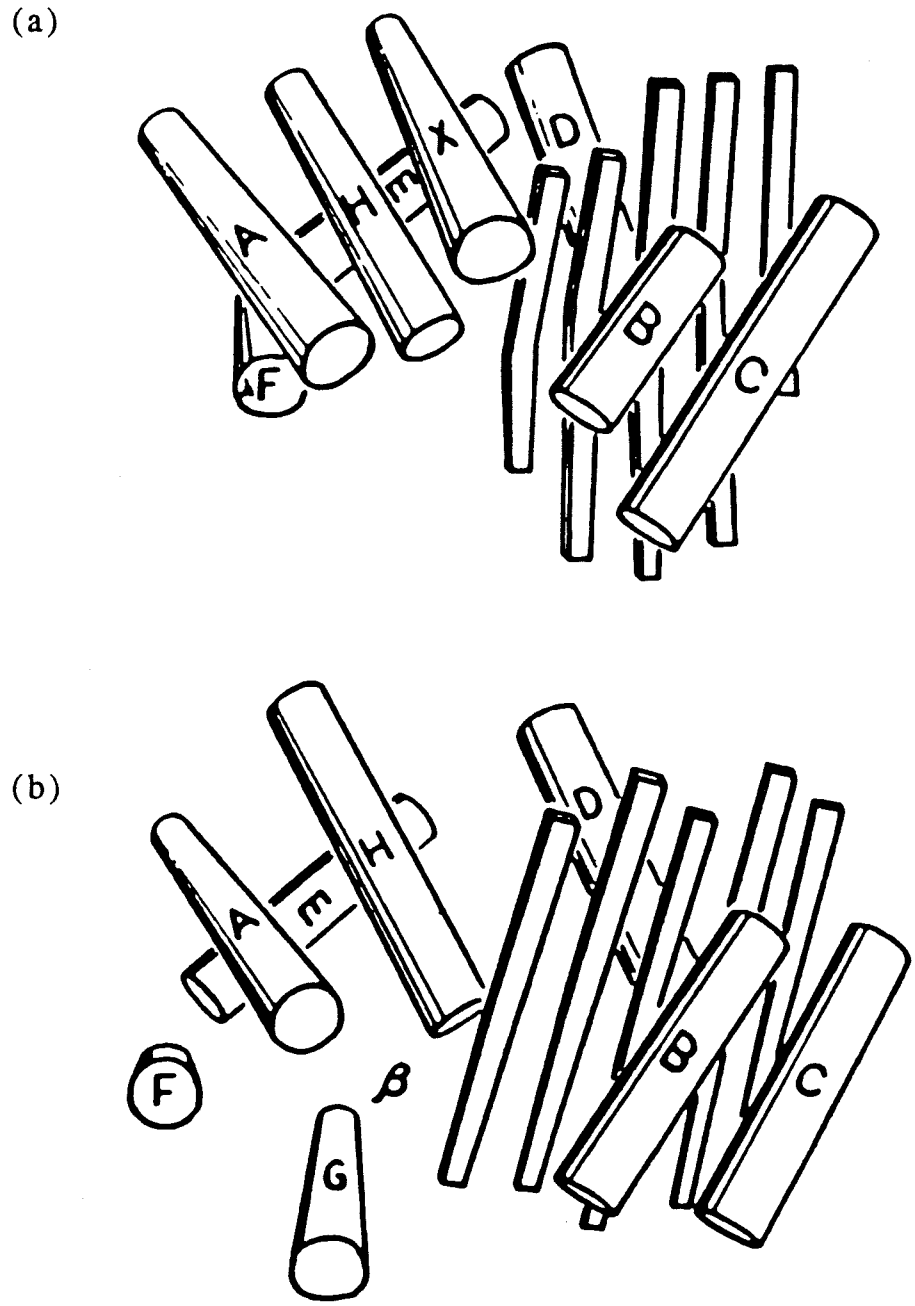

Figure 4. Secondary structures of (a) *Bacillus licheniformis* β–lactamase and (b) R61 carboxypeptidase (DD-peptidase) from *Streptomyces* R61. The site of β–lactam binding to the DD-peptidase is indicated by β. Notice the unique helices X and G (20).

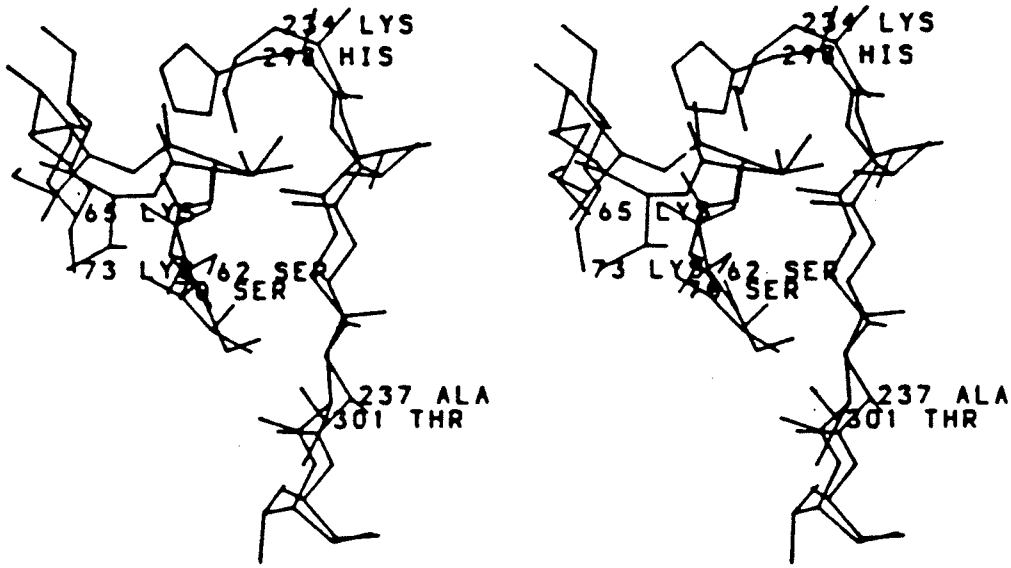

Figure 5. Superposition of the binding sites of DD-peptidase R61 and *B. licheniformis* β–lactamase. Serine 70 and lysine 234 belong to the β–lactamase (16).

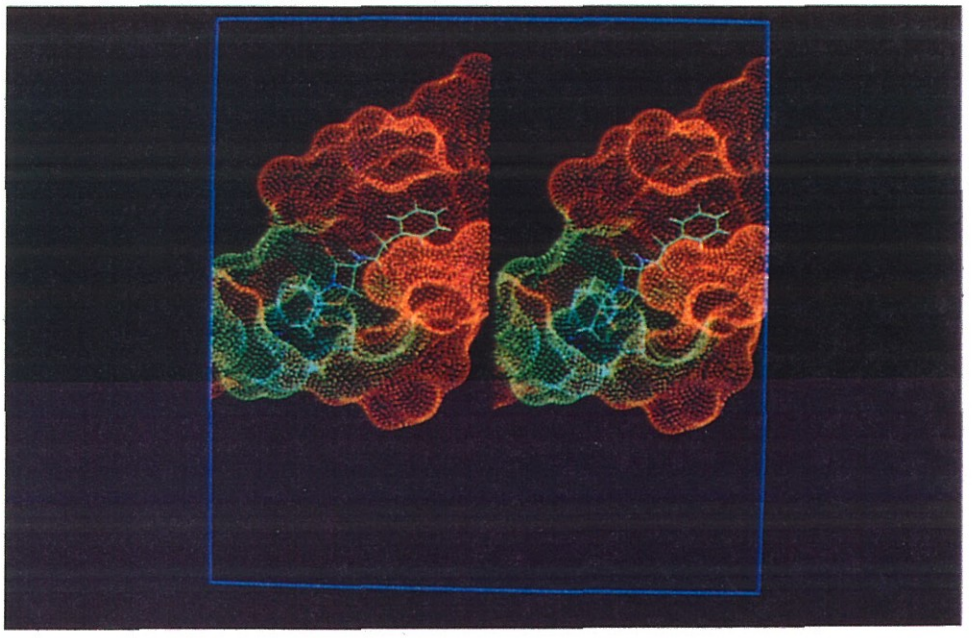

Figure 6. Surface representation of the RTEM-1 active site color coded according to electrostatic potential. Orange designates neutral potential and blue, relatively positive potential. The only residue that lacks a counter ion is lysine 234, which is the obvious blue depression in the background of the diagram. Benzylpenicillin is shown bound in the active site (the electrostatic surface display was calculated without the antibiotic).

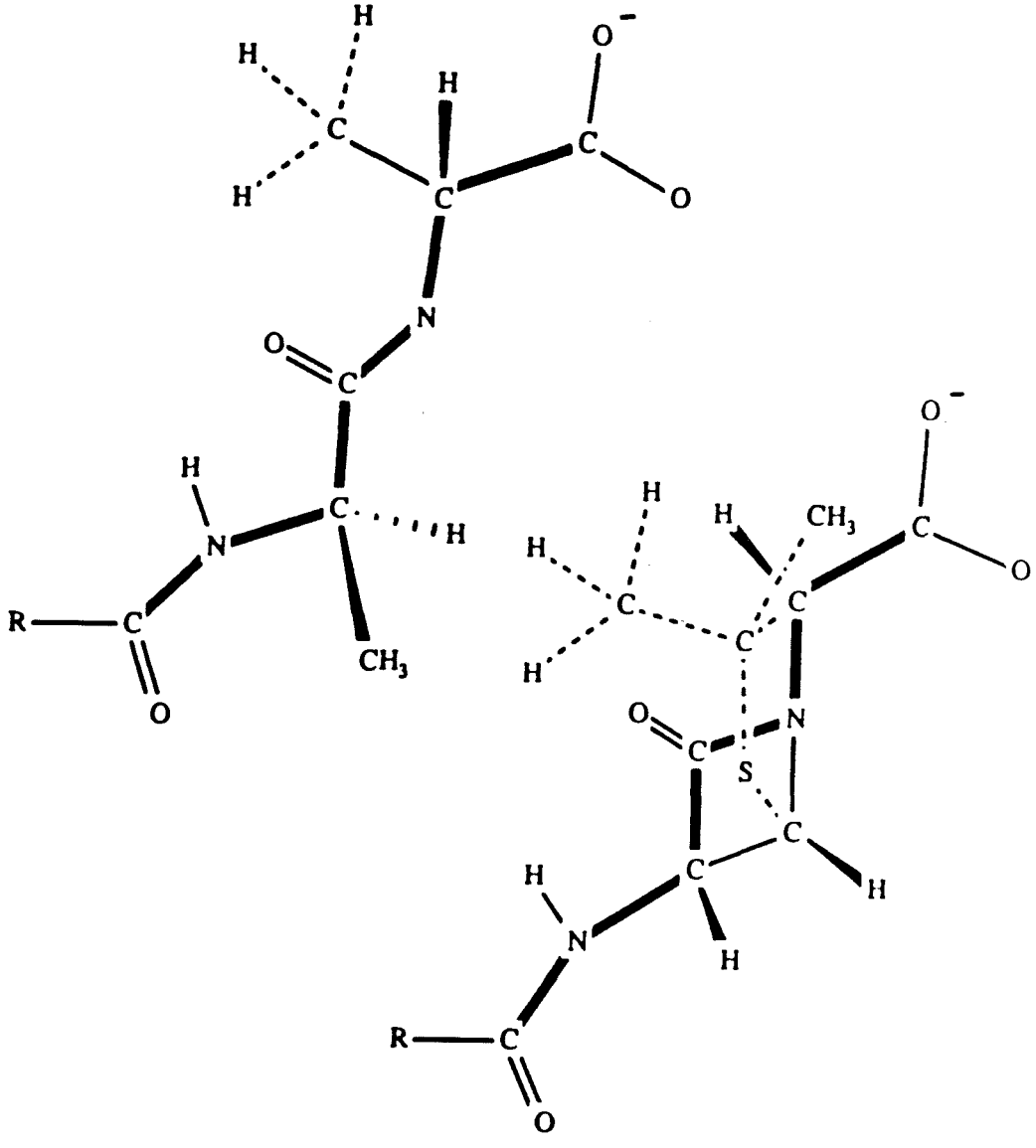

Figure 7. The structures of a D-Alanyl-D-Ala dipeptide (left) and a β–lactam antibiotic (right). The molecules are representative substrates of the DD-peptidases and the β–lactamases respectively (19).

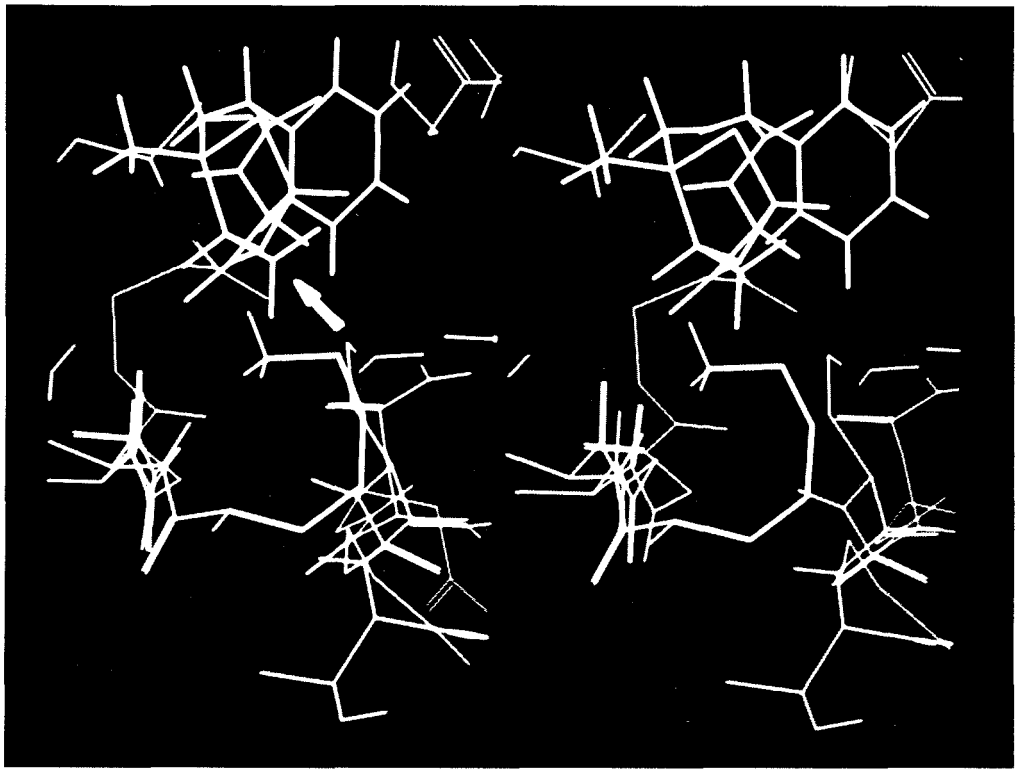

Figure 8. Molecular model of the salt bridge between Lysine 234 and the C3 carboxylate in the RTEM-1/benzylpenicillin complex. The two charged groups are separated by 3.0 Å.

complexed with cephalosporin C, the carboxylate of the substrate and the imidazole of histidine 298 are separated by 5Å (23). Taking into account the uncertainty in the x-ray structure (2.3Å resolution), this indicates that in the complex these two charges could benefit from a mutually stabilizing electrostatic interaction. Class A β–lactamases do not form long-lived complexes with β–lactam antibiotics, and so there is no direct crystallographic evidence supporting interaction between the ammonium group of lysine 234 and the C3 carboxylate of the β–lactam antibiotics. Computer-generated models of β–lactam substrates bound to the class A β–lactamase active site, however, have implicated the intermolecular salt bridge in these complexes (Figure 8).

To test the hypothesis that the C3 carboxylate and the ammonium group of lysine 234 in RTEM-1 β–lactamase interact electrostatically in enzyme/substrate complexes, and to make specific assessments of the catalytic and structural roles of lysine 234 in the function of RTEM-1, we have performed site-saturation mutagenesis at lysine 234 and have characterized the structural and functional properties of some key mutants.

Materials and Methods

Enzymes and Chemicals

Restriction enzymes, T4 DNA ligase, T4 polynucleotide kinase, and buffers for each enzyme were purchased from International Biotechnologies, Inc. (New Haven, CT) (IBI) or Boehringer Mannheim Biochemicals (BMB). All β–lactam antibiotics were from Sigma Chemical Company. Kanamycin sulfate was from BMB. (^{35}S)-ATP

was from Amersham. Isopropyl-β-D-thiogalactoside (IPTG) was from IBI.

Bacterial Strains

Plasmid pBR322-Xho and derivatives were harbored in *E. coli* strain HB101. Plasmid pJN and derivatives were harbored in *E. coli* strain D1210. Cells were propagated on L broth (10 g tryptone, 5 g yeast extract, and 5 g in one litre) or for protein expression experiments X broth (25 g Bactotryptone, 7.5 g yeast extract, 20 ml 1 M Mg_2SO_4, and 50 ml 1 M Tris-HCl pH 7.5 per litre).

Computer Modeling

Molecular modeling was carried out on an Evans and Sutherland ES390 graphics terminal and a Digital Equipment Incorporated VAXstation 3500 operating Biograf V2.1 available from BioDesign Inc. (Pasadena, CA). Specific methods have been described previously (24)

Site-Saturation Cassette Mutagenesis at Lysine 234

The site-saturation technique for introducing multiple mutations at a single site in the amino acid sequence of a protein is well established (25-27). Using this method, the 20 natural amino acids were introduced at position 234 in the pBR322 encoded RTEM-1 β–lactamase protein. Degenerate duplex DNA oligonucleotides, which code for all 20 amino acids and the amber codon at position 234, were synthesized by incorporating equimolar amounts of all four bases at the first and second positions of the lysine 234 codon and equimolar amounts of G and C at the third position of the lysine 234 codon (Figure 9). In a three-piece ligation the library of 32 double-stranded synthetic DNA oligomers, each having 49

base-paired nucleotides, was inserted between a unique *Xho*1 and a *Bgl*1 restriction site of the plasmid pBR322-Xho provided by William J. Healey and Kim O'Connor (Figure 9).

Preparation of Plasmid DNA

Plasmids were purified from bacterial cultures by the alkaline lysis method (28). Large-scale preparations (500 ml cultures) were purified by cesium chloride gradient ultracentrifugation (0.95 g/ml CsCl, 20 h, 45,000 rpm) using established procedures (29). For small-scale preparations (2 ml cultures), cells were grown to saturation, pelleted, incubated at room temperature in 100 µl of solution I (50 mM glucose, 25 mM Tris-HCl pH 8.0, 10 mM EDTA, 1 mg/ml lysozyme) for approximately five minutes at room temperature, resuspended in 200 µl of solution II (0.2 N NaOH, 1% SDS) and incubated on ice for approximately five minutes. 150 µl of solution III (60 ml 5M KOAc, 11.5 ml AcOH, to 100ml) were added, the precipitate was removed by centrifugation, the supernatant was extracted with 200µl of 1:1 phenol/chloroform, and the sample was ethanol precipitated. The resulting DNA was used for both restriction analyses and sequencing reactions.

Restriction Digests of Plasmid DNA

Restriction digests were performed under the recommended conditions, using the buffers provided by IBI or BMB. Typically about 1 µg of plasmid DNA (25% of a 2 ml prep) was digested with 5 to 10 units of enzyme in a total volume of 20 µl for at least 2h at 37°C. Restriction analyses were performed by standard procedures on 1.2% agarose gels (30). Restriction fragments for use in ligation reactions were prepared by digesting 20µg of DNA, separating

restriction fragments on agarose gels, excising bands containing the desired DNA, and isolating the DNA with a UEA electroeluter (IBI) (31).

Oligonucleotide Synthesis and Purification

Oligonucleotides were synthesized by the Caltech Microchemical Facility or the University of Southern California School of Medicine. Oligonucleotides were purified by preparative polyacrylamide gel electrophoresis (15% acrylamide, 1mm thick gel, 0.07 μmoles per lane, 500 volts, 12 to 16 h) using standard procedures (32). Gels were visualized by UV shadowing with fluorescent TLC plates. The high molecular weight band in each purification was excised, crushed, and incubated overnight in 3 ml of 2 M NaCl buffered at pH 7.0 with 10 mM Tris-HCl. The samples were desalted on G-25 Sephadex spin columns, and concentrations were measured by UV spectroscopy.

Kinasing and Annealing of Oligonucleotides

100 picomoles of each purified oligonucleotide were incubated in 25 μl of IBI kinase buffer with 5 units of T4 polynucleotide kinase for 1 h at 37°C. Reactions were terminated by heating to 65°C for 10 min. Pairs of complementary oligonucleotides were annealed by mixing the kinase reactions, diluting to 100 μl with medium salt buffer (10 mM Tris-HCl pH 7.5, 10mM Mg Cl_2, 50 mM NaCl, 1mM EDTA), heating to 95°C, and using a 2 litre water bath, allowing the reactions to cool over a period of about 1.5 h to room temperature. The resulting duplex oligomers were used in ligation reactions with no further purification.

Ligation of Restriction Fragments and Synthetic DNA Inserts

The three-fragment ligation (Figure 9), was carried out as follows. Approximately 0.04 pmol of *Xho*1/*Bam*H1 3051 base pair fragment and 0.04 pmol *Bam*H1/*Bgl*1 1256 base pair fragment were combined with 0.4 pmol kinased duplex oligomer prepared as described above. The mixture was incubated overnight at 16°C in 10 mM Tris-HCl, pH 8.0, 5 mM $MgCl_2$, 5 mM DTT, 1 mM ATP, and 5U of T4 DNA ligase in a total volume of 25 µl.

Transformation of Ligated DNA

Competent *E. coli* HB101 were prepared and transformed using established procedures (33). Typically 10 µl of each ligation reaction were used to transform 200 µl of competent cells.

Sequencing of Plasmid DNA

Plasmid DNA was sequenced by the Sanger method with the United States Biological (USB) Sequenase kit according to the manufacturer's recommended procedures (34). About 2 µg of double-stranded DNA (25% of the yield obtained from 2 ml cultures as described above) were denatured by boiling for 4 min with sequencing primer (5 µl of 0.07 µmoles of crude oligonucleotide per 750 µl 10 mM Tris-HCl pH 7.0) and immediately put on dry ice/ethanol. The 10 µl mixtures were thawed and sequenced using minor modifications to the USB potocol provided with the Sequenase kit. Reactions were analyzed on 5% polyacrylamide gels and visualized by standard autoradiographic procedures (35).

Protein Expression

Mutant β–lactamase genes were subcloned into the expression plasmid pJN (36) by inserting the *Bam*H1/*Eco*R1 restriction fragment

of pJN, which contains the *tac* promoter and the kanamycin resistance gene, in place of the tetracycline resistance gene of pBR322 (Figure 10). Typically, 1-litre cultures (grown in XB broth: 25g Bactotryptone, 7.5 g yeast extract, 20 ml 1 M Mg_2SO_4 and 50 ml 1 M Tris-HCl pH 7.5 per litre) of *E. coli* strain D1210 harboring the mutant pJN plasmids were grown to late log phase when IPTG was added to a final concentration of 0.1 mM. The cultures were incubated for an additional 45 min and pelleted at 10,000 rpm in a GSA rotor. Osmotic extrusion of periplasmic proteins containing the crude β–lactamase mutants was accomplished by modifications of established procedures (37). Pellets from 1-litre cultures were suspended in 60 ml ice cold sucrose solution (25 ml 1 M Tris-HCl, pH 7.0, 450 g sucrose, 0.5 g Na_2EDTA per 1 litre) and stirred for approximately 30 min at 4°C. Cells were pelleted (10,000 rpm, GSA rotor, 20 min), resuspended in 60 ml of ice cold water, stirred for 30 min, and pelleted again (13,000 rpm, GSA rotor, 30 min). The supernatant was filtered (0.2μ), concentrated by ultrafiltration (Amicon YM10 membrane, 10 kD MW cutoff) to between 5 and 10 ml, and fractionated with FPLC ion-exchange chromatography as described below.

Protein Purification

The purification protocol for RTEM-1 and mutants described below is the fruit of a series of experiments designed to optimize the preparative separation of these proteins and to investigate the effects of pH, the identity of the counter ion, the type of buffer, and the type of column used in the ion-exchange chromatography.

After extrusion from the periplasmic space as described in "***Protein Expression,***" mutant and wild-type RTEM-1 β–lactamases were purified by ion-exchange chromatography. Extrudates were filtered (0.2μ), then typically the equivalent of one half of a one litre culture (2 ml of the concentrated extrudate) was applied to a Pharmacia MonoQ HR10/10 anion-exchange column. Separation conditions and buffers were: flow rate, 1ml/min; temperature, 4°C; Buffer A, 25 mM triethanolamine-HCl (TEA-HCl), pH 7.65; Buffer B, 25 mM TEA-HCl, 1 M sodium chloride, pH 7.65. The gradient was t=0 min, 100% A; t=3 min, 100% A; t=28 min, 81% A, 19% B; t=33 min, 100% B. Purity of fractions was assessed by polyacrylamide gel electrophoresis (PAGE) with Coomassie blue staining.

Phenotypic Screening Techniques

Cultures of *E. coli* strain HB101 harboring plasmid pBR322 containing mutant β–lactamase genes were grown to saturation, diluted 10^5-fold, and plated on agar containing concentrations of ampicillin, benzylpenicillin, cephalosporin C or cephalothin that varied from 10 to 100 μg/ml (cephems) or 10 to 2500 μg/ml (penams). Plates were incubated overnight and the number of growing colonies was counted to estimate the maximum concentration upon which mutants retained the ability to confer resistance on the HB101 host bacteria.

Circular Dichroism Spectroscopy

All circular dichroism (CD) spectra were measured with a Jasco model J600 spectropolarimeter interfaced with an IBM model 50 PS2 computer operating the Jasco V1.37 software package. Unless otherwise stated, instrument parameters for wavelength-based

acquisitions were set as follows: band width 2 nm, scan rate 20 nm min^{-1}, time constant 2 sec, number of scans 1. Spectra were measured at room temperature in 100mM potassium phosphate buffer pH 7.0 using a 10mm path length cell. Instrument parameters and other methods employed for time-based acquisitions are described below and in Chapter 4.

Reaction Kinetics

Steady-state kinetic parameters for wild-type and mutants of RTEM-1 were measured using a novel method, the development of which is described in Chapter 4. The method is based on changes in chiroptical properties of penam and cephem antibiotics upon hydrolysis of the β–lactam chromophore. The rigid fused ring system of these compounds puts the β–lactam chromophors in asymmetric environments, giving them strong CD spectra, which are eliminated upon hydrolysis (Figure 11).

Using a Jasco J600 spectropolarimeter in the time-based acquisition mode, rates of ampicillin hydrolysis were monitored at 234.0 nm where the molar ellipticity [θ] of ampicillin is maximal at $[\theta]=4.38X10^2$ deg $M^{-1}\,cm^{-1}$, and the molar ellipticity of the hydrolysis product is undetectable (Figure 11) ([θ] is defined as $[\theta]=\theta/cl$ where θ is the measured ellipticity in degrees, c is the molar concentration, and l is the path length in cm) (38). Reaction conditions were: 100 mM potassium phosphate buffer, pH 7.0, ionic strength 125 mM, 30°C. Initial velocity data were collected during the linear portion of each reaction, typically between the first 20 to 60 seconds. Substrate concentrations were varied from approximately five times K_M to one half the K_M value in all analyses. Initial velocity data were analyzed

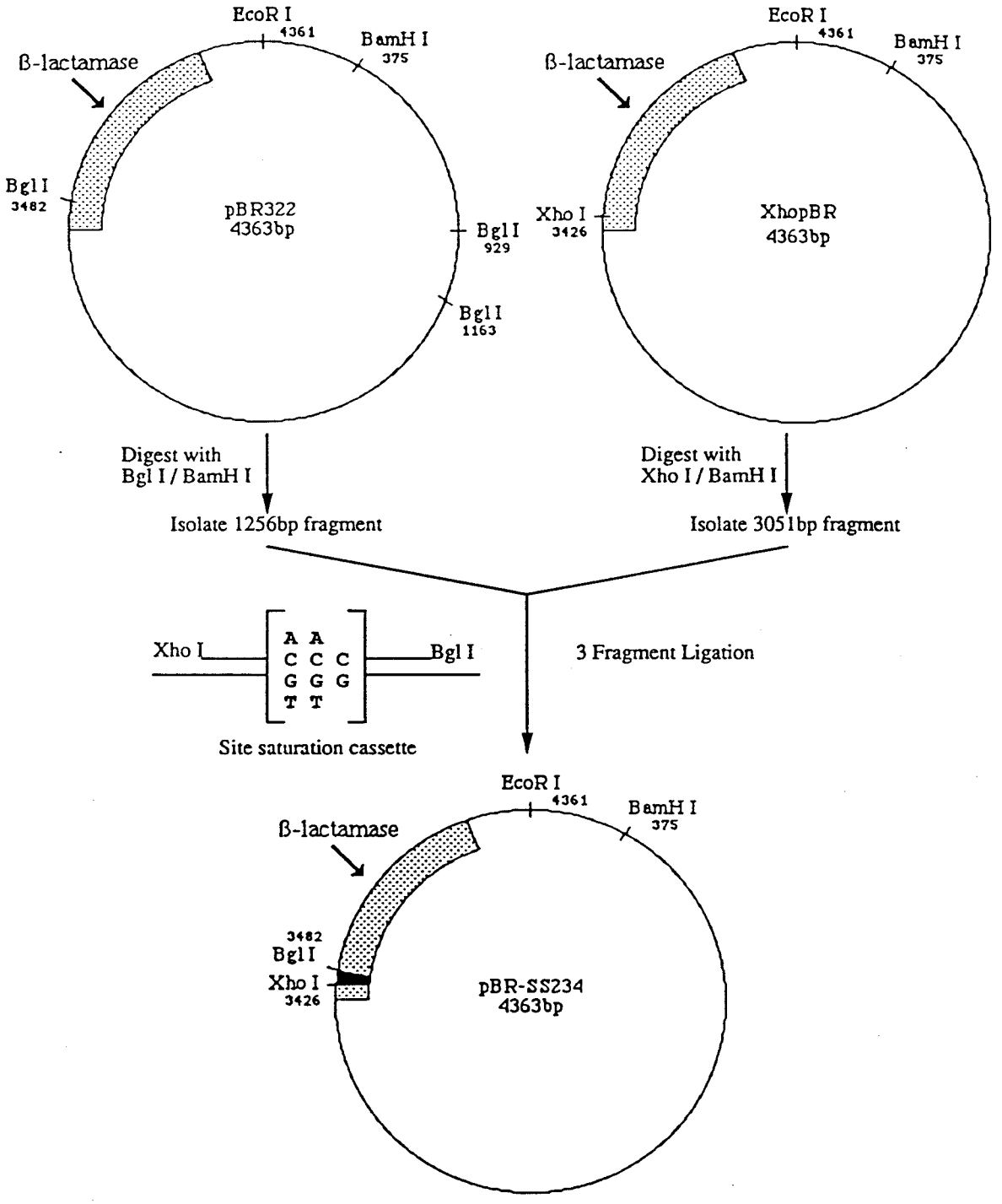

Figure 9. The three-fragment ligation scheme used to site-saturate lysine 234 in RTEM-1 β–lactamase.

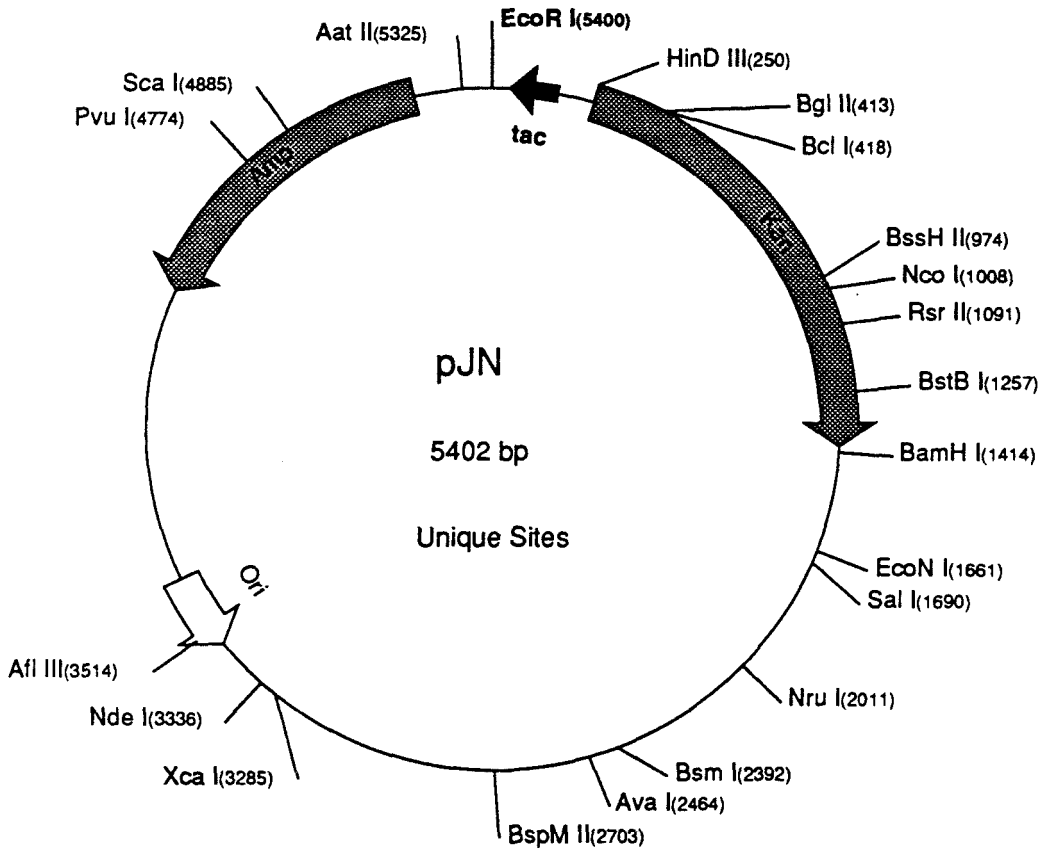

Figure 10. Restriction map of the expression plasmid pJN (36). Mutant β-lactamase genes were subcloned by inserting the *EcoR*1/*Bam*H1 1416 base pair fragment of pJN between the *EcoR*1 and *Bam*H1 sites of pBR322.

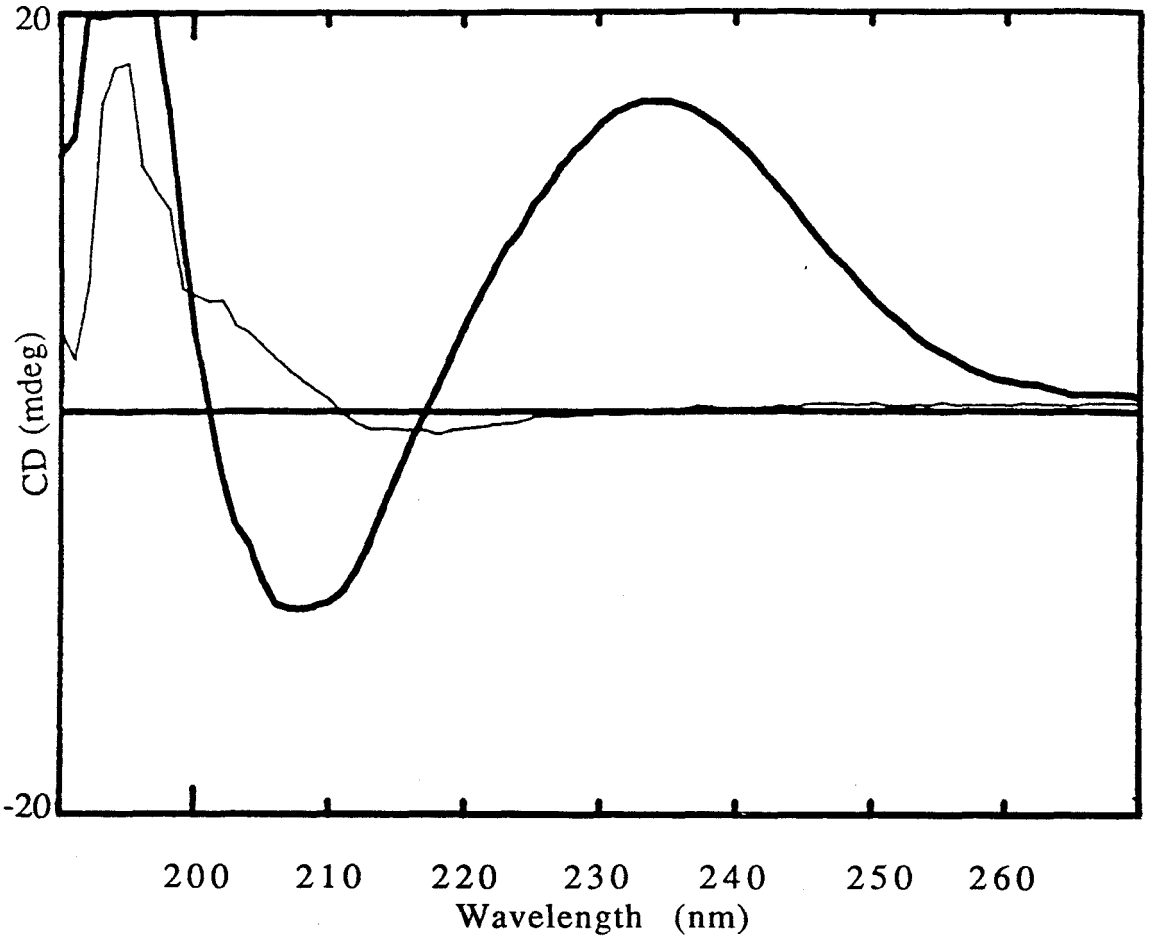

Figure 11. CD spectra of 0.5 mM ampicillin (heavy line) and 0.5 mM hydrolyzed ampicillin (light line).

by Hanes Plots (39). The steady-state kinetic parameters for hydrolysis of benzylpenicillin were measured using the methods described here for ampicillin, except that hydrolysis was monitored at 231.8 nm as described in Chapter 4.

Results

Site-Saturation at Lysine 234

The site-saturation cassette mutagenesis method was used to introduce 18 of the possible 19 mutant amino acids at position 234 in RTEM-1 β-lactamase. Plasmids from approximately 210 tetracycline-resistant transformants were sequenced in efforts to identify all 19 mutations expected at position 234. The unidentified mutant is K234W.

Phenotypic Screening

The abilities of mutant β-lactamases to confer resistance to ampicillin, benzylpenicillin, cophalothin, and cephalosporin C on *E. coli* HB101 was assessed by determining the maximum concentration of antibiotic upon which mutant colonies are able to grow on agar plates. Phenotypic data are recorded in Table 1. The mutant most resistant to the effects of the penam antibiotics is K234R, which grows on 1250 and 1750 μg/ml of ampicillin and benzylpenicillin, respectively, as compared to wild type, which grows on well over 2000 μg/ml of each of these antibiotics. The K234R mutant is no more resistant to the cephem antibiotics (cephalosporin C and cephalothin) than the other lysine 234 mutants. None of the mutants have any detectable resistance to cephalothin. With the exception of K234V and K234A, which have resistant phenotypes to 50 μg/ml of

cephalosporin C, all other mutants have resistant phenotypes to 60 μg/ml of cephalosporin C.

Protein Purification

For wild-type and mutant β–lactamases, a purification procedure was developed based on the well-known osmotic extrusion method followed by fractionation of crude periplasmic proteins by FPLC using a Pharmacia MonoQ anion-exchange column. Using the optimized separation conditions, wild type and mutants of RTEM-1 eluted with retention times of approximately 17 minutes (Figure12). All detectable β–lactamase activity eluted with this prominent peak (Figure 13). The yield of wild-type and mutant proteins was similar at from 1 to 3 mg of protein per liter of cell culture. As judged by PAGE (Coomassie blue staining) and scanning densitometry, the purity of proteins prepared by these methods was greater than 99.9%, the major impurity being a low molecular weight protein (between 3 and 8 kD) that was not detected in all preparations.

Circular Dichroism of Mutant Proteins

The CD spectra for three RTEM-1 mutants at position 234 are compared to the spectrum of wild-type in Figure 14. The spectra of the mutants are essentially identical to that of the wild-type enzyme. This result indicates that mutations at position 234 do not significantly disrupt the native secondary structure of RTEM-1. The spectra are not, however, necessarily sensitive to subtle changes in tertiary structure caused by the mutations.

Kinetic Properties of Mutant Proteins

The steady-state kinetic parameters of four RTEM-1 mutants and the wild-type enzyme were measured using a novel kinetic method

Table 1. Phenotypic activity of lysine 234 mutant RTEM-1 β–lactamases. Numbers given are the highest concentration (μg/ml) of antibiotic on which mutant colonies grew. Abbreviations are AP, ampicillin; BP, benzylpenicillin; CO, cephalothin; CC, cephalosporin C.

Amino Acid at 234	AP	BP	CO	CC
Wild Type (lysine)	2000	2000	50	100
Ala	15	35	0	50
Arg	1250	1750	0	60
Asn	15	25	0	60
Asp	15	35	0	60
Cys	15	35	0	60
Gln	10	25	0	60
Glu	10	25	0	60
Gly	10	25	0	60
His	0	35	0	60
Ile	15	35	0	60
Leu	0	35	0	60
Lys	2000	2000	30	100
Met	15	35	0	60
Phe	0	25	0	60
Pro	0	25	0	60
Ser	10	25	0	60
Thr	15	35	0	60
Trp	NA	NA	NA	NA
Tyr	0	35	0	60
Val	15	35	0	50

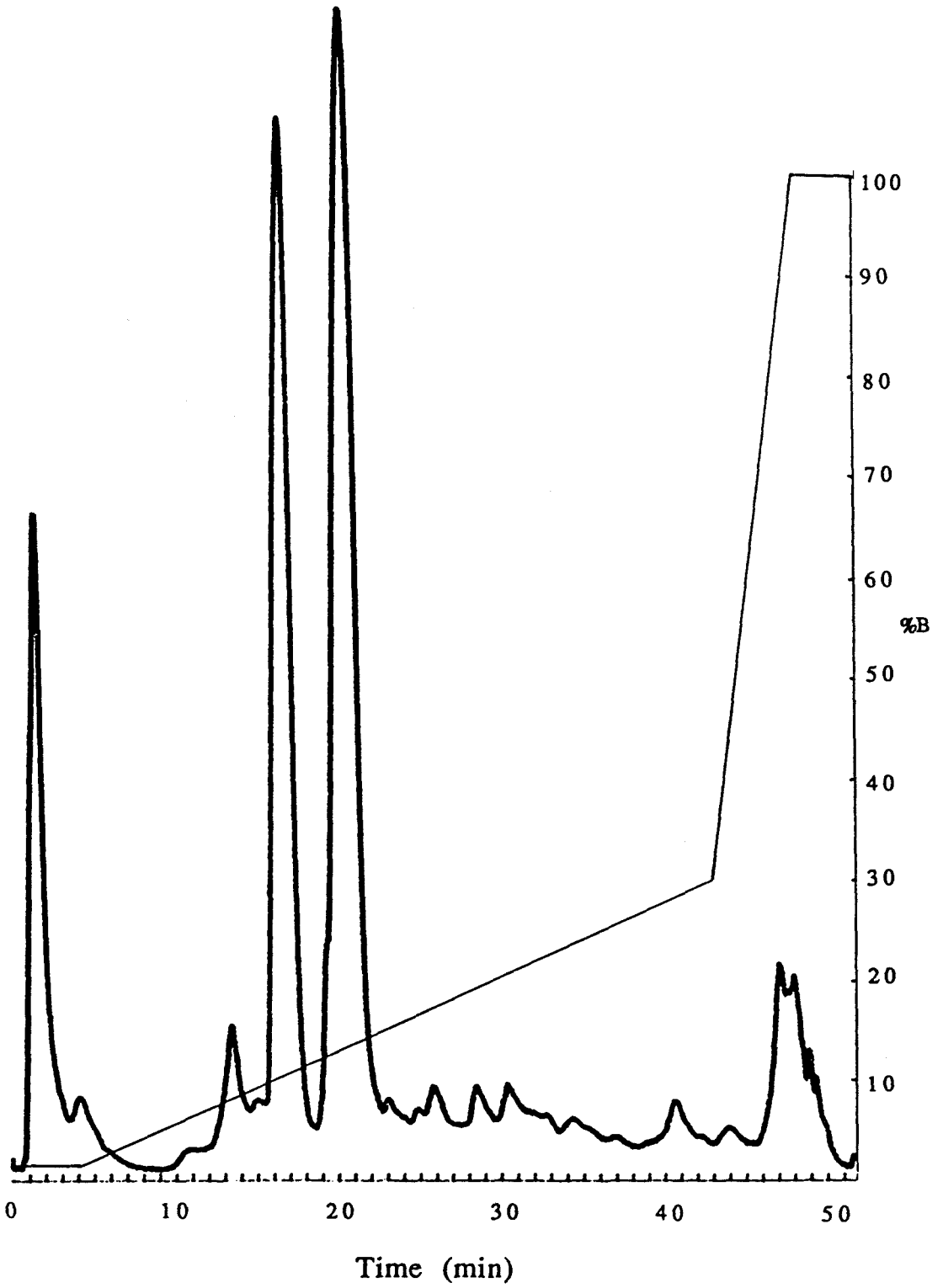

Figure 12. FPLC chromatogram of crude periplasmic proteins prepared as described in the text. The prominent peak at 17 min is wild type RTEM-1 β–lactamase.

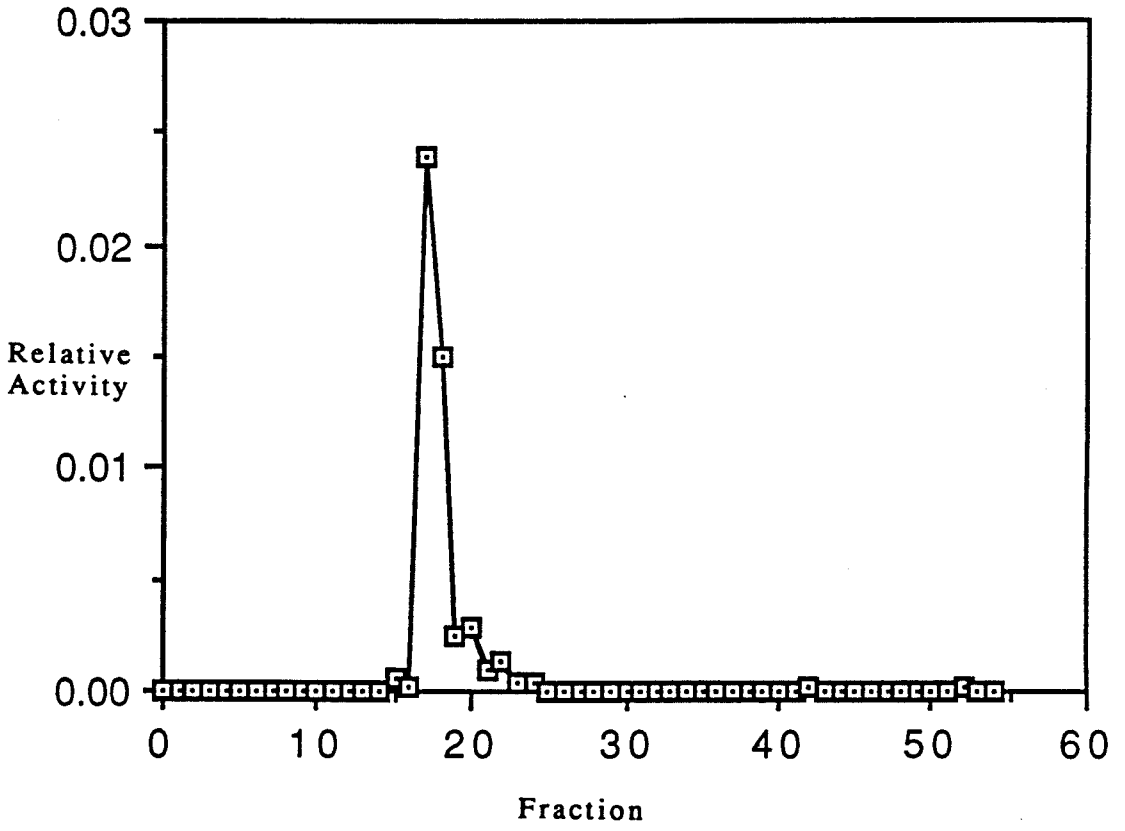

Figure 13. Activity profile of chromatogram in Figure 12. Activity is hydrolysis rate towards benzylpenicillin.

Figure 14. CD spectra of three lysine 234 mutants and wild-type RTEM-1 β–lactamase. Spectra were measured at room temperature, 100 mM potassium phosphate buffer, pH 7.0. Within error caused by base line variability, the spectra are identical.

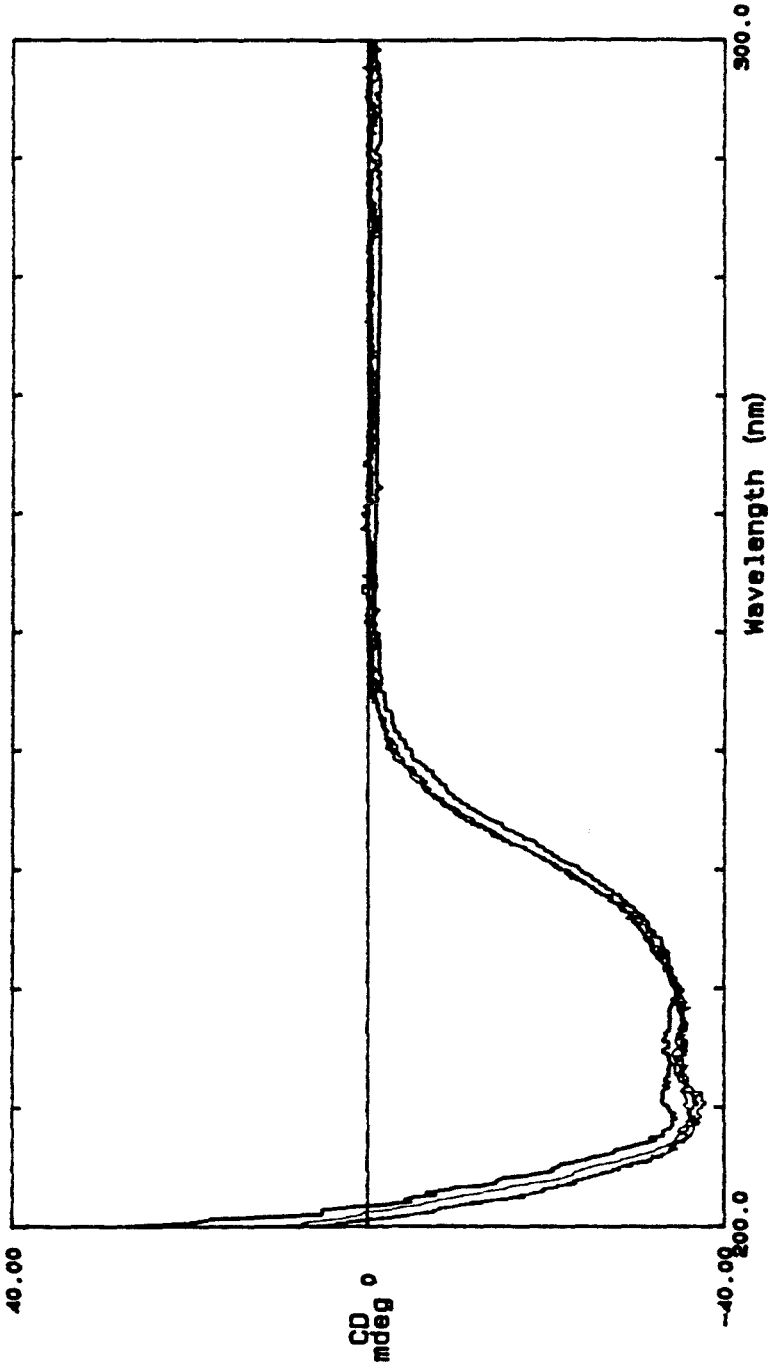
40.00
CD
mdeg 0
-40.00
200.0
300.0
Wavelength (nm)

Table 2. Steady-state rate constants for hydrolysis of ampicillin by wild type and mutants of RTEM-1 β–lactamase. Conditions were pH 7.0, 30°C. Units are k_{cat}, s^{-1}; K_M, μM; k_{cat}/K_M $s^{-1}M^{-1}$. Values marked with an asterisk (*) were measured by S. S. Carroll.

Enzyme	k_{cat}	K_M	k_{cat}/K_M	rel.
K234K (WT)	1482	10.50	$1.41X10^{8}$	1.00
K234E	1553	14000	$1.11X10^{5}$	$7.82X10^{-4}$
K234V	62	17600	$3.52X10^{3}$	$2.49X10^{-5}$
K234R	951	133	$7.15X10^{6}$	$5.07X10^{-2}$
K234Q	138	22000	$6.27X10^{3}$	$4.42X10^{-5}$
K73R*	0.30	43	$6.98X10^{3}$	$4.92X10^{-5}$
K73C*	0.25	21	$1.19X10^{4}$	$8.38X10^{-5}$

based on CD spectroscopy (Chapter 4). The k_{cat} and K_M values of K234E, K234R, K234V, and K234Q mutants are collected in Table 2. These data show that mutations at position 234 primarily affect the apparent ability of the wild-type enzyme to bind ampicillin.

Substituting lysine 234 of the wild-type enzyme with glutamate, valine, or glutamine, causes an increase of at least three orders of magnitude in the K_Ms of these enzymes. Substituting the positively charged lysine 234 of the native enzyme with arginine, also a positively charged residue, has a smaller effect on the apparent ability of the enzyme to bind ampicillin, as indicated by the 10-fold larger K_M of this mutant compared to wild-type. The ability of RTEM-1 to catalyze hydrolysis of ampicillin under pseudo-first-order conditions is relatively unaffected by mutations at position 234. Of the four mutations analyzed, none results in a reduction in k_{cat} by more than a factor of 24 over the value of the wild-type enzyme. K234E suffered the largest decrease in k_{cat}, while the data collected for K234R and K234E shows, within experimental error, that these mutations do not affect the ability of the native enzyme to catalyze the reaction under saturating substrate concentrations. The average relative activity ([k_{cat}/K_M mutant]/[k_{cat}/K_M wild-type]) of the "charged mutants" (K234E and K234R) is about 1000 times that of the "neutral mutants" (K234Q and K234V) (Table 2).

Discussion

We have used site-directed mutagenesis to understand how RTEM-1 β–lactamase binds and catalyzes the hydrolysis of β–lactam antibiotics. This assessment of the role of lysine 234 in catalysis by

RTEM-1 answers some fundamental questions concerning general properties of electrostatic interactions in proteins and specific features of the class A β–lactamase mechanism:

1. Is lysine 234 essential for maintaining structural stability of RTEM-1 β–lactamase?

2. Does lysine 234 participate in substrate binding or catalysis by RTEM-1 β–lactamase?

3. What are the effects of replacing lysine 234 with other amino acids on RTEM-1 activity?

4. Does the ammonium group of lysine 234 interact electrostatically with the β–lactam antibiotics?

5. How much free energy of binding does the putative salt bridge provide in the ground-state Michaelis complex?

6. How much does the salt bridge stabilize the rate-limiting transition state as compared to the ground-state Michaelis complex?

7. What is the effective dielectric constant in the active site of RTEM-1?

Three observations imply that the mutations at position 234 do not significantly disrupt the folded structure of the enzyme. First, the resistances of the mutant colonies are reduced *uniformly*. If the reduced activity was a result of destabilization of the folded protein with a concomitant increase in susceptibility to cellular protease activity, one would expect that conservative mutations (hydrophilic residues) would have less pronounced effects than nonconservative mutations (hydrophobic or negatively charged residues). Second,

four mutants purified by ion-exchange chromatography have the same retention time on anion-exchange columns and yields comparable to wild type were obtained for each. Yields would decrease and retention times would change if the mutations caused partial unfolding of the enzyme. Third, the CD spectra of three mutants, two with nonconservative substitutions (K234V and K234E) and one with a relatively conservative substitution (K234Q), are identical to that of the wild-type enzyme (Figure 14). While these observations indicate that mutating the lysine 234 surface residue does not cause significant disruptions in the secondary structure of the wild-type enzyme, they do not preclude subtle changes in tertiary structure that could significantly alter the catalytic properties of the enzymes.

Phenotypes of mutants at position 234 in RTEM-1 indicate that the best substitute for lysine 234 is arginine, since all other mutations have more severely deleterious effects on the *in vivo* activity of the enzyme (Table 1). With the notable exception of the arginine mutant, phenotypes are indistinguishable and independent of the identity, and thus the physical characteristics of, the side chain with which lysine 234 is replaced. We conclude that negative, neutral, and histidine substitutions have comparable *in vivo* activities and that a positive charge about four methylene units distant from the α–carbon of residue 234 is a requirement for *in vivo* activity sufficient to confer high resistance to the β–lactam antibiotics on the host *E. coli.* HB101.

The steady-state kinetic parameters were measured for four mutant enzymes in which the positively charged lysine 234 was

substituted with either of two neutral side chains, a negatively charged side chain, or a positively charged side chain (Table 2). The neutral and negative mutations (K234Q, K234V, and K234E) increase the Michaelis constant (K_M) for ampicillin hydrolysis by over three orders of magnitude, but have only small effects on the enzyme's ability to catalyze the reaction under saturating (pseudo-first-order) conditions. The positive mutation (K234R) causes the smallest increase in K--an order of magnitude--and within experimental error, no reduction in k_{cat}.

Although the steady-state rate constants for these mutants are directly related to their binding and catalytic properties, the commonly held assumption that the Michaelis constant (K_M) is equal to the equilibrium-binding constant (K_S) is not valid for wild-type RTEM-1 and is not necessarily valid for mutants of this enzyme. The K_M, given in terms of elementary rate constants in Figure 15, is 44% of K_S for benzylpenicillin and wild-type RTEM-1 (40). This is because the first-order rate constant for breakdown of the enzyme/substrate complex, k_{-1}, is comparable to both k_2, the first-order rate constant for acylation, and k_3, the first-order rate constant for deacylation of the active-site serine. Based on the following reasoning, the K_S values of the lysine 234 mutants can be approximated as two times the experimentally determined K_M values.

Since the mutant k_{cat}s are comparable to the wild-type value, neither the rate of deacylation (k_3) nor the rate of acylation (k_2) is slowed significantly by mutation (k_{cat} is the lower limit on these elementary rate constants). For any single mutant, either k_2 or k_3 could be faster than the wild-type rates, *but not both*, since this

would be manifested as an increase in k_{cat}, which is not observed. It appears unlikely, however, that any of the mutations would cause significant increases in k_2 or k_3, since these reactions require an active-site geometry with a precisely positioned oxyanion hole, nucleophilic serine, and other important catalytic residues that if disrupted by mutation, would less effectively stabilize transition states.

The identical k_{cat}s of the mutants and the wild-type enzyme indicate that at least one of the rate constants remains unperturbed by the mutations. It would be surprising if the mutations have a marked effect on k_2 but no effect on k_3 (or *vice versa*). Furthermore, if the mutations did affect k_2 or k_3, then substituting lysine 234 with amino acids having a wide range of physical properties such as charge, steric bulk, and hydrophilicity, should have differential effects on the rates, which they do not.

The rate of dissociation of the ground-state enzyme/substrate complex (k_{-1}) is probably greater for the mutants than for the native enzyme, because eliminating the putative stabilizing influence that lysine 234 has on the Michaelis complex would increase the free energy of the complex more than the energy of the dissociated species. Thus K' (Figure 15) for the mutants is approximately k_{-1}/k_1, the equilibrium-dissociation constant, and $k_3/(k_2+k_3)$ is about 0.5, since as is the case with the wild-type enzyme, k_2 and k_3 for the mutants, according to the previous argument, must be approximately equal. Although the mutations might affect k_1, the rate of formation of the enzyme/substrate complex, this does not change the fractional contribution that K_S makes to K'. To summarize, since k_2 and k_3 are

neither increased nor decreased significantly by the mutations, and since k_{-1} is probably increased by the mutations, to a good approximation the mutant equilibrium-dissociation constants (Ks) are two times the experimentally determined K_M values.

Using Equation 2, the free energy difference between the wild-type Michaelis complex and four mutant complexes were calculated from the experimentally determined K_M values (Table 3) (41).

$$\Delta\Delta G_{app} = -RT\ln(K_{Mmt}/K_{Mwt})$$

Equation 2. $\Delta\Delta G_{app}$, the measured change in free energy of formation of the ground state enzyme/substrate complex caused by a mutation. K_{Mmt} is the Michaelis constant for the mutant, K_{Mwt} is the Michaelis constant of wild type. Since both K_Ms are about twice the equilibrium dissociation constants $\Delta\Delta G_{app} = \Delta\Delta G_{bind}$ (see text for explanation).

The increase in free energy for the ground-state ampicillin/K234E complex relative to the wild-type/ampicillin complex, $\Delta\Delta G_{app}$, is 4.32 kcal mol^{-1}. This energy is not necessarily equal to the stabilizing energy of a specific interaction, $\Delta\Delta G_{bind}$, for example, a salt bridge or hydrogen bond, between the substrate and lysine 234. In general, apparent binding energies measured from amino acid substitution experiments do not accurately reflect the incremental binding energy attributable to the wild-type amino acid, and assuming so can lead to inaccurate estimates of incremental binding energies (42).

In the present case the lysine 234 mutants not only are deprived of the benefits of interacting favorably with the substrate through

the lysine 234 side chain; they also have to contend with the effects of the substrate interacting with the replacement side chain, which for some mutants might be a favorable and for others an unfavorable interaction. The apparent change in binding energy ($\Delta\Delta G_{app}$) resulting from a mutation at position 234 that does not perturb the enzyme structure is the difference of the free energy of the mutant side chain interacting with the substrate ($\Delta\Delta G_{mt}$) and the wild-type side chain interacting with the substrate ($\Delta\Delta G_{bind}$):

$$\Delta\Delta G_{app} = \Delta\Delta G_{mt} - \Delta\Delta G_{bind}$$

$\Delta\Delta G_{mt}$, like $\Delta\Delta G_{bind}$, is composed of two free energy terms, the free energy of transferring the substrate from bulk solvent to the active site (ΔG_S), and the free energy of transferring the active site to the bound substrate (ΔG_E):

$$\Delta\Delta G_{mt} = \Delta G_S + \Delta G_E$$

If the wild-type side chain has been effectively truncated by the mutation, it does not interact with the bound substrate, and so ΔG_E is zero. If the bound substrate remains exposed to bulk solvent in the Michaelis complex, then ΔG_S is also zero and consequently, $\Delta\Delta G_{app}$ can be approximated as $\Delta\Delta G_{bind}$.

For the lysine 234 mutants, phenotypic data, kinetic data, and molecular modeling indicate that $\Delta\Delta G_{mt}$ is zero, and so $\Delta\Delta G_{app}$ is approximately $\Delta\Delta G_{bind}$, the incremental binding energy provided by the side chain of lysine 234. The indistinguishable phenotypes of the 234 mutants (with the notable exception of K234R) suggests that the mutant side chains do not affect the catalytic properties of the enzyme, including its ability to bind the substrate. This is not surprising, considering that the mutations effectively truncate the

four-carbon methylene linker between the α–carbon and ammonium group that is characteristic of the wild-type lysine residue. Molecular modeling of mutations at position 234 indicates that mutant side chains are too distant from the bound substrate to affect binding, and that the carboxylate of the substrate is at least partially exposed to bulk solvent in the Michaelis complex. The most convincing evidence that supports inconsequential roles for the mutant side chains, that is $\Delta G_{E=0}$, comes from kinetic data, which show that whether the mutant side chain is neutral/hydrophilic, neutral/hydrophobic, or negatively charged, the apparent change in binding energy is the same. This indicates that mutant side chains are not close enough to interact with the bound substrate. The measured changes in apparent binding energy are, accordingly, good estimates of the incremental binding energy supplied by the substrate/lysine 234 interaction.

The approximate 4.5 kcal mol^{-1} of stabilization energy supplied by the lysine 234/substrate interaction is too large to be attributable to a single hydrogen bond between an uncharged donor and an uncharged acceptor. Fersht's group have estimated that the energies of uncharged hydrogen bonds are between 0.5 and 1.5 kcal mol^{-1}, and have determined that deleting a charged moiety of a pair that interact electrostatically weakens binding by 3 to 6 kcal mol^{-1} (43). We conclude that the ammonium group of lysine 234 in RTEM-1 β–lactamase interacts through a charged hydrogen bond with the conserved carboxylate of the β–lactam antibiotics and stabilizes the ampicillin/wild-type RTEM-1 complex by 4.5 kcal mol^{-1}.

Compiled in Table 3 are the stabilization energies that lysine 234 provides to species along the reaction pathway. $\Delta\Delta G_{bind}$ for the ground-state Michaelis complex (ES) relative to the free enzyme and free substrate (E+S), $\Delta\Delta G_{bind}$ for the rate-limiting transition state (ES*) relative to ES, and $\Delta\Delta G_{bind}$ for ES* relative to E+S are derived from the ratio of the substrate-binding constants (K_{smt}/K_{swt}), the ratio of the first-order rate constants (k_{catmt}/k_{catwt}), and the ratio of the apparent second-order rate constants ($(k_{cat}/K_s)_{mt}/(k_{cat}/K_s)_{wt}$) respectively (see Table 3 legend). The average difference in stabilization energy between ES and ES* calculated for K234Q, K234E, and K234V is only 1.1 kcal mol^{-1}. This indicates that lysine 234 in RTEM-1 β–lactamase leads to improved catalytic efficiency through uniform binding of ground- and transition-state species (44); the conserved carboxylate of the β–lactam antibiotics is a "handle" that is gripped uniformly by the ammonium "hand" of lysine 234 throughout the RTEM-1 catalyzed reaction. The idea of uniform binding of transition- and ground-state species runs almost counter-intuitive to the concept of catalysis by selective stabilization of the transition state first introduced by Haldane and later by Pauling (45,46). A limited number of mutations that reveal uniform binding of ground and transition states have been reported in the literature, including three mutations in *Bacillus stearothermophilus* tyrosyl-tRNA synthetase (T51C, Y34F, and Y169F) (47-49), three mutations in *E. coli* dihydrofolate reductase (L54I, L54G, and L54N) (50), and the notable first example of a uniform binding nucleotide in a ribozyme (the nucleotide at position -3 from the cleavage site in the *Tetrahymena thermophila* ribozyme) (51,52).

The effective dielectric constant in the RTEM-1 active site calculated from Equation 1, assuming single negative and positive charges for the substrate carboxylate and the enzyme ammonium groups, respectively, a separation distance of 3.0 Å (estimated from molecular modeling methods), and an interaction energy of 4.5 kcal mol^{-1}, is 25.

The wide range of literature values for the dielectric constants of proteins does not stem from the use of faulty experimental or theoretical methods (53-55). At the interface between protein and water, which have low and high dielectric constants, respectively, electrostatic energies are difficult to evaluate. The effective dielectric constant in the active site of RTEM-1 is not only specific to the RTEM-1 active site, but is probably also specific to the interaction between the carboxylate and ammonium groups of the said species, and is not expected to be the same for charged species that interact nearby in the active site.

The small $\Delta\Delta G_{app}$ of the arginine mutant (1.45 kcal mol^{-1}) indicates that this positive side chain is functionally equivalent to the wild-type lysine. The small decrease in stabilization energy caused by substituting lysine with arginine is surprising, considering the different steric and electronic properties of these amino acids. This result contrasts with the more dramatic decrease in activity caused by substituting lysine with histidine (Table 1). Apparently the "stubby" side chain of the latter amino acid does not allow its positive charge to come close enough to the substrate to interact in the enzyme/substrate complexes.

Ellerby *et al.* have substituted lysine 234 in β–lactamase from *Bacillus licheniformis* (BL) with glutamate and alanine and have measured the steady state kinetic parameters for the hydrolysis of ampicillin by the glutamate mutant (15). The primary structures of BL and RTEM-1 are 33% homologous overall and 75% homologous within the active-site residues, and it is believed that the two enzymes have the same tertiary fold, which has been revealed in the crystal structure of BL (57). Although the roles predicted *a priori* for lysine 234 in BL and RTEM-1 are that they perform the same function, comparison of kinetic data measured for the glutamate mutants of each enzyme reveals a distinct difference in the function of lysine 234 (Table 4). Deleting the stabilizing effects of lysine 234 increases the K_Ms of BL and RTEM-1 by two and three orders of magnitude respectively; however, because the wild-type K_M for BL is 10-fold higher than RTEM-1, both glutamate mutants have K_Ms of about 14 mM. The mutation has no effect on the k_{cat} of RTEM-1 but decreases k_{cat} of BL by two orders of magnitude, revealing that lysine 234 in BL is a differential binding residue, which contrasts to the uniform binding role it plays in catalysis by RTEM-1. Why in these two structurally and functionally equivalent enzymes would the same amino acid be recruited to stabilize different species along the reaction pathway? Moreover, how do the structures of the two proteins bring about the difference in the function of lysine 234?

Figure 16 shows how the reaction velocities catalyzed by each enzyme and the glutamine mutants vary as a function of substrate concentration. In BL, lysine 234 selectively binds the transition state, providing an advantage over RTEM-1 under conditions of high

substrate concentration when the reaction rate is limited by kcat. At low substrate concentration, lysine 234 works for RTEM-1 by binding the ground state, and so under these conditions gives RTEM-1 a selective advantage over BL. A plausible explanation for these differences is that the typical β–lactam antibiotic concentrations encountered by the *E. coli* and *B. licheniformis* hosts of RTEM-1 and BL, respectively, have influenced the divergent evolution of two enzymes that are optimized for different reaction conditions. Alternatively, the *E. coli* cell might be sensitive to lower concentrations of antibiotics than the *B. licheniformis* cell is. Precisely how the two structures alter the function of lysine 234 is more difficult to explain. The two enzymes have 18 of 24 active-site amino acids in common. Perhaps one or more of the nonconserved amino acids result in the observed difference in properties; however, it seems equally likely that variability in parts of the proteins well removed from the active sites could be responsible.

The results of these experiments support the hypothesis that the ammonium group of lysine 234 interacts electrostatically with the carboxylate of β–lactam antibiotics in enzyme/substrate complexes and support a uniform binding role for lysine 234 in catalysis by RTEM-1 β–lactamase.

$$E + S \underset{k_{-1}}{\overset{k_1}{\rightleftharpoons}} ES \xrightarrow{k_2} E\text{-}Acyl \xrightarrow{k_3} E + P$$

$$K_s = \frac{k_{-1}}{k_1} = 96\ \mu M \qquad K_m = \left(\frac{k_{-1} + k_2}{k_1}\right)\left(\frac{k_3}{k_2 + k_3}\right) = 42\ \mu M$$

$$k_{cat} = \frac{k_2 k_3}{k_2 + k_3} = 980\ s^{-1} \qquad K' = \left(\frac{k_{-1} + k_2}{k_1}\right) = 119\ \mu M$$

$$k_1 = 123\ \mu M^{-1} s^{-1}$$
$$k_{-1} = 11800\ s^{-1}$$
$$k_2 = 2800\ s^{-1}$$
$$k_3 = 1500\ s^{-1}$$

Figure 15. The acyl-enzyme mechanism of the class A β−lactamases. E is the enzyme, S is the substrate, ES is the Michaelis complex, E-Acyl is the acyl-enzyme, and P is the product. The steady-state rate constants are shown in terms of the elemental rate constants. Ks is the equilibrium dissociation constant for E and S, KM is the Michaelis constant, and kcat is the pseudo-first-order rate constant. The elemental rate constants were measured by Christensen *et al.* (40).

Table 3. Stabilization energy (kcal mol^{-1}) provided by lysine 234 to intermediates along the RTEM-1 reaction pathway. E is the free enzyme, S is the free substrate, ES is the ground-state Michaelis complex, and ES* is the rate-limiting transition state. Values for lysine 73 mutants are derived from data collected by S. S Carroll and are included for purposes of comparison.

Enzyme	ΔΔG[ES*-ES] (kcat derived)	ΔΔG[ES-(E+S)] (Ks derived)	ΔΔG[ES*-(E+S)] (kcat/KM derived)
K234K (WT)	0	0	0
K234E	-0.03	4.32	4.29
K234V	1.90	4.45	6.35
K234R	0.27	1.45	1.72
K234Q	1.42	4.59	6.01
K73R*	5.10	0.84	5.94
K73C*	5.21	0.42	5.63

Table 4. Kinetic comparison of ampicillin hydrolysis by *Bacillus licheniformis* 749/C (BL) and *E. coli* RTEM-1 (RTEM-1) β–lactamases and the K234E mutants of each. Conditions were pH 7.0, 30°C. Units are kcat, s^{-1}; KM, μM; kcat/KM $s^{-1}M^{-1}$; ΔΔG, $kcalmol^{-1}$. E is the free enzyme, S is the free substrate, ES is the ground-state Michaelis complex, and ES* is the rate-limiting transition state. BL numbers were measured by Ellerby *et al.*(15).

Enzyme	kcat	KM	kcat/KM	rel.
(wild types)				
RTEM-1	1482	10.50	$1.41X10^{8}$	1.00
BL	2241	210	$1.06X10^{7}$	1.00
(K234E mutants)				
RTEM-1	1553	14000	$1.11X10^{5}$	$7.87X10^{-4}$
BL	21.1	13700	$1.50X10^{3}$	$1.40X10^{-4}$

Enzyme	ΔΔG[ES*-ES] (kcat derived)	ΔΔG[ES-(E+S)] (Ks derived)	ΔΔG[ES*-(E+S)] (kcat/KM derived)
RTEM-1			
K234E	0.0	4.3	4.3
BL			
K234E	2.8	2.5	5.3

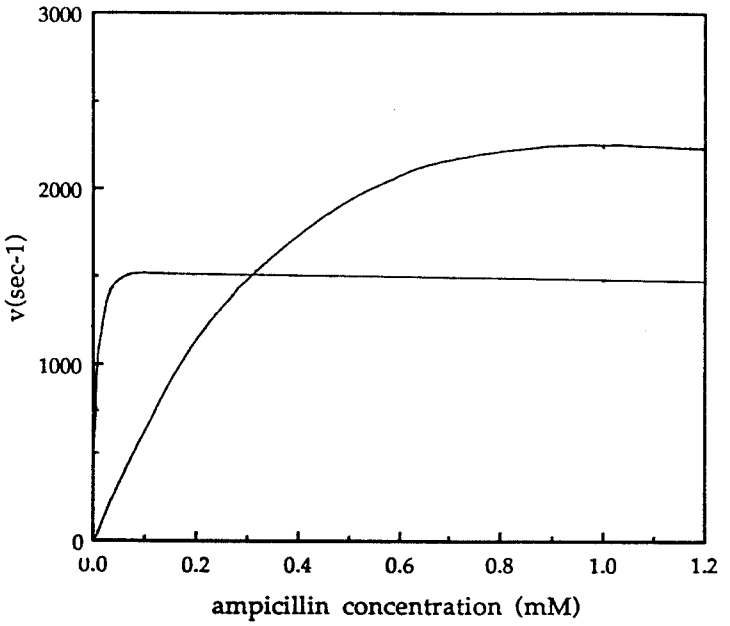

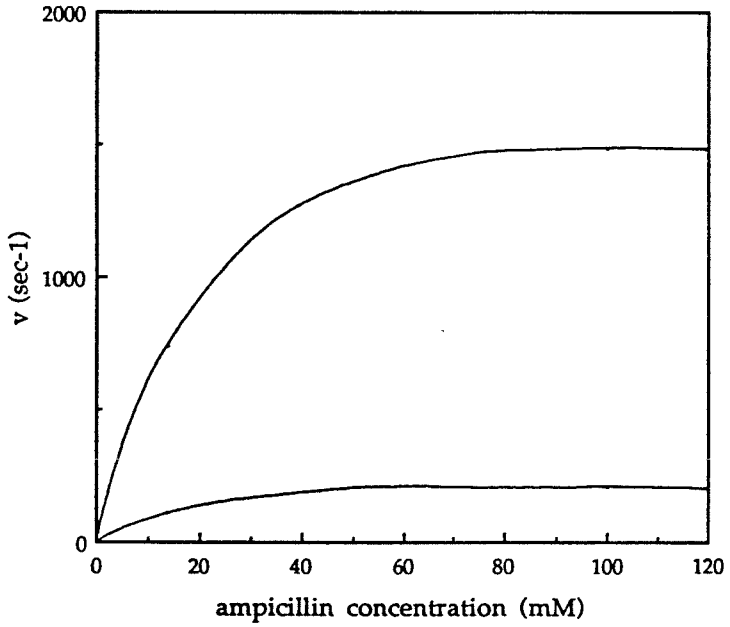

Figure 16. Plot of reaction velocity (v) vs. substrate concentration (s) for (a) wild type *Bacillus licheniformis* 749/C (BL) and *E. coli* RTEM-1 (RTEM-1) β–lactamases and (b) the K234E mutants of each enzyme. In (b) the BL rates have been multiplied by 10X for illustrative purposes.

References

1. Arnone, A.(1972) *Nature (London)*, **237**, 148.
2. Bode, W. and Schwager, P. (1975) *J. Mol. Biol.*, **98**, 693.
3. Middleton, S. and Kantrowitz, E. (1988) *Biochemistry*, **27**, 8653.
4. Fersht, A. (1989) *Biochemistry*, **28**, 6841.
5. Lowe, D., Winter, G., and Fersht, A. (1987) *Biochemistry*, **26**, 6038.
6. Cronin, C. and Kirsch, J. (1988) *Biochemistry*, **27**, 4572.
7. Graf, L., Craik, C., Patthy, A., Roczniak, S., Fletterick, R., and Rutter, W. (1987) *Biochemistry*, **26**, 2616.
8. Warshel, A. (1978) *Proc. Natl. Acad Sci. U.S.A.*, **75**, 5250.
9. Kraut, J. (1977) *Annu. Rev. Biochem.*, **46**, 331.
10. Schulz, G. and Schirmer, R. (1979) *Principles of Protein Structure*, Springer-Verlag, New York, p. 31.
11. Gilson, G. and Honig, B. (1987) *Nature (London)*, **330**, 84.
12. Mehler, E. and Eichele, G. (1984) *Biochemistry*, **23**, 3887.
13. Hopfinger, A (1973) in *Conformational Properties of Macromolecules*, Academic Press, New York, p. 59.
14. Hertzberg, O. and Moult, J. (1987) *Science*, **236**, 694.
15. Ellerby, L., Escobar, W., Fink, A., Mitchinson, C. and Wells, J (1990) *Biochemistry*, **29**, 5797.
16. Knox, J. and Kelly, J. (1989) in *Chemical and Biochemical Problems in Molecular Recognition*, Stanley Roberts ed., Royal Society of Chemistry, London.
17. Frere, J. and Joris, B. (1985) *Crit. Rev. Microbiol.*, **11**, 299.

18. Joris, B., Ghuyser, J.-M., Dive, G., Renard, A., Dideberg, O., Charlier, P., Frere, J.-M., Kelly, J., Boyington, J., Meows, P., and Knox, J. (1988) *Biochem. J.*, **250**, 313.

19. Tipper, D. and Strominger, J. (1965) *Proc. Natl. Acad Sci. U.S.A.*, **54**, 1133.

20. Kelly, J., Dideberg, O., Charlier, P., Wery, J., Libert, M., Meows, P., Knox, J., Duez, C., Fraipont, C., Joris, B., Dusart, J., Frere, J., and Ghuysen, J.-M. (1986) *Science*, **231**, 1429.

21. Jaszberenyi, J. and Gunda, T. (1975) *Prog. Med. Chem.*, **12**, 395.

22. Varetto, L., Frere, J.-M., and Ghuysen, J.-M. (1987) *FEBS lett.*, **225**, 218.

23. Kelly, J., Knox, J., Zhao, H., Frere, J.-M., and Ghuysen, J.-M. (1989) *J. Mol. Biol.*, **209**, 281.

24. Chapter 2 of this thesis.

25. Schultz, S. and Richards, J. (1986) *Proc. Natl. Acad Sci. U.S.A.*, **83**,1588.

26. Richards, J. (1986) *Nature (London)*, **323**, 11.

27. Dalbadie-McFarland, G., Cohen, L., Riggs, A., Moln, C., Itakura, K., and Richards, J. (1982) *Proc. Natl. Acad Sci. U.S.A.*, **79**, 6409.

28. Ish-Horowicz, D. and Burke, J. (1981) *Nuc. Acids Res.*, **9**, 2989.

29. Maniatis, T., Fritsch, E., and Sambrook, J. (1982) *Molecular Cloning A laboratory Manual*, Cold Spring Harbor Laboratory, Cold Spring Harbor, p. 93.

30. *ibid*, 150.

31. Anonymous (1988) International Biotechnologies Inc., Hew Haven, CT.

32. Berger, S. and Kimmel, A., eds. (1987) *Methods in Enzymology*, **152**, 71.

33. Hanahan, D. (1983) *J. Mol. Biol.*, **166**, 557.

34. Anonymous (1988) "U. S. Biochemicals Sequenase Manual," United States Biochemical, Cleveland, OH.

35. Maniatis, T., Fritsch, E., and Sambrook, J. *Ibid*, 478.

36. Nietzel, J. (1987) Ph. D. thesis (California Institute of Technology, Pasadena, CA)

37. Fisher, J., Belasco, J., Khosla, S., and Knowles, J. (1980) *Biochemistry*, **19**, 2895.

38. Cantor, C. and Shimmel, P. (1980) *Biophysical Chemistry*, W. H. Freeman and Co., San Fransisco, p. 413.

39. Hanes, J. (1932) *Biochem J.*, **26**, 1406.

40. Christensen, H., Martin, M., and Waley, S. (1990) *Biochem. J.*, **266**, 853.

41. Fersht, A. (1985) *Enzyme Structure and Mechanism, second Ed.*, W. H. Freeman and Co., New York, p. 302.

42. Fersht, A. (1988) *Biochemistry*, **27**, 1577.

43. Leatherbarrow, R. and Fersht, A. (1986) *Potein Eng.*, **1**, 7.

44. Albery, W. and Knowles, J. (1976) *Biochemistry*, **15**, 5631.

45. Haldane, J. (1930) *Enzymes*, Longmans, Green and Co., London, p. 182, (reprinted MIT Press, Cambridge MA, 1965).

46. Pauling, L. (1946) *Chem. Eng. News*, **24**, 1375.

47. Ho, C. and Fersht, A. (1986) *Biochemistry*, **25**, 1891.

48. Wells, T. and Fersht, A. (1986) *Biochemistry*, **25**, 1881.

49. Wells, T. and Fersht, A. (1985) *Nature (London)*, **316**, 656.

50. Murphy, D. and Benkovic, S. (1989) *Biochemistry*, **28**, 3025.

51. Hershlag, D. and Cech, T. (1990) *Biochemistry*, **29**, 10159.

52. Hershlag, D. and Cech, T. (1990) *Biochemistry*, **29**, 10172.

53. Rees, D. (1980) *J. Mol. Biol.*, **141**, 327.

55. Warshel, A. (1987) *Nature (London)*, **330**, 15.

56. Russel, A., Thomas, P., and Fersht, A. (1987) *J. Mol. Biol.*, **193**, 803.

CHAPTER 4

Measuring Enzyme Kinetics with Circular Dichroism Spectroscopy

Introduction

Kinetic characterization of the first known enzyme, sucrase, otherwise known as "invertase," was by polarographic methods (1,2). The original assay was based on measuring the optical activity of reaction mixtures that contained proportions of substrate and product sugars (Figure 1). Considering the historical significance, simplicity, and ease of carrying out kinetic measurements based on optical rotatory dispersion (ORD), it is surprising that methods like the one developed for sucrase are not widely used by enzymologists. Indeed, relatively few assay methods based on optical activity of substrates or products of enzymatic reactions have been developed. This work demonstrates that real-time measurements of optical properties such as ORD or circular dichroism (CD) can be used to determine the steady-state rate constants of enzymes.

The range of potential applications for the methods we describe makes this work of general interest to enzymologists who rely on kinetics as a primary resource in mechanistic studies. We report a CD-based method for measuring the steady-state rate constants of two enzymes, β-lactamase and ribulose 1,5-bisphosphate carboxylase/oxygenase (rubisco), and comment on the general applicability of CD for measuring enzymatically catalyzed reaction rates.

Materials and Methods

Chemicals

All β-lactam antibiotics, ribulose-1,5-bisphosphate, phosphoglycerate, phosphoglycolate, and ribulose-1,5-bisphosphate

carboxylase/oxygenase were from Sigma Chemical Company. Kanamycin sulfate was from Boehringer Mannheim Biochemicals (BMB). Isopropyl-β-D-thiogalactoside (IPTG) was from International Biotechnologies, Inc. (New Haven, CT) (IBI).

Protein Expression

β–lactamase genes were subcloned into the expression plasmid pJN by inserting the *Bam*H1/*Eco*R1 restriction fragment of pJN, which contains the *tac* promoter and the kanamycin resistance gene, in place of the tetracycline resistance gene of pBR322 (see Chapter 3) (3). Typically, 1-litre cultures (grown in XB broth: 25g Bactotryptone, 7.5 g yeast extract, 20 ml 1 M Mg_2SO_4 and 50 ml 1 M Tris-HCl pH 7.5 per litre) of *E. coli* strain D1210 harboring the pJN plasmids were grown to late log phase when IPTG was added to a final concentration of 0.1 mM. The cultures were incubated for an additional 45 min and pelleted at 10,000 rpm in a GSA rotor. Osmotic extrusion of periplasmic proteins including the crude β–lactamases was accomplished by modifications of established procedures (4). Pellets from 1-litre cultures were suspended in 60 ml ice cold sucrose solution (25 ml 1 M Tris-HCl, pH 7.0, 450 g sucrose, 0.5 g Na_2EDTA per 1 litre) and stirred for approximately 30 min at 4°C. Cells were pelleted (10,000 rpm, GSA rotor, 20 min), resuspended in 60 ml of ice-cold water, stirred for 30 min, and pelleted again (13,000 rpm, GSA rotor, 30 min). The supernatant was filtered (0.2μ), concentrated by ultrafiltration (Amicon YM10 membrane, 10 kD MW cutoff) to between 5 and 10 ml, and

fractionated with FPLC ion-exchange chromatography as described below.

Protein Purification

After extrusion from the periplasmic space mutant and wild-type RTEM-1, β-lactamases were purified by ion-exchange chromatography. Extrudates were filtered (0.2μ), then typically the equivalent of one half of a one-litre culture (2 ml of the concentrated extrudate) was applied to a Pharmacia MonoQ HR10/10 anion-exchange column. Separation conditions and buffers were: flow rate, 1ml/min; temperature, 4°C; Buffer A, 25 mM triethanolamine-HCl (TEA-HCl), pH 7.65; Buffer B, 25 mM TEA-HCl, 1 M sodium chloride, pH 7.65. The gradient was t=0 min, 100% A; t=3 min, 100% A; t=28 min, 81% A, 19% B; t=33 min, 100% B. Wild-type and mutant β-lactamases eluted at approximately 17 min (Chapter 3). Purity of fractions was assessed by polyacrylamide gel electrophoresis (PAGE) with Coomassie blue staining.

Circular Dichroism and Optical Rotatory Dispersion Spectropolarimetry

All CD and ORD spectra were measured with a Jasco model J600 spectropolarimeter interfaced with an IBM model 50 PS2 computer operating the Jasco V1.37 software package. ORD spectra were collected using the ORD attachment for the J600 spectropolarimeter available from Jasco.

Instrument parameters for routine wavelength-based CD acquisitions were set as follows: band width 2 nm, scan rate 20 nm min^{-1}, time constant 2 s, number of scans 1. Spectra were measured

at room temperature in 100 mM potassium phosphate buffer pH 7.0 using a 10 mm path length cell.

Reaction Kinetics

Steady-state kinetic parameters for wild-type and mutant RTEM-1 β-lactamases were measured by monitoring the change in ellipticity of reaction mixtures at either approximately 230 nm for hydrolysis of penams or approximately 260 nm for hydrolysis of cephems. For example, using the Jasco J600 spectropolarimeter in the time-based acquisition mode, rates of ampicillin hydrolysis were monitored at 234 nm, where the molar ellipticity [θ] of ampicillin is maximal at $[\theta]=4.38X10^2$ deg M^{-1} cm^{-1} and the molar ellipticity of the hydrolysis product is undetectable ([θ] is defined as $[\theta]=\theta/cl$, where θ is the measured ellipticity in degrees, c is the molar concentration, and 1 is the path length in cm) (5). Acquisition parameters were chosen to maximize the signal-to-noise ratio. Typically, the time constant was from 2 to 0.5 s and the slit width was 1500 μm. Unless otherwise stated, reaction conditions were 100 mM potassium phosphate buffer, pH 7.0, ionic strength 125 mM, temperature 30°C. The working enzyme concentration was from $1X10^{-10}$ M to $1X10^{-12}$ M (estimated from an extinction coefficient of 29,400 M^{-1} cm^{-1} (6)). Initial velocity data were collected during the linear portion of each reaction, typically between the first 20 to 60 seconds. Substrate concentrations were varied from approximately five times K_M to one half the K_M value in all analyses. In order to obtain maximum accuracy from the method, antibiotic solutions were made up *immediately prior to use* because appreciable hydrolysis was

observable by CD within less than two hours. Slopes of linear portions of reaction curves were calculated by linear regression, and initial velocity data were analyzed by Hanes Plots (7). Steady-state kinetic parameters derived from full time course experiments were derived from nonlinear least squares fitting of reaction curves to the integrated Michaelis-Menten equation (8).

Results and Discussion

A CD Assay for Measuring β-lactamase Catalyzed Reaction Rates

The β-lactam chromophore of the β-lactam antibiotics exhibits strong circular dichroism as a consequence of the asymmetric character of the fused ring system common to these compounds (Figure 2) (9-11). The penam antibiotics display a positive CD at *ca.* 230 nm and the cephem antibiotics, because of the presence of a carbon/carbon double bond, display a positive CD at *ca.* 260 nm and a negative CD at *ca.* 230 nm (Figures 3-5). Antibiotic ellipticities are linear functions of concentration between approximately 1 μm and 10 mM (Figures 6-8, Table 1). This range can be extended to at least 100 mM by using a 1 mm or 0.1 mm path length cell. In contrast to the strong optical activities of β-lactam antibiotics, the hydrolysis products are optically inactive.

By measuring the ellipticity as a function of time at 230 nm (penams) or 260 nm (cephems) of samples containing the β-lactam antibiotic and β-lactamase, it is straightforward to derive hydrolysis rates (Figure 9). The concentration of antibiotic can be varied, and

initial hydrolysis rates can be plotted by the conventional Hanes or Eadie-Hofstee methods to obtain steady-state rate constants for the enzyme used in the assay (Figures 10-14).

The effect of temperature on the CD spectra of the β-lactam antibiotics is negligible between 25°C and 35°C; however, the ellipticities of these compounds have moderate pH dependencies, which should be taken into account in studies designed to determine pH/hydrolysis rate profiles. The ellipticity of ampicillin varies by about 10% over the pH range from 6.0 to 8.0 (Figure 15). This variance is not expected to be the same for cephem antibiotics or even other penam antibiotics, and accordingly, it should be determined for each compound used in pH studies.

The largest contributing error in β-lactamase turnover numbers (i.e., kcats) determined by either CD or conventional UV spectroscopy comes from uncertainty in the concentration of active enzyme in reaction mixtures, a quantity that is normally measured by UV spectroscopy (6). By measuring ellipticities at 222 nm of stock enzyme solutions, CD spectroscopy can be used to estimate the fraction of folded (active) enzyme in solution. The molar ellipticity of wild-type RTEM-1 β-lactamase at 222 nm is $[\theta] = 3.03 \times 10^7$ M^{-1} cm^{-1} (Figures 16 and 17). Since ellipticities at 222 nm for proteins are a direct function of secondary structure content, unfolded protein or contaminants that absorb but are not optically active will not interfere with CD measurements of enzyme concentration. Some preparations will, however, have fractions of inactive but normally folded enzyme that is indistinguishable from active protein by CD.

The complete hydrolysis curve for 230 μM ampicillin (*ca.* 5 X KM) is shown in Figure 18; the theoretical curve (smooth line) described by the integrated Michaelis-Menten equation is fit to the experimental data (8). Although the data appear to fit the calculated curve quite well, in several experiments kcats and KMs measured from these curves varied by several hundred percent according to how much of the reaction curve was used in the curve-fitting procedures For example, if in one case 90% and in another 95% of the experimental data were fitted to the theoretical equation, significantly different results were obtained from each fit. If the extent of the reaction (% of substrate hydrolyzed at the longest time for which data were collected) was held constant, and the initial substrate concentration was varied, a similar result was obtained. These effects are probably due to product inhibition, enzyme inactivation, or a combination of the two. No experiments were performed to further investigate this; however, it can be concluded that RTEM-1 β–lactamase, steady-state kinetic parameters measured from time course experiments are at best rough estimates.

When compared to the traditional UV spectroscopy method for monitoring hydrolysis of β–lactam antibiotics (12), CD spectroscopy offers several advantages. The detection limit of most penams by CD spectroscopy is about 10 μM as compared to the approximate 50 μM detection limit by UV spectroscopy. This allows more accurate determination of KMs, binding constants, and apparent second-order rate constants (kcat/KM). Unlike UV absorbance, high concentrations of enzymes required in some assays do not interfere significantly with CD quantification. In assays designed to characterize enzymes

with high KMs, the substrate concentration must be increased beyond the upper limit accurately measurable at the optimum wavelengths by UV spectrophotometry. Concentrations from 5 μM to 100 mM are readily measured by CD, giving this method a dynamic range of 10^5.

The hydrolysis products of the antibiotics do not exhibit CD characteristis of asymmetric β-lactams because internal bond rotation results in time-averaged symmetric environments for chromophores of these molecules. However, the molar ellipticity of unhydrolyzed β-lactam antibiotics rivals that of the most optically active compounds. For example, ammonium-D-camphorsulphonate ($[\theta] = 7.9X10^1$ deg M^{-1} cm^{-1}) and D-(-)-pantolactone ($[\theta] = 1.62X10^2$ deg M^{-1} cm^{-1}), two common CD standards, have molar ellipticities of less than 20% and 25%, respectively, of ampicillin (13,14). The 100% change in the strong ellipticity of β-lactam antibiotics upon hydrolysis contrasts with the moderate change in UV absorbance upon hydrolysis of these compounds (about 22% for ampicillin) (Figure 19). Since the product of the reaction does not interfere with CD quantification of the substrate, as is the case with the UV method, there is no uncertainty in the initial substrate concentration caused by time delays between the start of the reaction and the start of CD data collection.

Using CD, equimolar amounts of β-lactamase and cephems can be detected simultaneously in reaction mixtures. For example, even though the molar ellipticities at the wavelength maxima for RTEM-1 and cephalothin differ by 10^5-fold ($[\theta]_{222nm} = 3.03X10^7$ deg M^{-1} cm^{-1} and $[\theta]_{260nm} = 4.38X10^2$ deg M^{-1} cm^{-1}, respectively), at 260 nm the relative ellipticity of cephalothin is 8.5 times greater than that of

RTEM-1. Consequently, one equivalent of a unique amid bond, the β−lactam, can be accurately quantified in the presence of 265 equivalents of peptide bond, the number of amino acids in RTEM-1. This affords the opportunity to perform experiments under second-order conditions ([E]=[S]), such as binding constant determinations (using inactive mutants, e.g., S70G) and stopped-flow transient-state kinetics, since CD spectra are generally sensitive to the environment of the chromophore (15,16), These experiments are not possible by monitoring absorption changes of conventional substrates upon binding or hydrolysis, since they are obscured by the spectrum of the enzyme.

We contend that CD is an effective analytical tool for measuring the rates of β−lactam hydrolysis by β−lactamase. As stated above, the CD β−lactamase assay has several advantages over the traditional UV method; however, the low cost of the UV method and the desirability of having available two independent methods for measuring the steady-state rate constants of β−lactamases is recognized.

A CD assay for Measuring Rubisco Catalyzed Reaction Rates

Ribulose 1,5-bisphosphate carboxylase/oxygenase (rubisco) initiates uptake of carbon dioxide into the biosphere by catalyzing carboxylation of ribulose 1,5-bisphosphate (RuBP) (Figure 20) (17,18). The enzyme reduces an estimated 10^{11} tons of CO_2 per year and is the most abundant enzyme on earth (19,20). In addition to the carboxylase reaction, the enzyme catalyzes oxygenation of RuBP in a puzzling "sugar-burning" reaction (Figure 20) (21). The unique

catalytic properties of rubisco and the importance of the enzyme in the contexts of environmental, agricultural, and economic issues have led to extensive biochemical, crystallographic, and mutagenic studies of the enzyme (22-24).

The rates of the carboxylation and oxygenation reactions which rubisco catalyzes are difficult to measure because of the lack of a convenient and accurate method of quantifying the reactant and product sugars. The widely used method employs $^{14}CO_2$ for the carboxylase reaction and an oxygen electrode for the oxygenase reaction (25). The procedures are cumbersome, time-consuming, and can be inaccurate (26).

Although RuBP is essentially transparent to UV and visible light, the carbonyl group of the compound has a weak absorption band ($\varepsilon<100$) at 280 nm, which is due to an n to $\pi*$ transition (27). This band is known to be an important determinant of circular dichroism properties of carbonyl groups in chiral molecules (28). The CD spectrum of RuBP shows a strong positive ellipticity at 280 nm of $[\theta]=19$ deg M^{-1} cm^{-1} (Figure 21). The products of the carboxylation and oxygenation reactions, phosphoglycerate and phosphoglycolate, respectively, are optically inactive (Figure 22), and so using methods similar to those described for measuring the steady-state rate constants of β–lactamase, the kinetics of the rubisco reactions can be measured with CD. By varying the concentrations of CO_2 and O_2, the K_Ms and k_{cat}s for these substrates can be determined in the presence of sufficient concentrations of RuBP to saturate the enzyme (400 μM) (25). The CO_2 and O_2 substrates do not interfere with the assay because they are neither chiral nor do they absorb light at 280 nm.

Since CD can accurately quantify concentrations of RuBP only as low as about 100 μM, and the RuBP KM of the enzyme from *Rhodopsirillum rubrum*, for example, is less than 10 μM (25), the RuBP KM of most bacterial enzymes cannot be accurately measured with CD. Although relatively fewer RuBP KMs have been measured for rubisco from higher plants, this quantity will be measurable by CD if the KM of soybean rubisco (180 μM) is typical for these enzymes (29).

We have demonstrated that CD spectroscopy is an effective analytical tool for measuring the steady-state rate constants of two important enzymes. The abundance of optically active substrates, cofactors, and products in enzymatic reactions suggests that CD methods might be useful for characterizing the kinetics of a wide range of biological reactions. The utility of the method derives from the selectivity of CD. A compound must be both chiral and light-absorbing to exhibit CD, and even if a spectrum is anomalous, the rates of subtle changes in the chemical structure or the physical environment of an optically active chromophore can be observed and associated with specific chemical reactions.

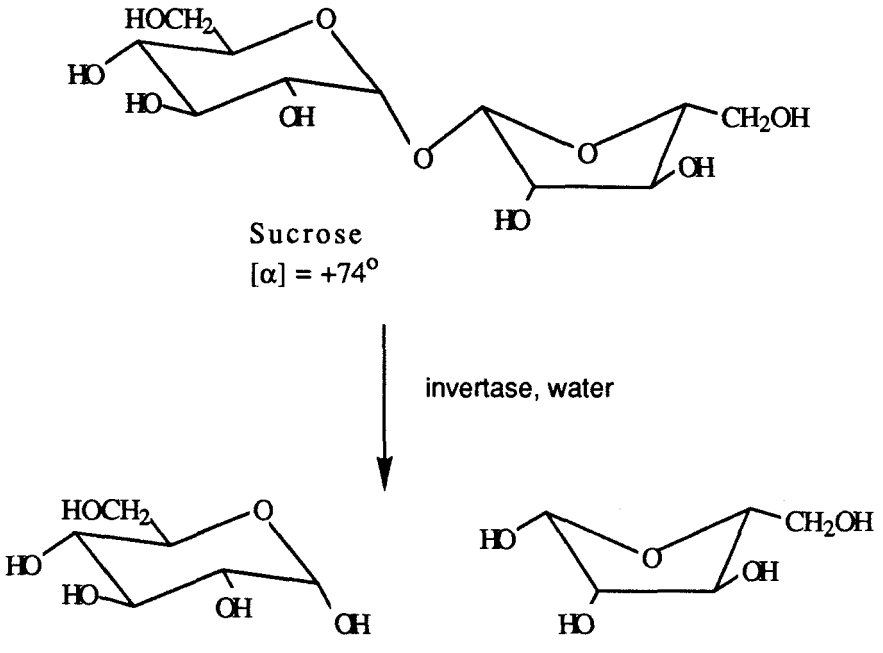

Figure 1. The hydrolysis of sucrose catalyzed by sucrase ("invertase"). The optical activities that are the basis for the original polarographic assay are shown.

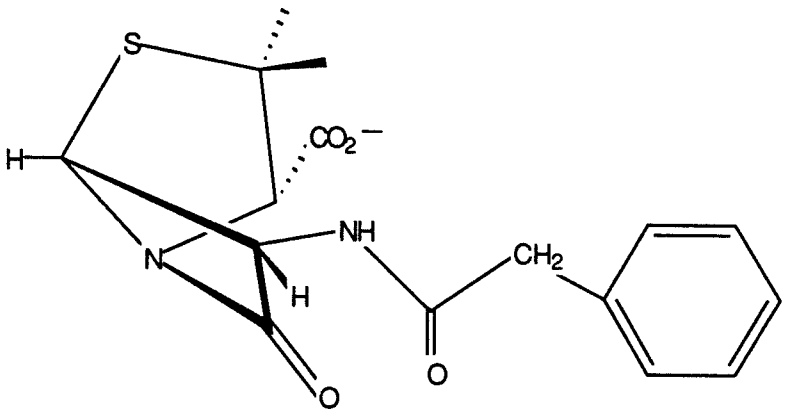

Figure 2. The asymmetric structure of the β–lactam antibiotics. The structure of benzylpenicillin is shown. The fused ring system is bent and rigid.

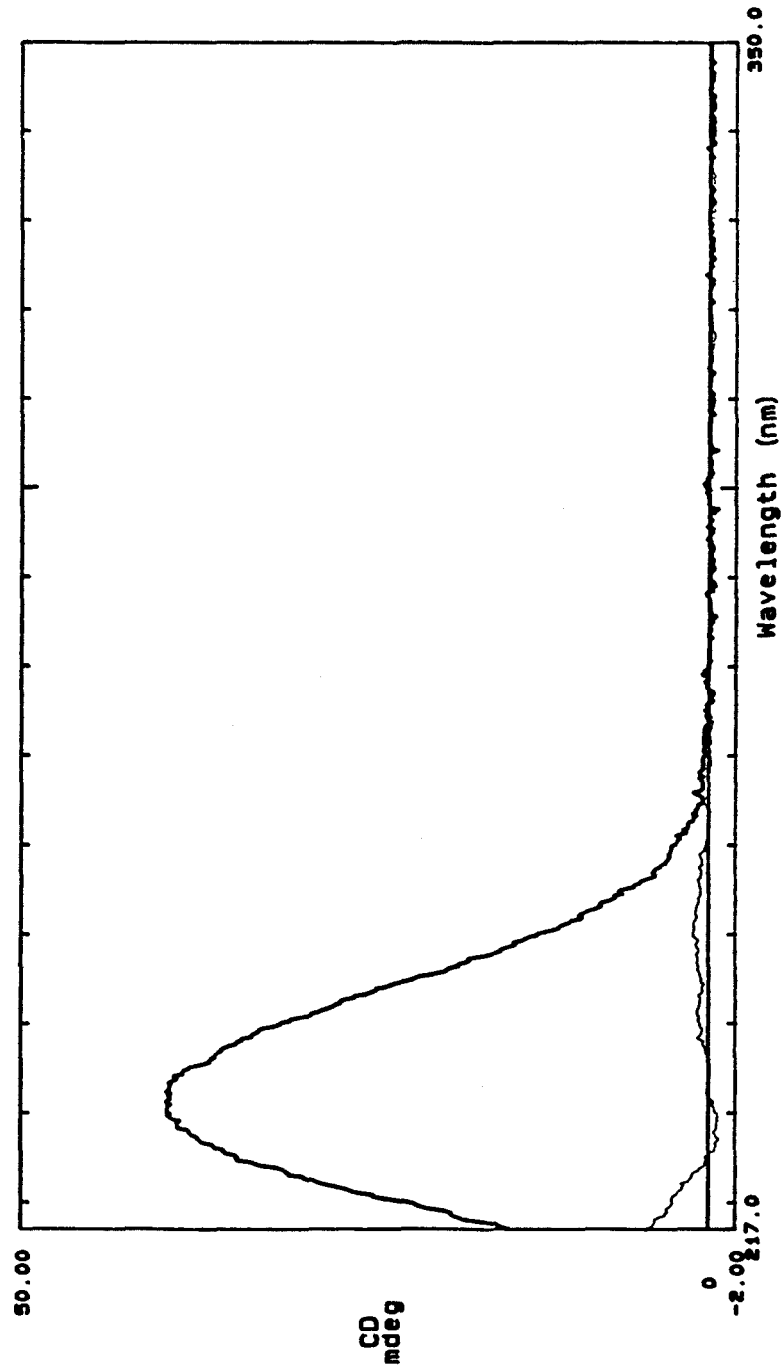

Figure 3. CD spectra of 1 mM benzylpenicillin (heavy line) and 1 mM hydrolyzed benzylpenicillin (light line). Conditions were: 100 mM potassium phosphate pH 7.0, 25°C, path length 1 mm.

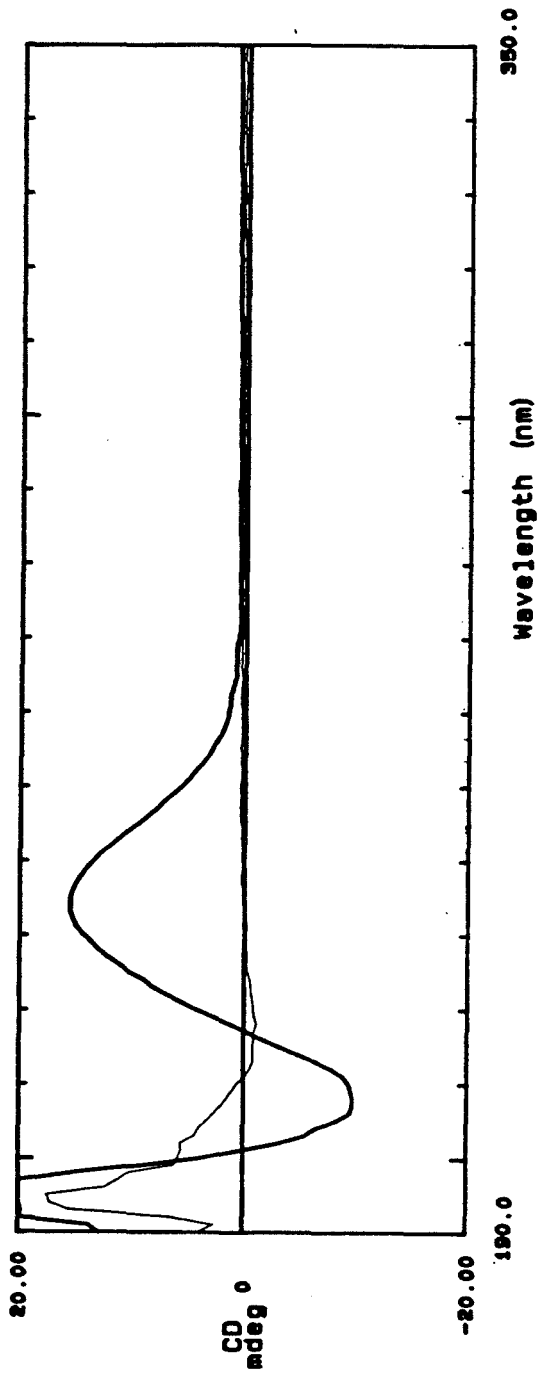

Figure 4. CD spectra of 0.5 mM ampicillin (heavy line) and 0.5 mM hydrolyzed ampicillin (light line). Conditions were: 100 mM potassium phosphate pH 7.0, 25°C, path length 1 mm.

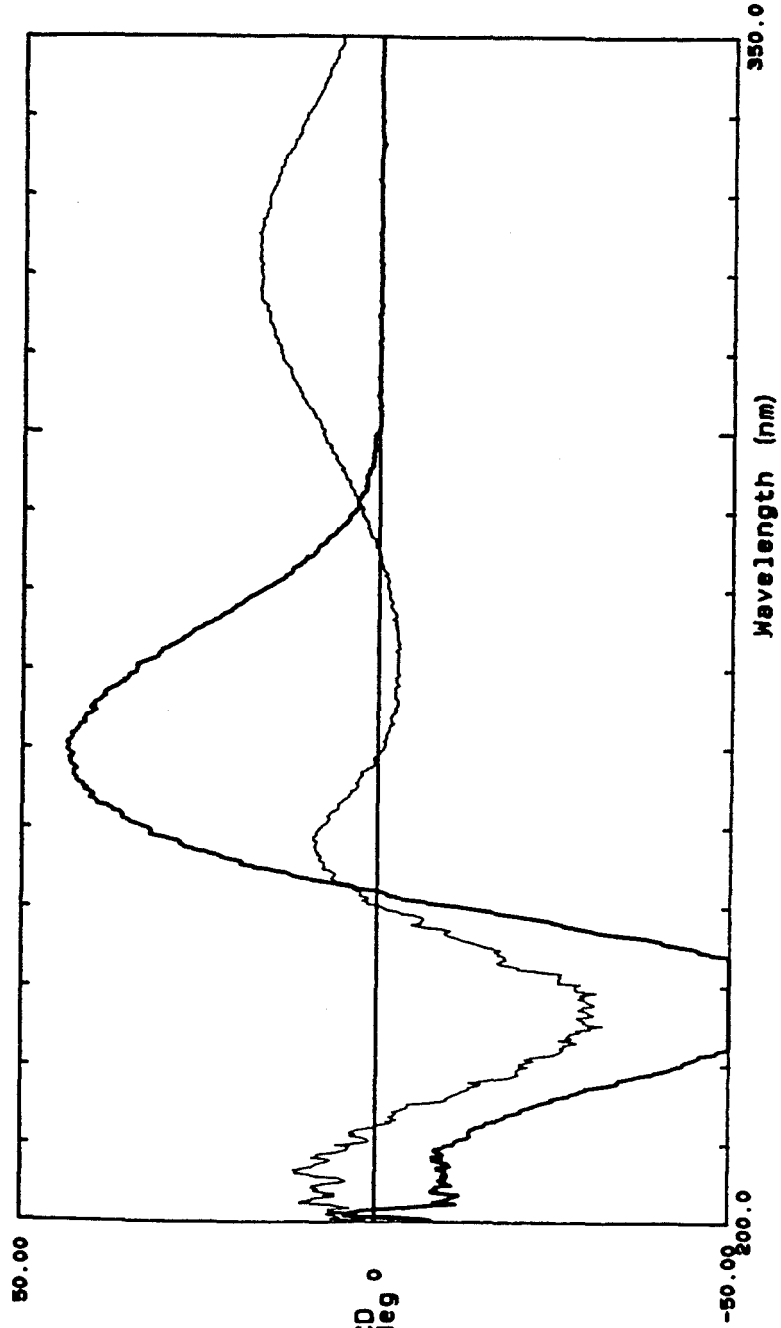

Figure 5. CD spectra of 1 mM cephalothin (heavy line) and 1 mM hydrolyzed cephalothin (light line). Conditions were: 100 mM potassium phosphate pH 7.0, 25°C, path length 1 mm.

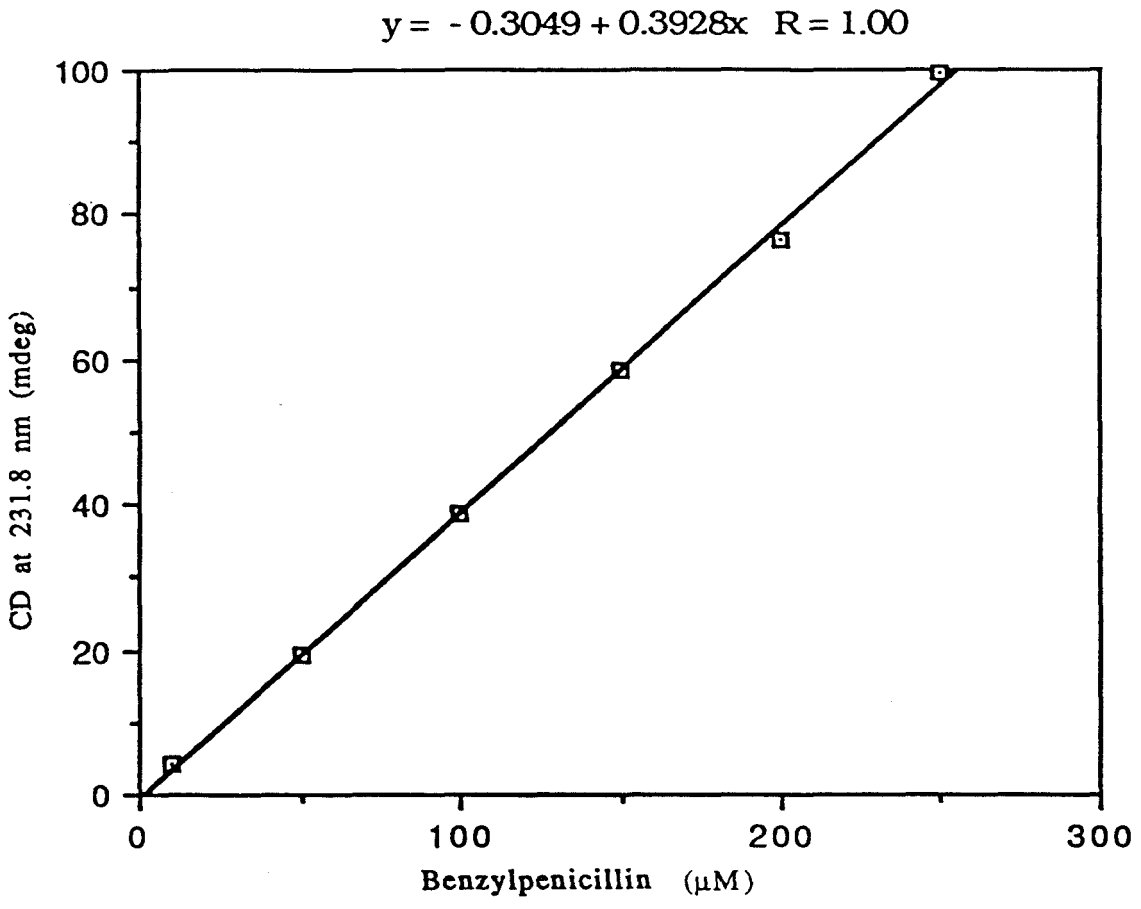

Figure 6. Plot of ellipticity at 231.8 nm versus benzylpenicillin concentration. The slope of the line (392.8 deg M^{-1} cm^{-1}) is the molar ellipticity of benzylpenicillin. Conditions were 100 mM potassium phosphate, 25°C, 10 mm path length.

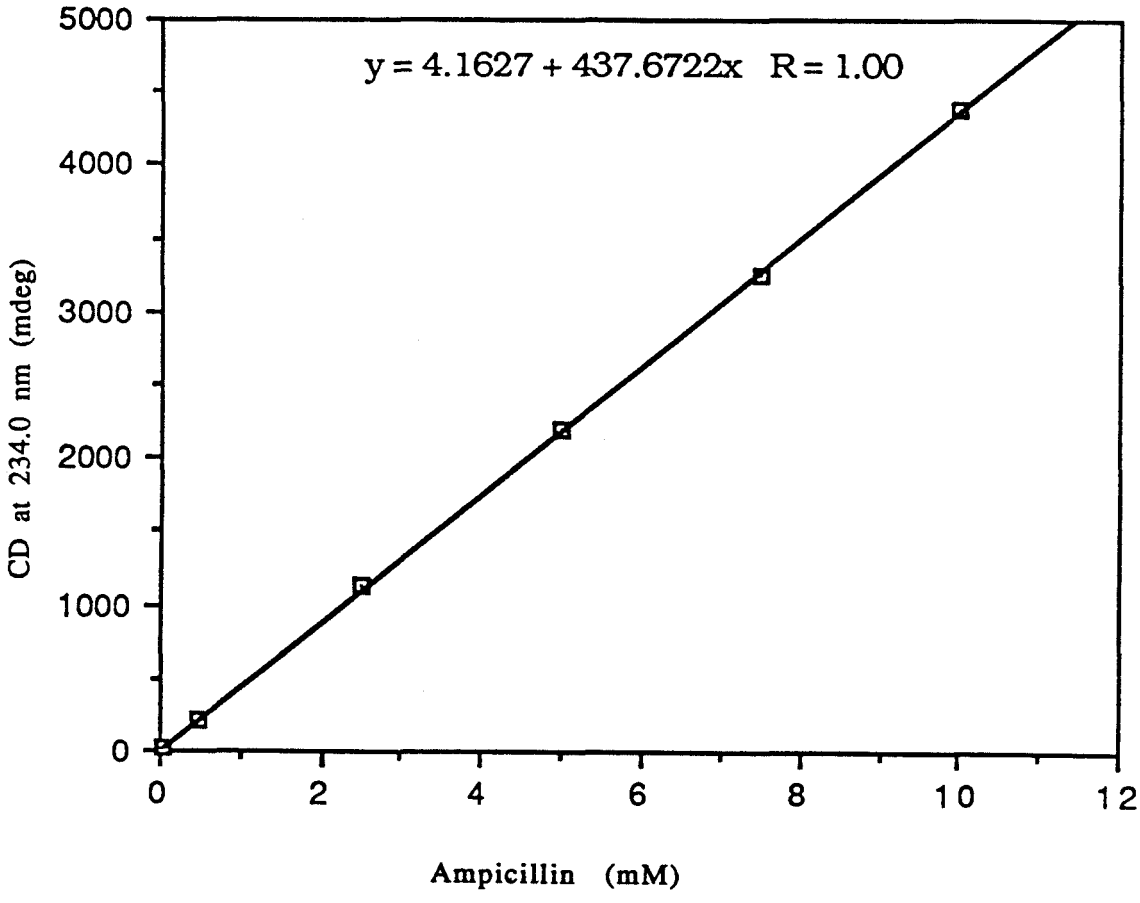

Figure 7. Plot of ellipticity at 234.0 nm versus ampicillin concentration. The slope of the line (437.7 deg M^{-1} cm^{-1}) is the molar ellipticity of ampicillin. Conditions were 100 mM potassium phosphate, 25°C, 10 mm path length.

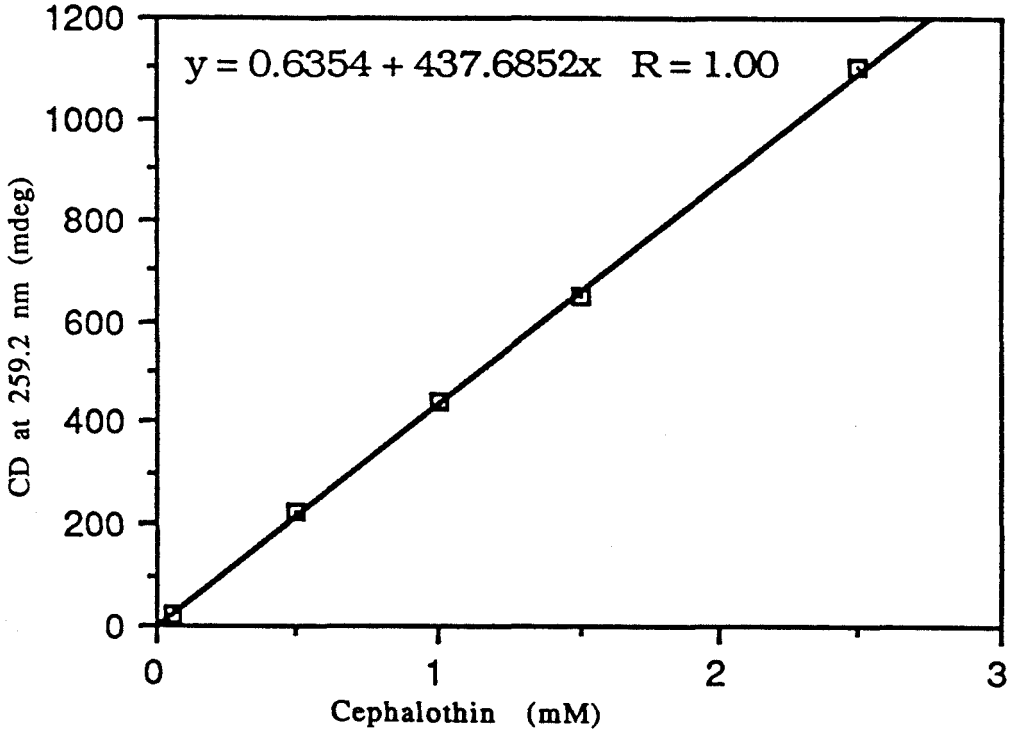

Figure 8. Plot of ellipticity at 259.2 nm versus cephalothin concentration. The slope of the line (437.7 deg M^{-1} cm^{-1}) is the molar ellipticity of cephalothin. Conditions were 100 mM potassium phosphate, 25°C, 10 mm path length.

Table 1. Molar ellipticities of some common β-lactam antibiotics. Values marked with an asterisk (*) were estimated from one measurement and should be considered rough estimates only (Purdie, N. and Swallows, K. (1985) *Anal. Chem.*, **59**, 1349.). Values measured in this laboratory are in boldface and have been determined by serial dilution experiments (see Figures 6-8). Estimated error in these values is less than 2%. Units of [θ] are deg M^{-1} cm^{-1}.

Antibiotic	[θ] (nm)
amoxicillin	+398 (230)*
ampicillin	**+437 (234.0)**
cloxacillin	+333 (230)*
dicloxacillin	+323 (230)*
methicillin	+265 (230)*
naficillin	+237 (230)*
oxacillin	+482 (230)*
benzylpenicillin	**+392 (231.8)**
penicillin-V	+363 (230)*
cephalexin	+395 (260)*
cephalothin	**+437 (259.2)**
cephapirin	+501 (260)*

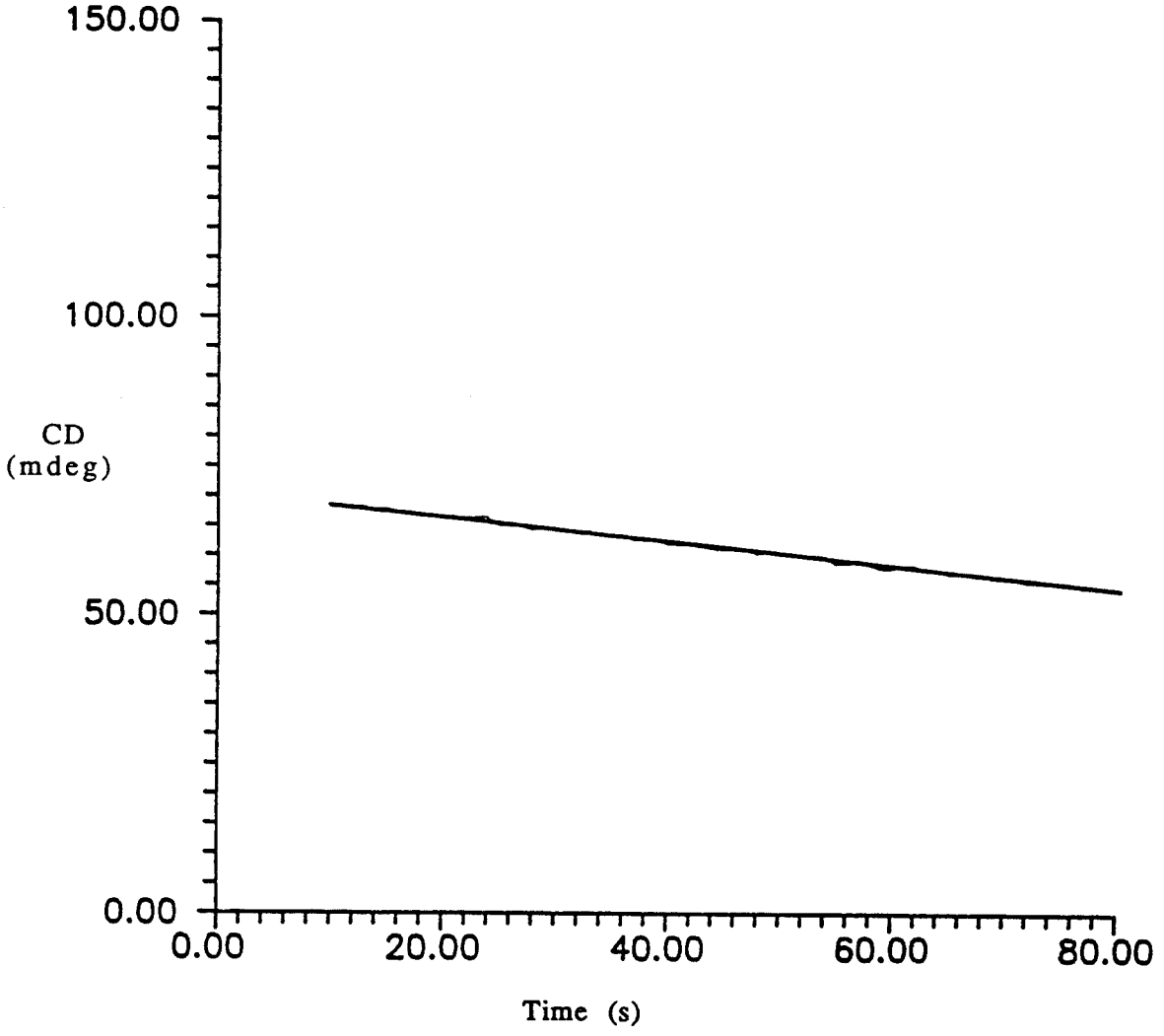

Figure 9. Plot of ellipticity at 234 nm versus time for the hydrolysis of 200 μM ampicillin by wild type RTEM-1 β–lactamase. Conditions were 100 mM potassium phosphate, pH 7.0, 30°C, 10 mm path length. The effects of noise are barely observable as a light line under a heavy line (theoretical, straight) from which the initial velocity of the reaction was calculated. The initial substrate concentration was estimated by extrapolating to time zero. Several experiments starting from different initial concentrations of ampicillin were combined to derive the wild type steady-state rate constants (see text and Figure 10).

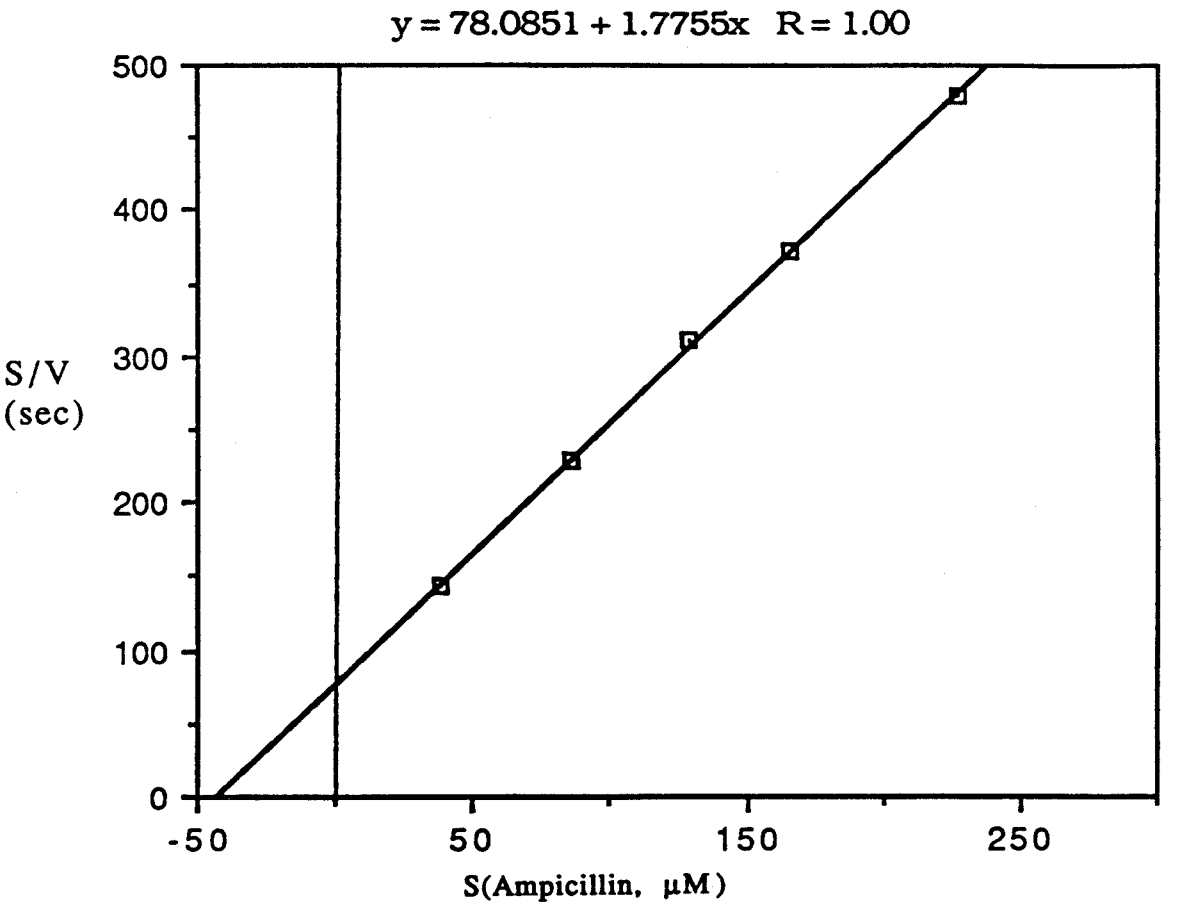

Figure 10. Hanes plot for ampicillin hydrolysis by wild type RTEM-1 β–lactamase. Conditions were 100 mM potassium phosphate, pH 7.0, 30°C, 10 mm path length. Enzyme concentration was $6X10^{-10}$ M. The X-intercept is -KM (44 μM) and the slope is 1/[E]kcat. The steady-state rate constants are KM=44 μM and kcat=939 s^{-1}.

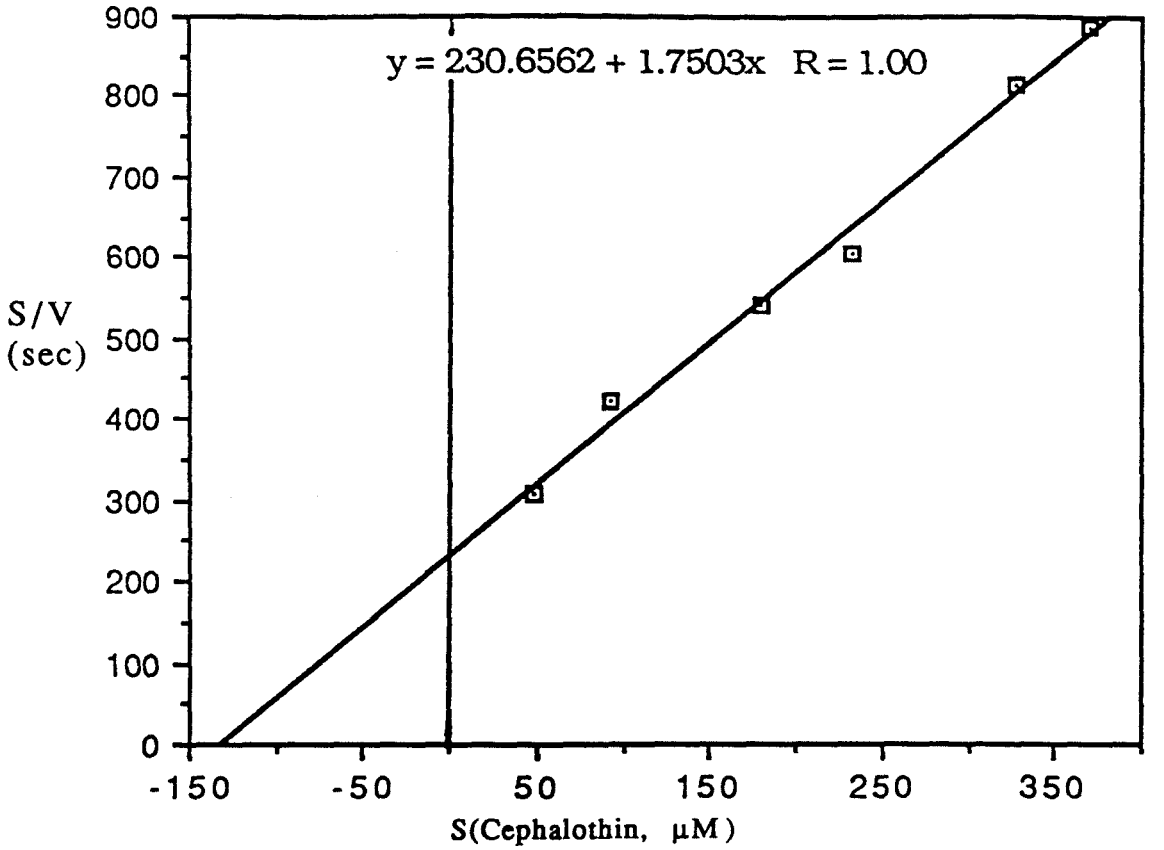

Figure 11. Hanes plot for cephalothin hydrolysis by wild type RTEM-1 β–lactamase. Conditions were 100 mM potassium phosphate, pH 7.0, 30°C, 10 mm path length. Enzyme concentration was $4.9X10^{-9}$ M. The steady-state rate constants are K_M=132 μM and k_{cat}=116 s^{-1}.

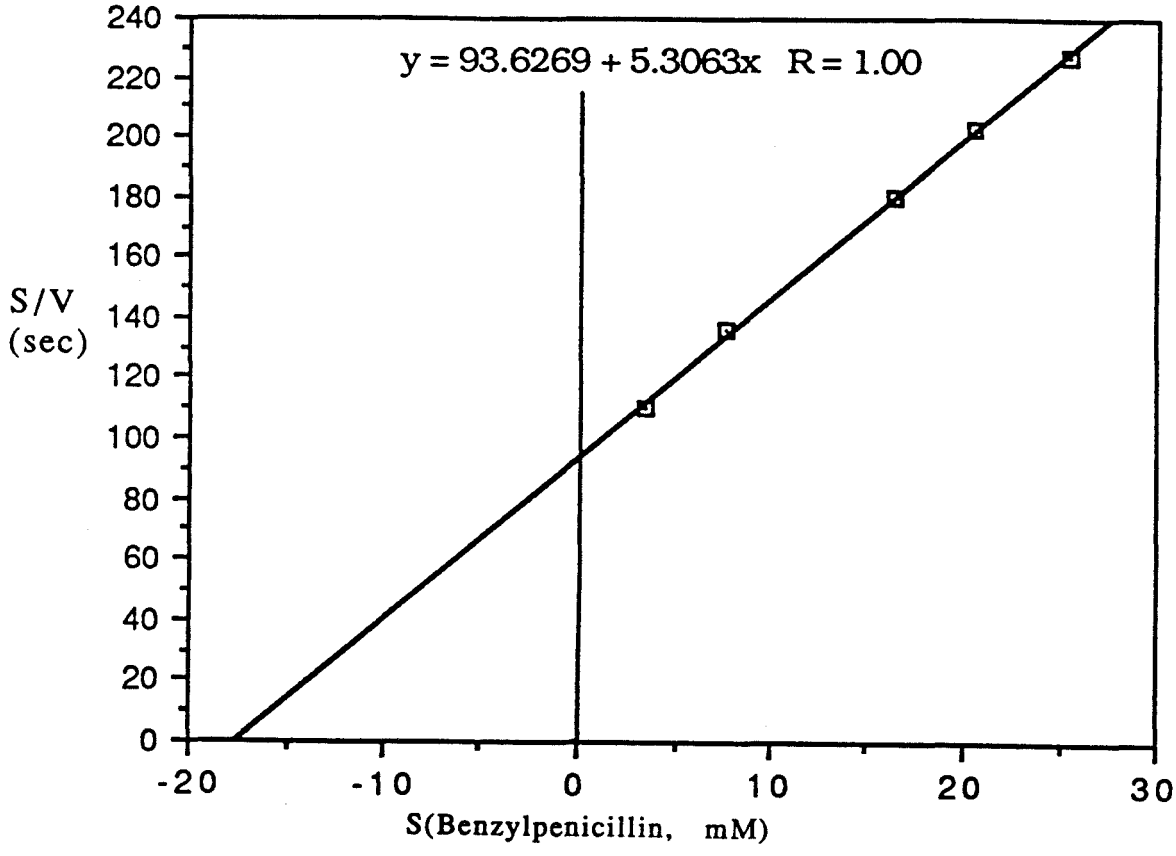

Figure 12. Hanes plot for benzylpenicillin hydrolysis by K234V mutant RTEM-1 β−lactamase. Conditions were 100 mM potassium phosphate, pH 7.0, 30°C, 10 mm path length. Enzyme concentration was $3.1X10^{-6}$ M. The steady-state rate constants are $K_M=17.6X10^3$ μM and $k_{cat}=61.6$ s^{-1}.

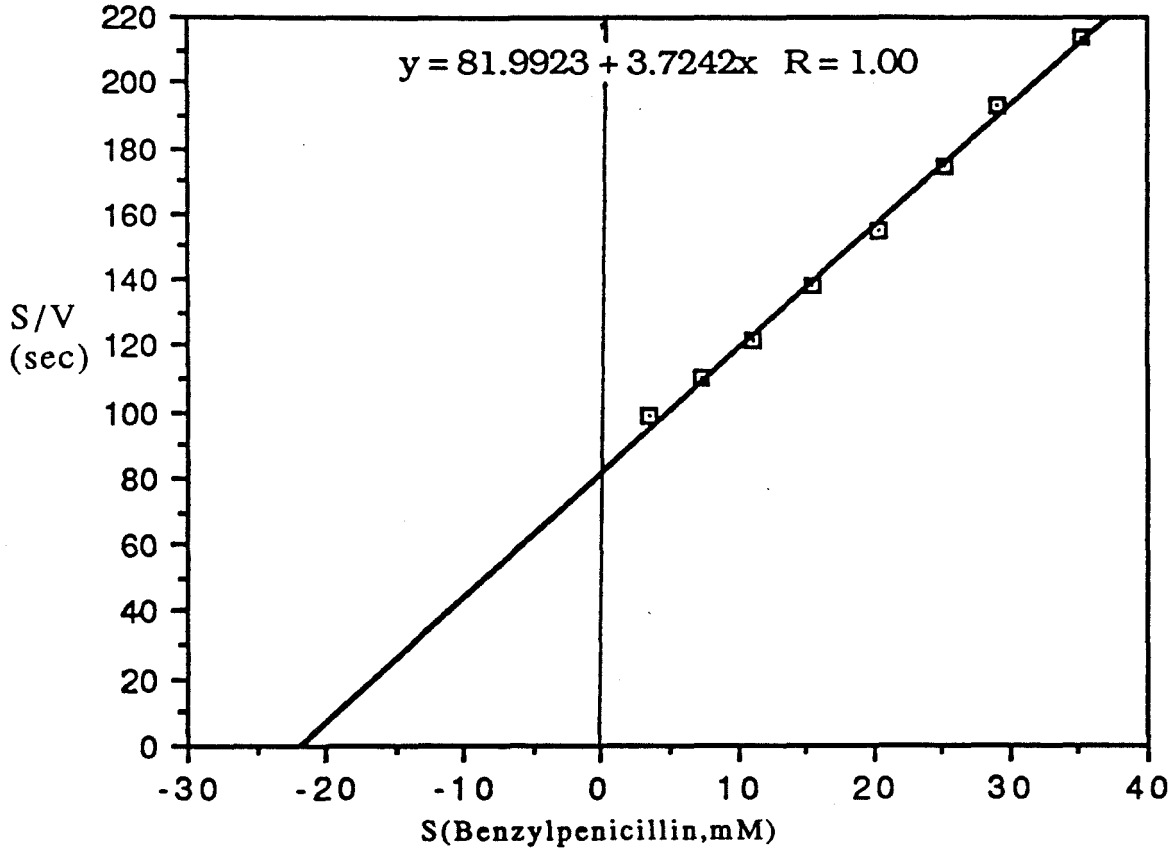

Figure 13. Hanes plot for benzylpenicillin hydrolysis by K234Q mutant RTEM-1 β-lactamase. Conditions were 100 mM potassium phosphate, pH 7.0, 30°C, 10 mm path length. Enzyme concentration was $1.9X10^{-6}$ M. The steady-state rate constants are $K_M=2.2X10^4$ μM and $k_{cat}=138$ s^{-1}.

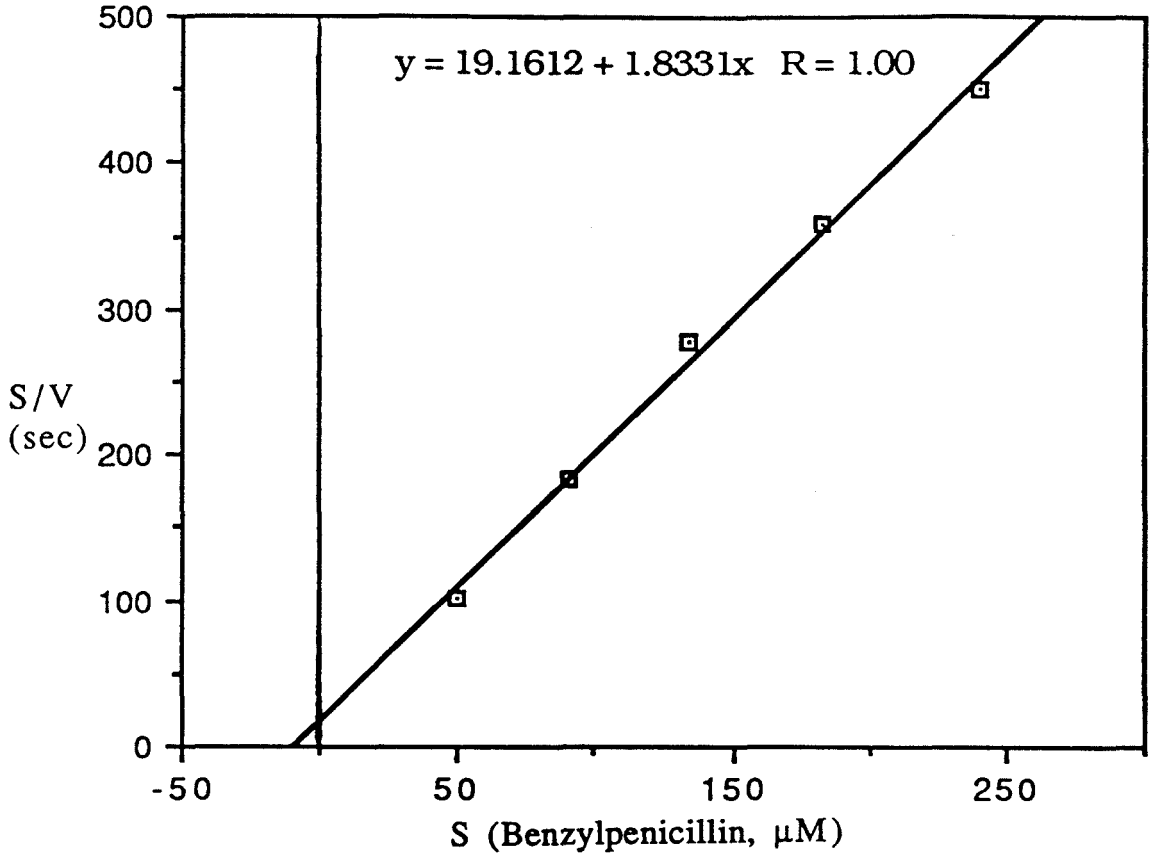

Figure 14. Hanes plot for benzylpenicillin hydrolysis by wild type RTEM-1 β–lactamase. Conditions were 100 mM potassium phosphate, pH 7.0, 30°C, 10 mm path length. Enzyme concentration was $3.7X10^{-10}$ M. The steady-state rate constants are K_M=10.45 μM and k_{cat}=1482 s^{-1}.

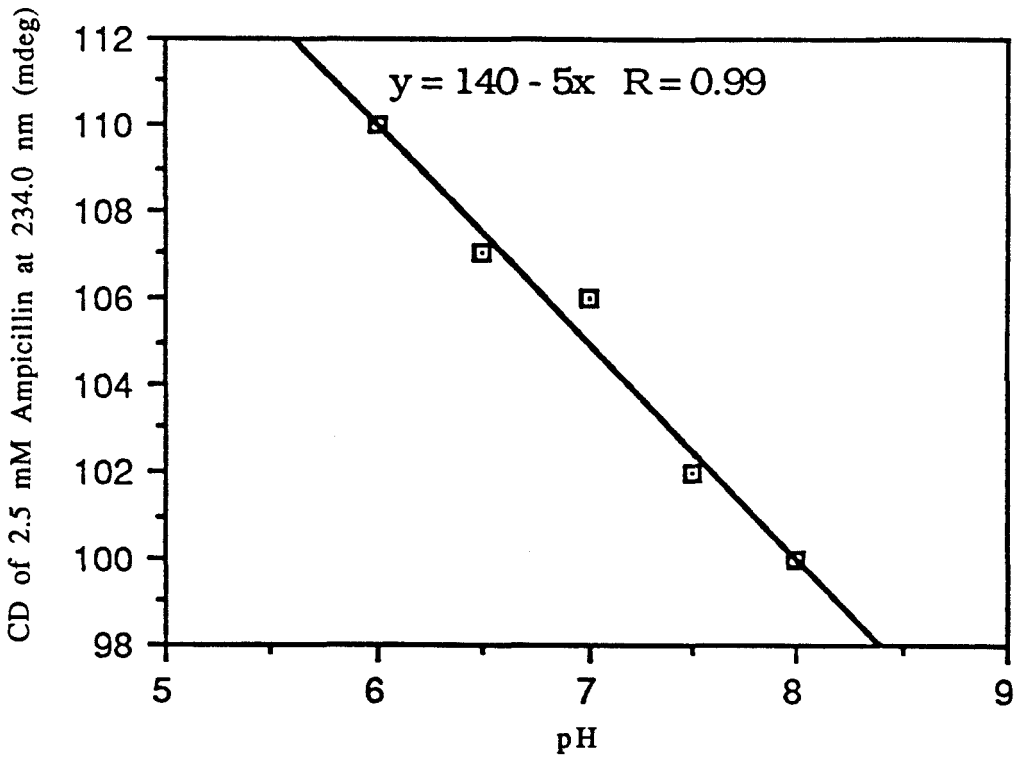

Figure 15. The ellipticity of 2.5 mM ampicillin as a function of pH. The pH dependency is approximately linear between pH 6 and pH 8. Conditions were 100 mM potassium phosphate, 25°C, 1 mm path length.

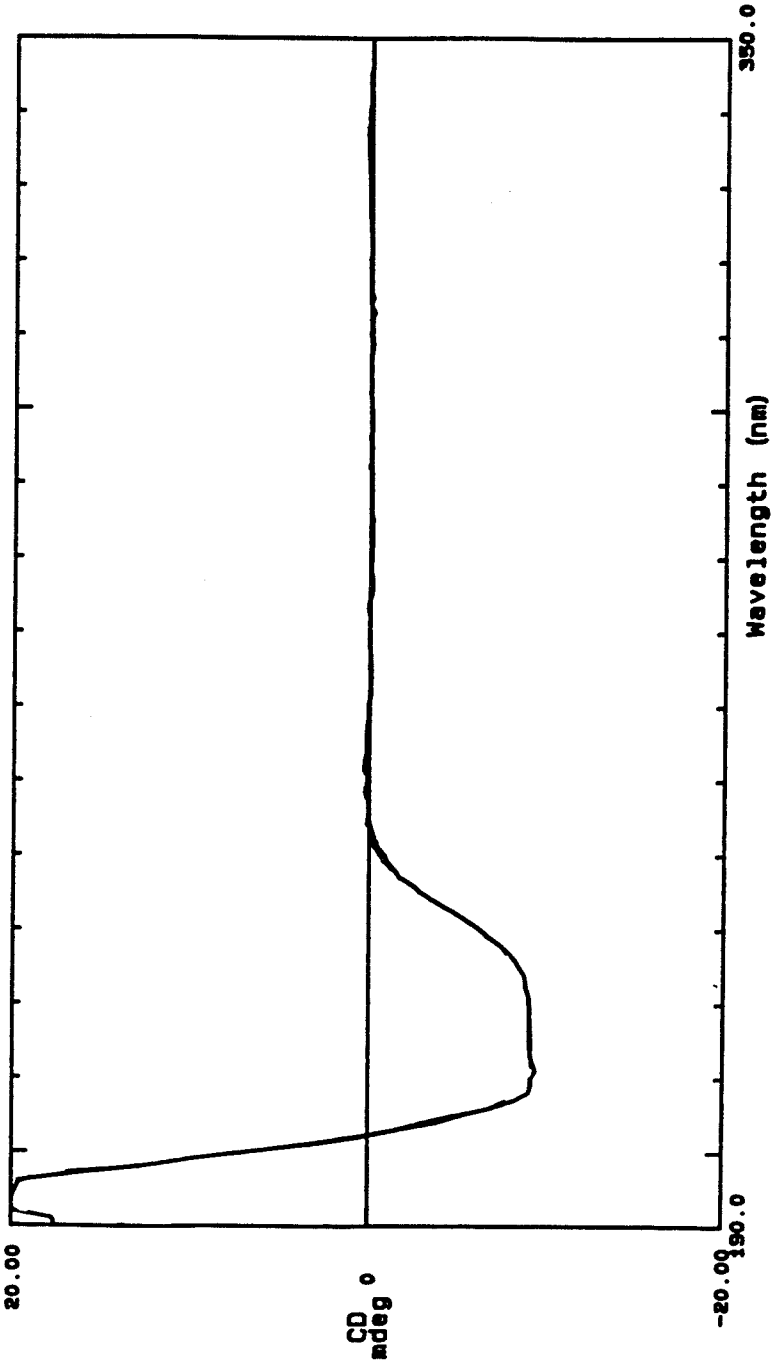

Figure 16. The CD spectrum of 2.5X10^{-6} M wild type RTEM-1 β-lactamase. Conditions were: 100 mM potassium phosphate pH 7.0, 25°C, path length 10 mm.

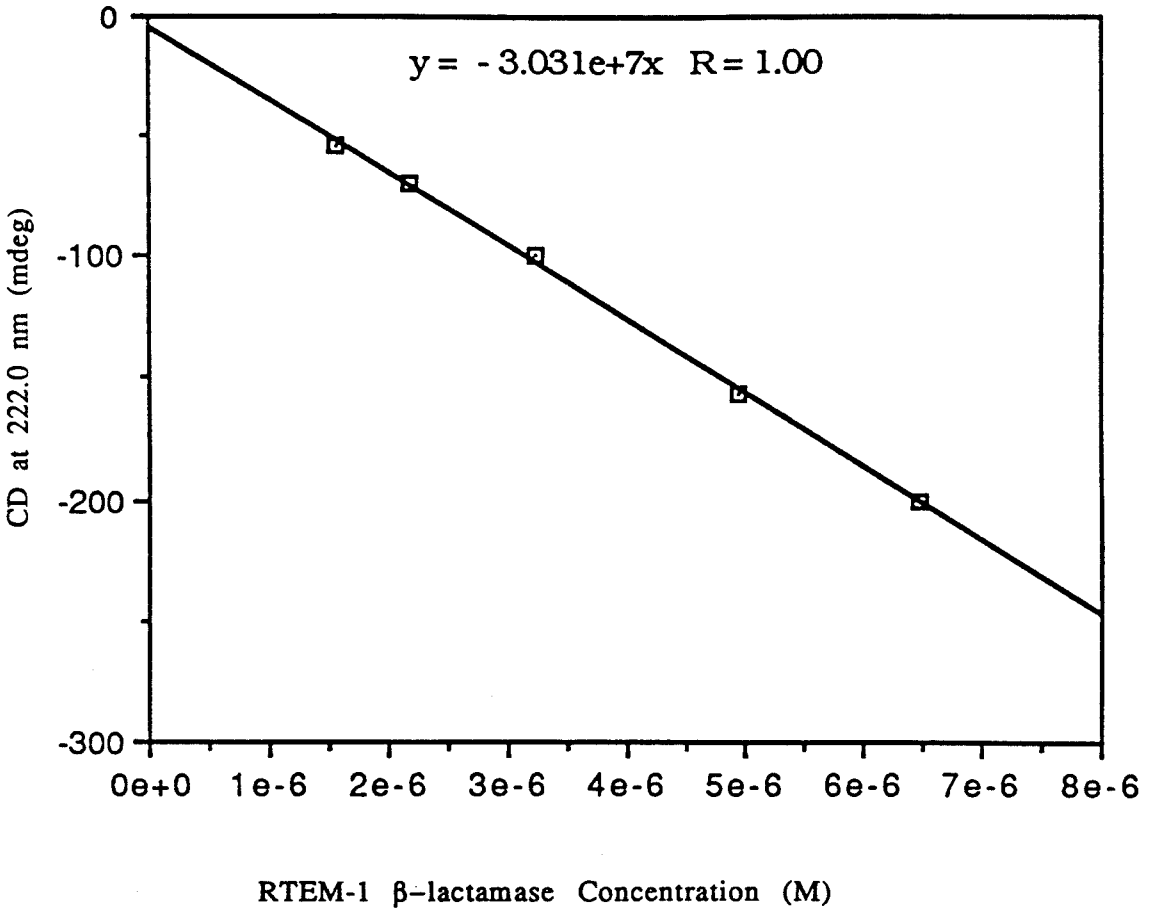

Figure 17. Ellipticity at 222 nm versus wild type RTEM-1 β-lactamase concentration $[\theta]_{222}=3.03X10^7$ deg M^{-1} cm^{-1}.

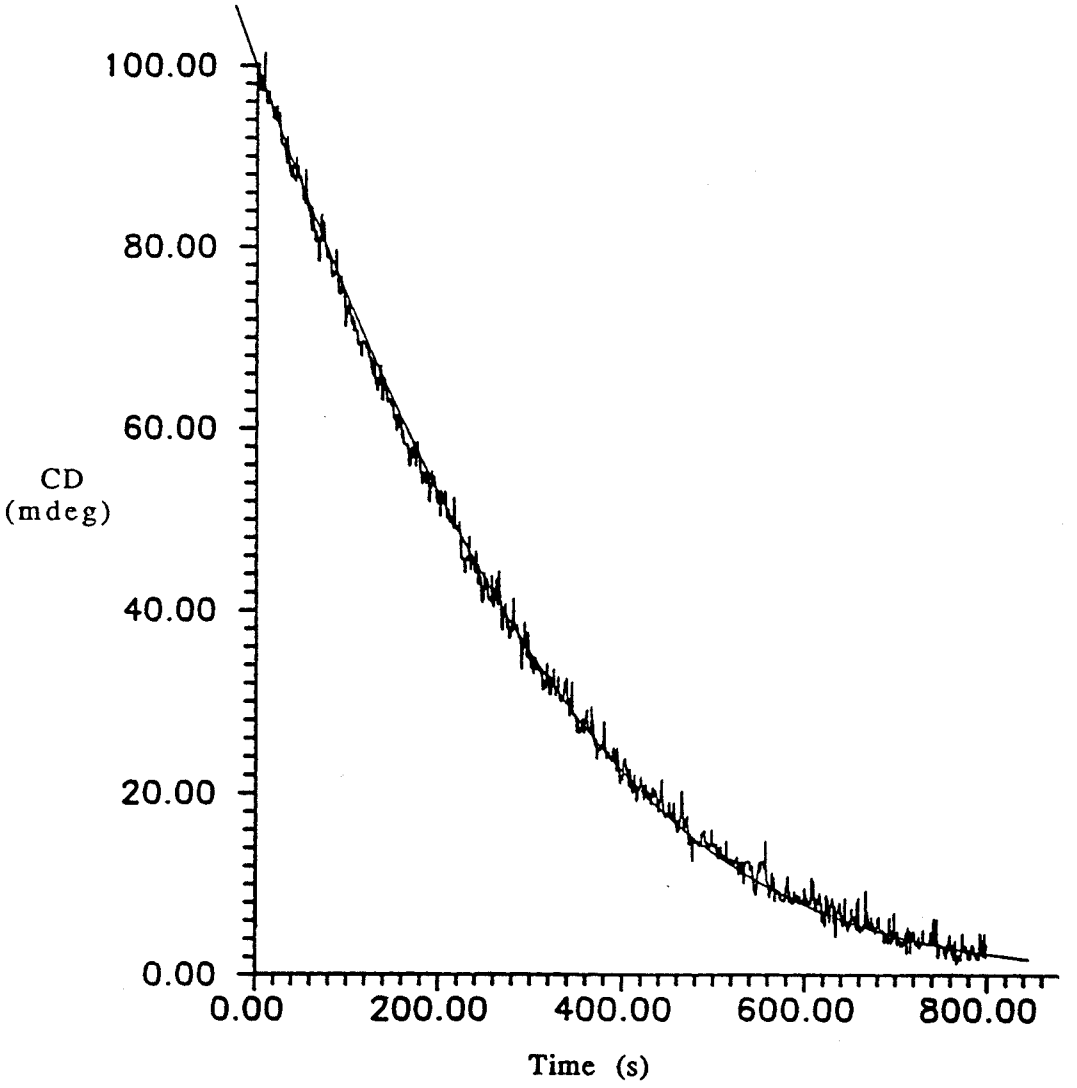

Figure 18. CD versus time for the hydrolysis of ampicillin by wild type RTEM-1 β–lactamase. Initial ampicillin concentration was about 230 μM. Conditions were 100 mM potassium phosphate pH 7.0, 30°C, 10 mm path length. Data were collected until 2% of the substrate remained unhydrolyzed.

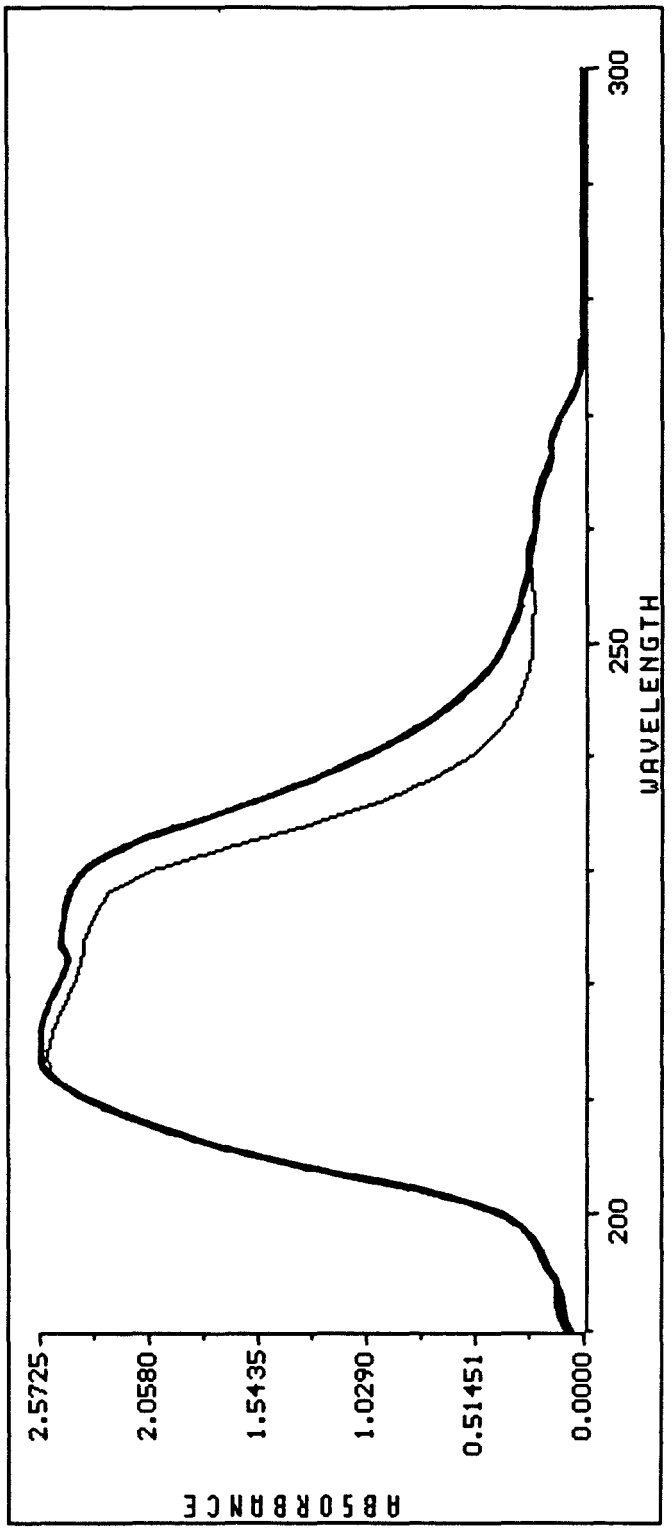

Figure 19. The UV spectra of 1 mM ampicillin (heavy line) and 1 mM hydrolyzed ampicillin (light line). Conditions were: 100 mM potassium phosphate pH 7.0, 25°C, path length 10 mm.

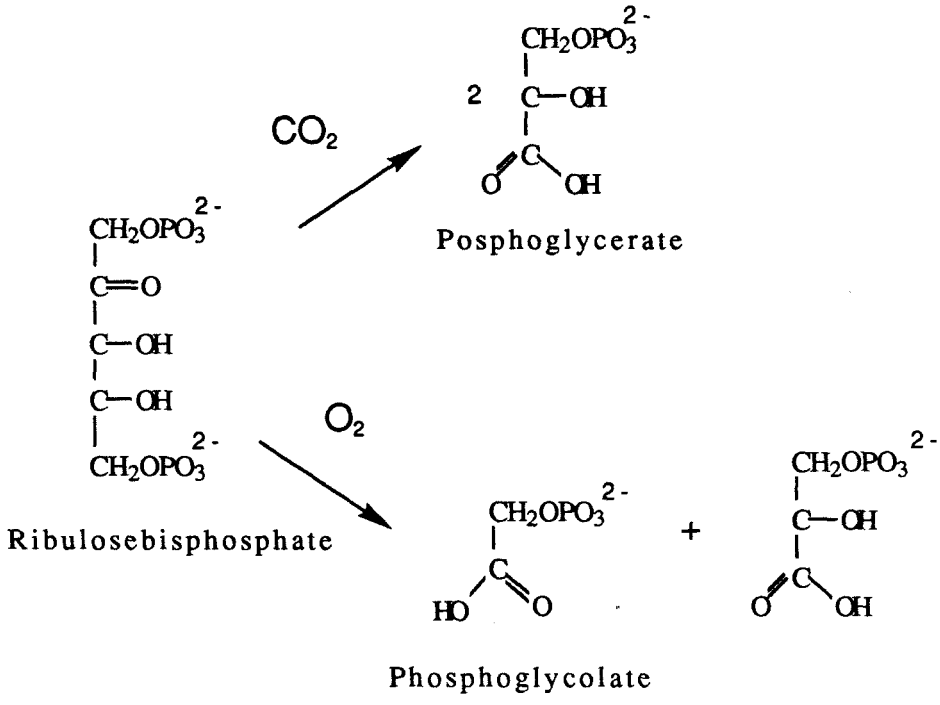

Figure 20. The reactions catalyzed by ribulose-1,5-bisphosphate carboxylase/oxygenase. The enzyme from spinach has a turnover number of a few per second, and KMs for CO_2 and O_2 are equal to about 15 μM and 600 μM, respectively (Jordan, B. and Ogren, W. (1984) *Planta*, **161**, 308.).

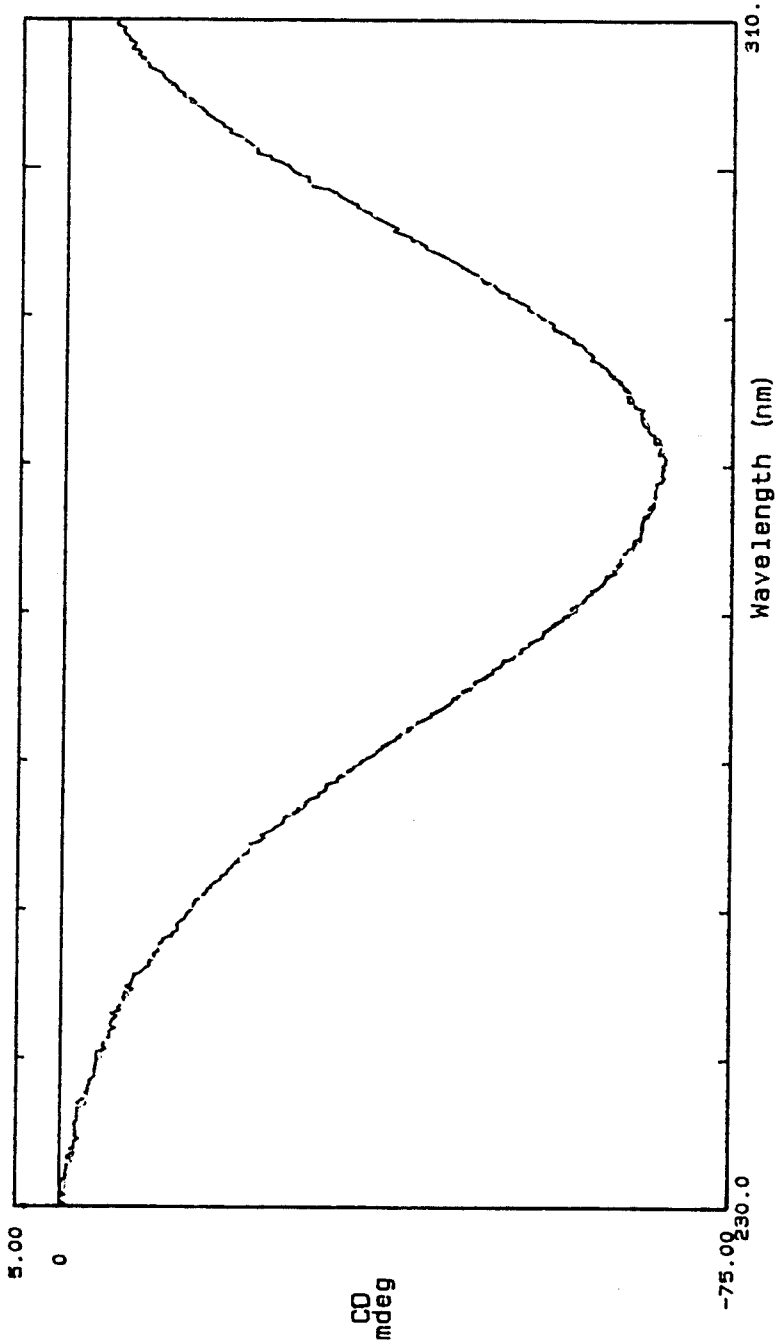

Figure 21. The CD spectrum of $3.57X10^{-3}$ M ribulose-1,5-bisphosphate. Conditions were 100 mM potassium phosphate pH 7.0, 30°C, 10 mm path length. The molar ellipticity is $[\theta]_{280.6}=19$ deg M^{-1} cm^{-1}.

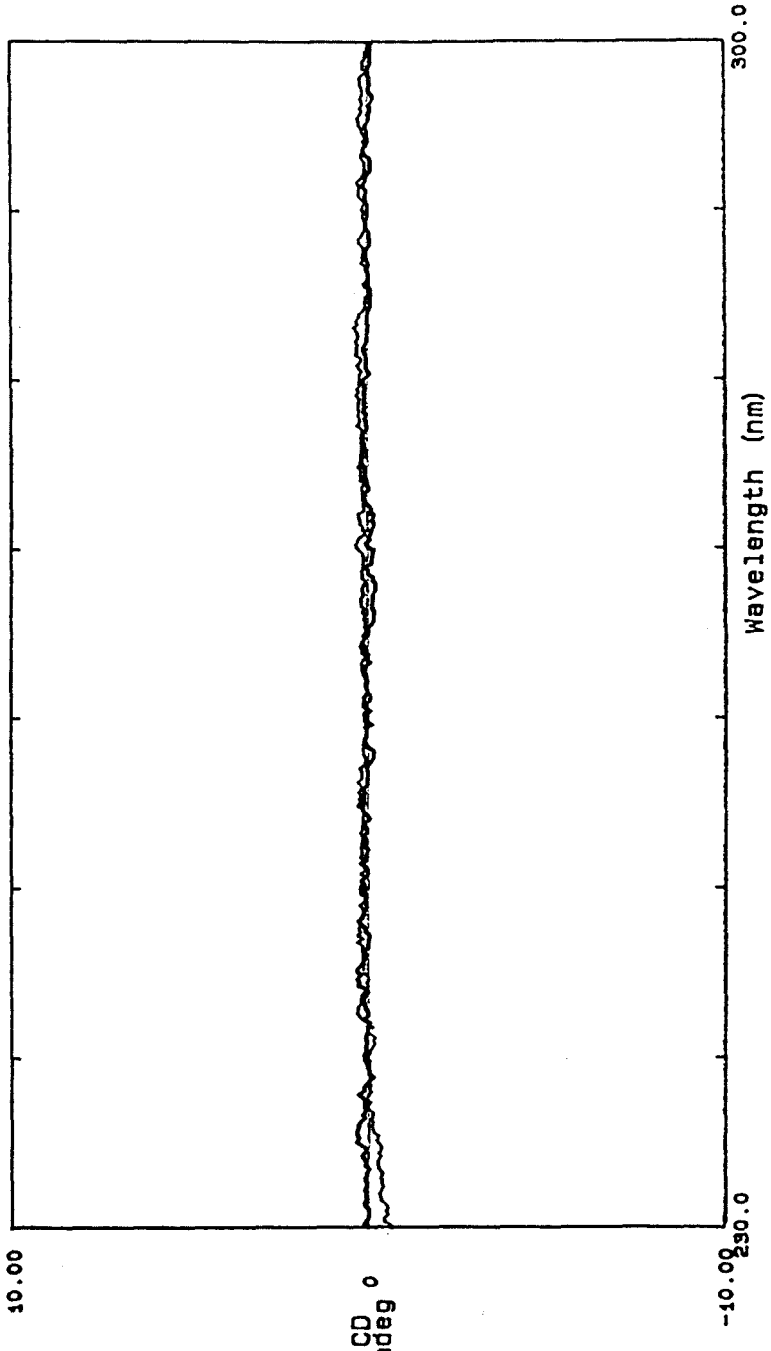

Figure 22. CD spectra of 1 mM phosphoglycolate (heavy line) and 1 mM phosphoglycerate (light line). Conditions were: 100 mM potassium phosphate pH 7.0, 25°C, path length 1 mm.

References

1. O'Sullivan, C. and Thompson, F. (1890) *J. Chem. Soc. (Trans.)*, **57**, 834.
2. Brown, A. (1892) *J. Chem. Soc. (Trans.)*, **61**, 369.
3. Nietzel, J. (1987) Ph. D. thesis (California Institute of Technology, Pasadena, CA)
4. Charm, S. and Matteo, C. (1972) *Methods Enzymol.*, **22**, 476.
5. Cantor, C. and Shimmel, P. (1980) *Biophysical Chemistry*, W. H. Freeman and Co., San Fransisco, p. 413.
6. Fisher, J., Belasco, J., Khosla, S., and Knowles, J. (1980) *Biochemistry*, **19**, 2895.
7. Hanes, J. (1932) *Biochem J.*, **26**, 1406.
8. Cornish-Bowden, A. (1979) *Fundamentals of Enzyme Kinetics*, Butterworths, London, p. 36.
9. Litman, B. and Schellman, J. (1965) *J. Chem. Phys.*, **69**, 978.
10. Rasmussen, C. and Higuchi, T. (1971) *J. Pharm. Sci.*, **60**, 1608.
11. Purdie, N. and Swallows, K. (1985) *Anal. Chem.*, **59**, 1349.
12. Waley, S. (1974) *Biochem J.*, **139**, 789.
13. Takakuwa, T., Konno, T., and Meguro, H. (1985) *Anal. Sci.*, **1**, 215.
14. Konno, T., Meguro, H., and Tuzimura, K. (1975) *Anal. Biochem.*, **67**, 226.
15. Stryer, L. and Blout, E. (1961) J. *Amer. Chem. Soc.*, **83**, 1411.
16. Neville, D. and Bradley, D. (1961) *Biochim. Biophys. Acta*, **50**, 397.
17. Walker, D., Leegood, R., and Sivak, M. (1986) *Phil. Trans. R. Soc. Lond. B*, **313**, 305.

18. Hartman, F., Stringer, C., Milanez, S., and Lee, E. (1986) *Phil. Trans. R. Soc. Lond. B*, **313**, 379.

19. Miziorko, H. and Lorimer, G. (1983) *Ann. Rev. Biochem.*, **52**, 507.

20. Eisenberg, D. Presented at the First Symposium of The Protein Society, San Diego, Ca., Aug. 9-13, 1987.

21. Lorimer, G. (1981) *Annu. Rev. Plant Physiol.*, **32**, 349.

22. Chapman, M., Suh, S., Curami, P., Cascio, D., Smith, W., and Eisenberg, D. (1988) *Science*, **241**, 4861.

23. Hartman, F., Soper, T., Niyogi, S., Mural, R., Foote, R., Mitra, S., Lee, E., Machanoff, R., and Larimer, F. (1987) *J. Biol. Chem.*, **262**, 3496.

24. McFadden, B., Torres-Ruiz, J., Daniell, H., and Sarojini, G (1986) *Phil. Trans. R. Soc. Lond. B*, **313**, 347.

25. Niyogi, F., Foote, R., Mural, R., Larimer, F., Mitra, S., Soper, T., Machanoff, R., and .Hartman, F. (1987) *J. Biol. Chem.*, **262**, 10087.

26. Keys, A. (1986) *Phil. Trans. R. Soc. Lond. B*, **313**, 325.

27. Silverstein, R., Bassler, G., and Morrill, T. (1981) *Spectrometric Identification of Organic Compounds, Fourth Ed.*, John Wiley and Sons, New York, p. 315.

28. Schellman, J. and Oriel, P. (1962) *J. Chem. Phys.*, **37**, 2114.

29. Laing, W., Ogren, W., and Hageman, R. (1974) *Pl. Physiol.*, **75**, 645.